PROLITH v7.2

PROLITH Workbook

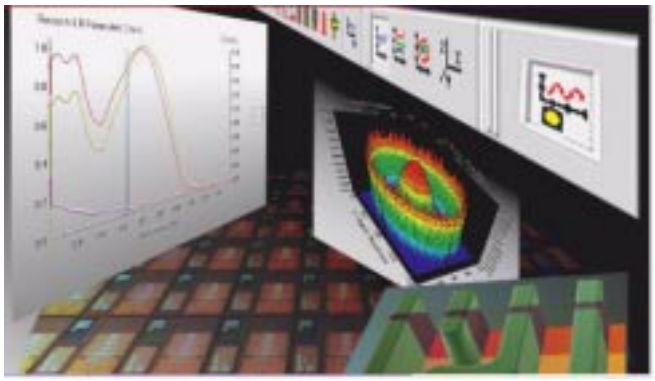

KLA-Tencor

Preface

KLA-Tencor has designed the PROLITH Workbook to be used as a tutorial. It should be a valuable learning tool for PROLITH users at all levels of experience. This version of the workbook is based on PROLITH version 7.2.

Some chapters address PROLITH functions that are optional and not included in the base PROLITH configuration.

About This Workbook

The workbook consists of a series of chapters that address a particular lithography problem or issue. Each chapter is organized as follows:

- Objective – A statement of the tutorial objective.
- Introduction – A brief overview of the lithography topic.
- Theory – A presentation of the theory needed to understand the problem or issue.
- Procedure – The hands-on portion of the tutorial. A guide to use PROLITH to address the issue.
- Summary – Review of what has been covered in the chapter.
- Questions – A list of questions and exercises for the user that are designed to deepen and test their understanding of the issue.
- Further Information – A listing of references on the topic.

Some of the Workbook chapters make reference to PROLITH files that are included for your use.

Getting Help

We always welcome comments regarding our suite of products and encourage users to contact us with recommendations or observations about using this product.

If you have questions about PROLITH after reviewing the printed documentation and online help, follow these steps:

- If the software was purchased from a distributor, please contact the distributor with unresolved questions.
- If the software was purchased directly from KLA-Tencor, or if you have questions that the distributor cannot answer, please contact us by any of the following methods:

Mailing address:

KLA-Tencor, Inc.
8834 N. Capital of Texas Highway
Suite 301
Austin, TX 78759

Telephone:

(512) 327-3781 (during business hours, U.S. Central Standard Time)

Fax:

(512) 327-1510

Email:

PROLITH_Support@KLA-Tencor.com

For questions, concerns, or comments regarding this document, send an email to Tech_Support@KLA-Tencor.com.

See also the following web site: www.KLA-Tencor.com/litho.

Table of Contents

Chapter 1
Using NILS to Judge Aerial Image Quality

Objective

This workbook example will explain the meaning and use of NILS, the normalized image log-slope, to judge the quality of an aerial image.

Introduction

In one sense, the aerial image is the source of the information being provided to the photoresist to define the final photoresist pattern. As such, it is important to judge the quality of an aerial image, with regards to how that image will ultimately be printed in resist. This workbook example will define one important metric, the Normalized Image Log-Slope (NILS), and show how this metric can be used to study the influence of various optical parameters on image quality.

In this workbook chapter, you'll learn how to:

- Generate a log-slope defocus curve
- Interpret the log-slope defocus curve to estimate depth of focus
- Use the log-slope defocus curve to understand the impact of wavelength and numerical aperture on depth of focus

Theory

Projection imaging tools, such as scanners, steppers, or step-and-scan tools, project an image of a mask pattern into air, and into the photoresist. The projected image in air is called the *aerial image*. It is the distribution of light intensity as a function of spatial position in the image plane. The aerial image is the source of the information that is exposed into the resist, forming a gradient in dissolution rates that enables the three-dimensional resist image to appear during development. The quality of the aerial image dictates the amount of information provided to the resist, and subsequently the quality and controllability of the final resist profile.

How do we judge the quality of an aerial image? If, for example, aerial images are known for two different values of the partial coherence, how do we objectively judge which is better? Historically, the problem of image evaluation has long been addressed for applications such as photography. The classical metric of image quality is the *image contrast* (Figure 1). Given a mask pattern of equal lines and spaces, the image contrast is defined by first determining the maximum light intensity (in the center of the image of

the space) and the minimum light intensity (in the center of the line) and calculating the contrast as

$$Image\ Contrast = \frac{I_{\max} - I_{\min}}{I_{\max} + I_{\min}} \quad (1)$$

Since the goal is to create a clearly discernible bright/dark pattern, ideally I_{min} should be much smaller than I_{max}, giving a contrast approaching 1.0 for a high-quality ("high contrast") image.

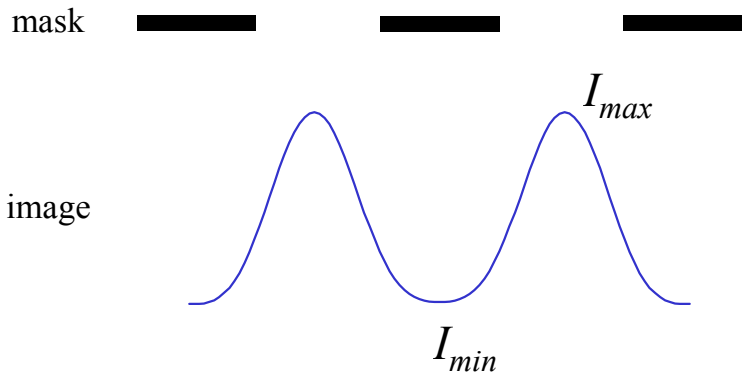

Figure 1: Image Contrast is the conventional metric of image quality used in photography and other imaging applications, but is not directly related to lithographic quality.

Although this metric of image quality is clear and intuitive, it suffers from some problems when applied to lithographic images. First of all, the metric is only defined for equal lines and spaces. Although it is possible to modify the definition of image contrast to apply, for example, to an isolated line or to a contact hole, it is not clear that these modified definitions are useful or comparable to each other. Secondly, the image contrast is only useful for patterns near the resolution limit. For large features the image contrast is 1.0, regardless of the image quality. Finally, and most importantly, the image contrast is not directly related to metrics of lithographic quality, such as resist linewidth control.

Fundamentally, the image contrast metric samples the aerial image at the wrong place. The center of the space and the center of the line are not the most important regions of the image. What is most important is the shape of the image near the nominal line edge. The edge between bright and dark determines the position of the resulting photoresist edge. This transition from bright to dark within the image is the source of the information concerning where the photoresist edge should be. The steeper the intensity transition, the better the edge definition of the image, and as a result the better the edge definition of the resist pattern. If the lithographic property of concern is the control of the photoresist linewidth (i.e., the position of the resist edges), then the image metric that affects this lithographic result is the slope of the aerial image intensity near the desired photoresist edge.

The slope of the image intensity as a function of position (dI/dx) measures the steepness of the image at the transition from bright to dark. However, to be useful it must be

properly normalized. For example, if one simply doubles the intensity of the light, the slope will also double, but the image quality will not be improved. Dividing the slope by the intensity will properly normalize the metric. The resulting metric is called the image log-slope.

$$Image\ Log-Slope\ =\ \frac{1}{I}\frac{dI}{dx}\ =\ \frac{d\ln(I)}{dx} \tag{2}$$

The log-slope is measured at the nominal (desired) line edge (Figure 2). The sign of the image log-slope is adjusted to remove sign differences between lines and spaces. Since variations in the photoresist edge positions (linewidths) are typically expressed as a percentage of the nominal linewidth, the position coordinate x can also be normalized by multiplying the log-slope by the nominal linewidth w. This gives the Normalized Image Log-Slope (NILS).

$$NILS\ =\ w\frac{d\ln(I)}{dx} \tag{3}$$

The NILS is the best single metric to judge the lithographic usefulness of an aerial image.

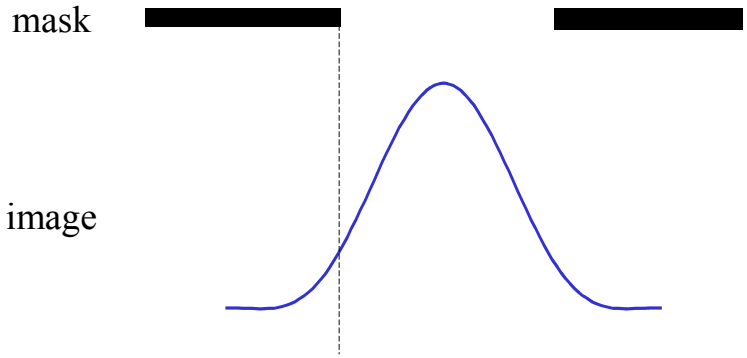

Figure 2. Image Log-Slope (or the Normalized Image Log-Slope, NILS) is the best single metric of image quality for lithographic applications.

An important property of the calculated NILS value is its relationship to the expected exposure latitude for a given process. By associating a change in position with a change in CD and a change in image intensity with a change in dose, equation 3 can be rearranged as follows:

$$\mathrm{NILS} = \frac{\mathrm{w}}{\mathrm{dx}}\cdot\frac{\mathrm{dI}}{\mathrm{I}} \approx 2\frac{\mathrm{w}}{\Delta\mathrm{CD}}\cdot\frac{\Delta\mathrm{I}}{\mathrm{I}} \approx 2\frac{\%\mathrm{Dose\ Error}}{\%\mathrm{CD\ Error}}$$

The ratio of the dose error to the CD error is the exposure latitude:

$$\text{Exposure Lattitude (\% dose change / 1\% CD change)} \approx \frac{\mathrm{NILS}}{2} \tag{4}$$

Equation (4) is appropriate for an "ideal" resist, where the resist completely develops away only in the regions where the dose is larger than some threshold value. A more general equation can be derived that is appropriate for a high-contrast resist described by the Lumped Parameter Model,

$$\frac{\partial \ln CD}{\partial \ln E} \approx \frac{2}{NILS} + \frac{2\gamma D}{CD}\left[\frac{I(CD/2)}{I(0)}\right]^{\gamma} \propto \frac{1}{\text{Exposure Latitude}} \qquad (5)$$

In the above equation, D is the thickness of the resist and γ is the resist contrast. In this expression, there are two distinct terms that are inversely proportional to the exposure latitude. The first, 2/NILS, corresponds to the term in Equation (4), which is a pure aerial image term. The second term includes the impact of the resist on exposure latitude, and includes the aspect ratio of the resist (*D/CD*), the resist contrast, and the ratio of the aerial image intensity at the edge of the pattern relative to that in the center of the space. The intensity at the center of the space is important to the develop process, where the middle of the space clears first. Whether we use Equation (4) or (5), we find that a higher NILS value will result in a higher exposure latitude.

Unfortunately, the NILS, like the aerial image itself, cannot be accurately measured for real lithographic images from a stepper or scanner. We can, however, calculate what we expect the NILS to be for any set of optical parameters, such as numerical aperture, partial coherence, wavelength, mask pattern, aberrations and defocus, using PROLITH.

How can the NILS be used? NILS can be used to investigate how optical parameters affect image quality. One of the most obvious examples is defocus. The effects of focus on an image are quite familiar to most of us from everyday examples such as on overhead projector: as an image goes out of focus, it gets blurry! Specifically, the edges become blurred so that it is harder to distinguish the exact point where the image transitions from bright to dark. In other words, the slope of the aerial image at the edge between bright and dark features is reduced as we go out of focus. Using our metric of image quality, the NILS decreases as the image goes out of focus.

Figure 3a shows the aerial image of a space at best focus, and at two levels of defocus. The "blurred" images obviously have a lower image log-slope at the nominal line edge compared to the in-focus image. By plotting the log-slope or the NILS as a function of defocus, one can quantify the degradation in aerial image quality as a function of defocus (Figure 3b). This log-slope defocus curve provides a very important tool for understanding how focus affects a lithographic process. For example, suppose one assumes that there is a minimum acceptable NILS value, below which the aerial image is not good enough to provide adequate resist images or linewidth control. In Figure 3b, for example, a minimum acceptable NILS value of 2.5 would mean that this imaging process can tolerate about ±1μm of defocus and still produce aerial images of acceptable quality. Thus, an estimate of the minimum acceptable NILS can lead to an estimate of the depth of focus.

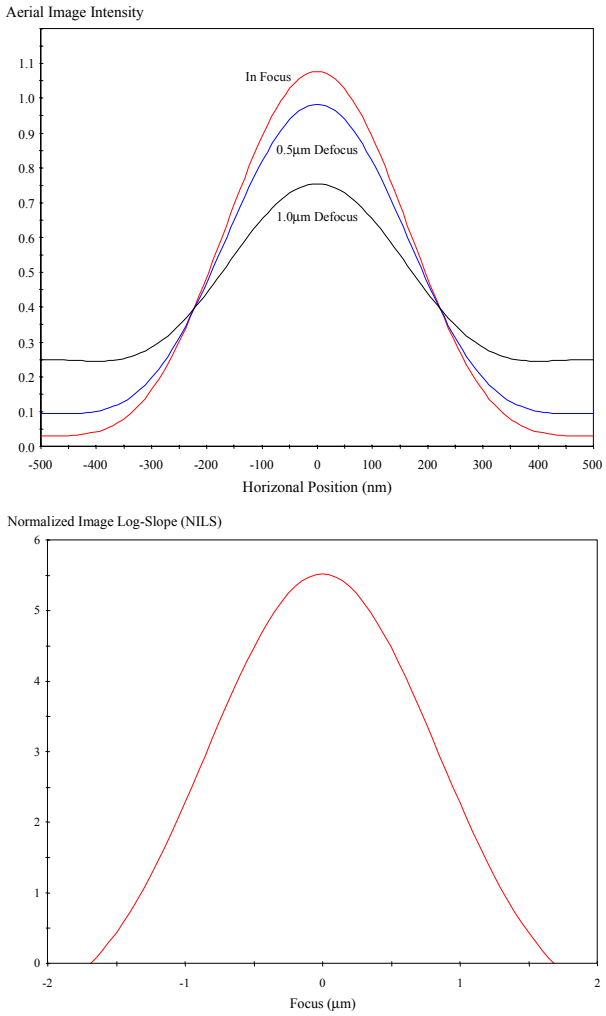

Figure 3: The effect of defocus is to "blur" an aerial image (top graph), resulting in reduced log-slope as the image goes out of focus (bottom graph).

Procedure

To see how the log-slope defocus curve can be used to understand imaging, consider the effects of wavelength and numerical aperture on the focus behavior of an aerial image. In PROLITH, set up the following input parameters. If a parameter is not listed, use the default:

Mask:

Mask Type: 1D Binary
Feature Type: Line
Nominal Feature Width: 500 nm
Pitch: 1000 nm
Mask Bias: 0

Imaging Tool:

Source Shape: Partially Coherent
Partial Coherence: 0.5
Wavelength: 365 nm
Bandwidth: 0
Numerical Aperture: 0.5

Next, run a custom simulation set. Select Focal Position as the input, setting the *Min*., *Max* and *Step* to 0, 2, and 0.1, respectively. Select the Aerial Image Group as the output. When the simulation is finished, set the Y-axis of the graph to be Normalized Image Log-Slope. Figure 4 shows the expected output.

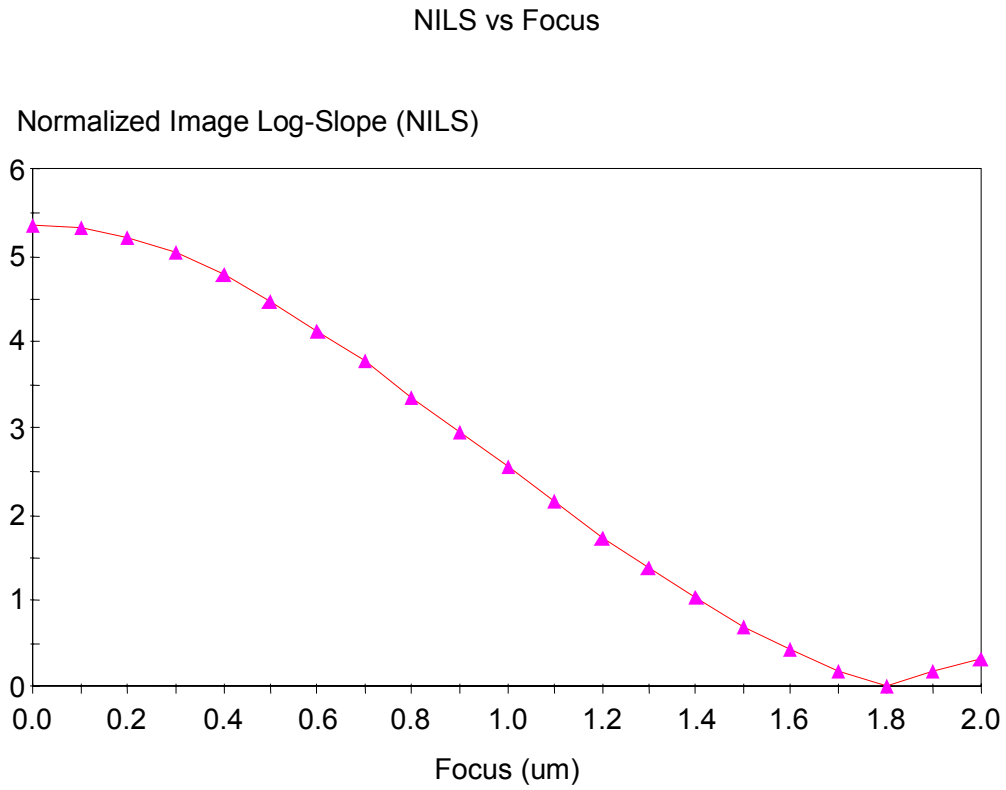

Figure 4: Typical log-slope defocus curve as calculated using a custom simulation set.

Now, add *Wavelength* as a second input to the custom set. Set the *Min*., *Max* and *Step*. to 250, 450, and 100, respectively. When the simulation is complete, change the graph type to Multi-Line, then set the *X-axis* to *Focal Position*, the *Y-axis* to *Normalized Image Log-Slope*, and the *Z-axis* to *Wavelength*. Figure 5 shows the results.

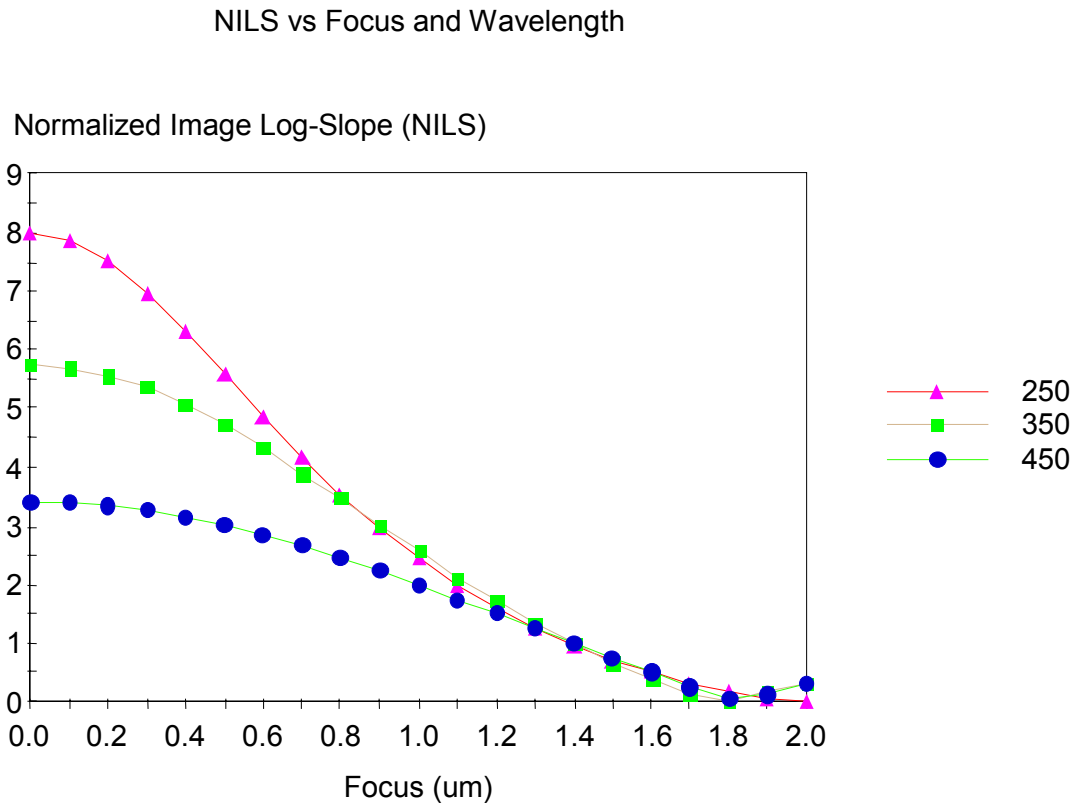

Figure 5: Impact of wavelength on the log-slope defocus curve for a given feature.

It is clear from the plot that the lower wavelength provides better image quality for all amounts of defocus. For any minimum acceptable value of NILS, the lower wavelength will allow acceptable performance over a wider range of focus. One could conclude that, for a given feature being imaged, the lower wavelength always provides better in-focus performance and better depth of focus.

As a final exercise, remove *Wavelength* from the input list and add *Numerical Aperture.* Set the *Min*., *Max* and *Step*. to 0.4, 0.6, and 0.1, respectively. When the simulation is complete, change the graph type to Multi-Line, then set the *X-axis* to *Focal Position*, the *Y-axis* to *Normalized Image Log-Slope*, and the *Z-axis* to *Numerical Aperture*. Figure 6 shows the results.

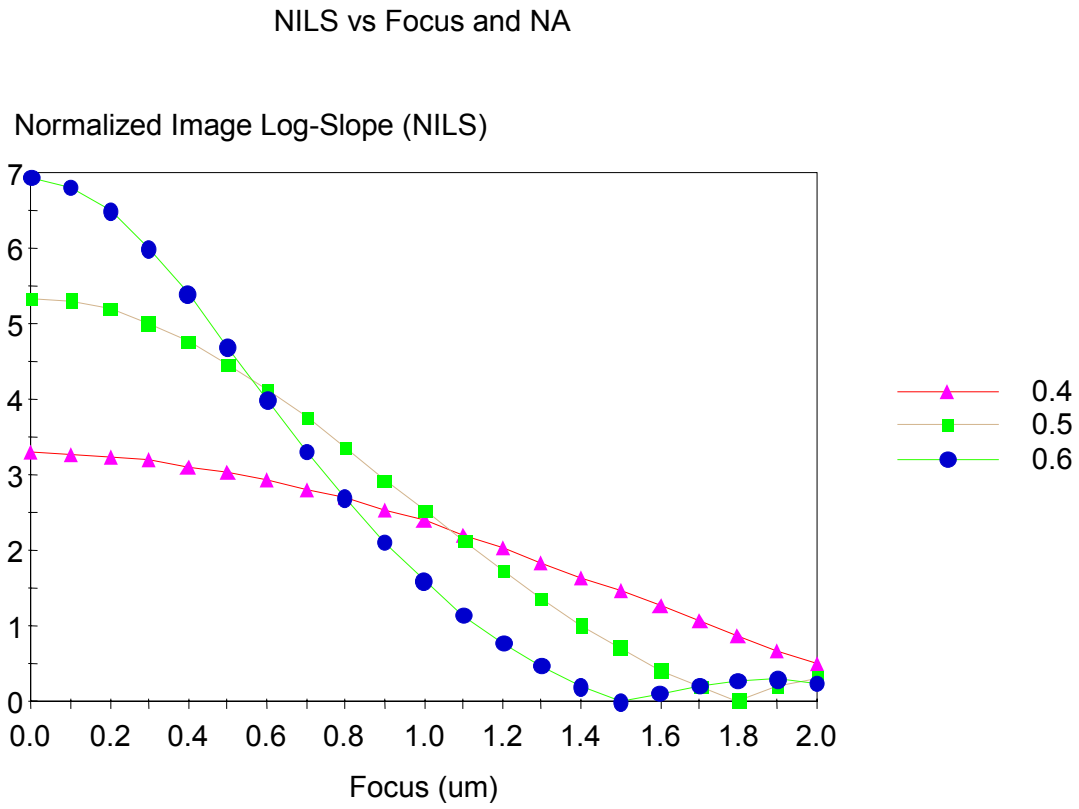

Figure 6: Impact of numerical aperture on the log-slope defocus curve for a given feature.

The impact of numerical aperture (NA) is more complicated, as shown in Figure 6. Here, the log-slope defocus curves for three different numerical apertures cross each other. If one picks some minimum acceptable NILS value, there will be an optimum NA that gives the maximum depth of focus (for example, a minimum NILS value of 3.5 has the best depth of focus when NA = 0.5). Using a numerical aperture above or below this optimum reduces the depth of focus.

Summary

NILS values are easy and fast to calculate and they provide a simple yet valuable metric of image quality. As an example, the log-slope defocus curve is one of the easiest ways to quantify the impact of defocus on image quality. By using NILS, we have quickly arrived at two fundamental imaging relationships: when imaging a given mask pattern, 1) lower wavelengths give better depth of focus, and 2) there is an optimum numerical aperture that maximizes the depth of focus.

Questions

See Appendix A for answers.

1. If a better quality photoresist requires a lower minimum acceptable NILS value compared to another resist, does the resist influence the choice of the optimum

wavelength (from the perspective of the NILS-estimated depth of focus)? If so, how?

2. The analysis above was performed assuming 500nm equal lines and spaces. Would the choice of the optimal wavelength and numerical aperture change for isolated features?
3. Wavelength is not an easily adjustable control knob for a manufacturing process but numerical aperture most often is programmable in modern imaging tools. What other stepper settings are easily changeable? How would one use NILS to optimize these stepper settings to achieve maximum depth of focus?

Further Information

For further information, see chapter 10 of *Inside PROLITH* and the following references:

C.A. Mack, "Using the Normalized Image Log-Slope, part 6: Development Path", *Microlithography World*, May 2002.

The Lumped Parameter Model is described in Chapter 9 of *Inside PROLITH*

Chapter 2
Defining Depth of Focus

Objective

This workbook example will explain how Depth of Focus (DOF) is used to measure process capability. We will develop a definition of DOF that is consistent and unambiguous and one that relates accurately to the manufacturability of a lithography process.

Introduction

Depth of Focus (DOF) is a commonly used – and misused – term. Since a consideration of DOF is fundamental to the lithography process, it is imperative that the lithographer has a clear definition of the term as well as a firm understanding of how this important metric is used.

In this workbook chapter, you'll learn how to:

- Define DOF in a simple and powerful way
- Use PROLITH to generate a Focus-Exposure (FE) matrix and FE process window
- Graphically represent systematic and random errors in the FE process window
- Determine the DOF based on a simple error analysis

Theory

Before one can begin to understand DOF, one must first understand what is meant by focus or focal position. We intuitively know what focus is from experience with common optical systems such as a camera or the human eye. For these systems, focus is adjusted by turning the bezel ring of a camera or flexing the muscles of the eye. The definition of focus for optical lithography is somewhat less intuitive. During the lithography process, the illumination system will project the image contained on the mask into the resist. The characteristics of the projected image will vary through the thickness of the resist, so we define the focal position as a position relative to the resist. For example, if the resist is 1000 nm thick and zero focus is defined as the mid-point of the resist, with positive values closer to the resist/air interface and negative values closer to the resist/substrate interface, the focal positions within the resist vary from –500 nm to +500 nm. (Note: It is possible to focus the system above or below the resist, so the full range of focal positions is larger than 1000nm. This will be shown below.)

As with a camera, the user of a stepper or scanner will try to set the focus or focal position to achieve optimum imaging. However, limitations in the photolithography

process cause the focal position to deviate from this desired value. These deviations are called focus errors. The focus errors, in general, have both random and systematic components. Since the errors are deviations from what was intended, they cause degradation in the image quality. With this simple understanding of focus, focal position and focus errors, we can now begin to define DOF.

In general, DOF can be thought of as the range of focus errors that a process can tolerate and still give acceptable lithographic results. A change in focus results in two major changes to the final lithographic result: the photoresist profile changes and the sensitivity of the process to other processing errors is changed. The first of these effects, the photoresist profile change, is the most obvious and the most easily observed consequence of defocus. Typically, photoresist profiles are described (in an oversimplified way) using three parameters: the linewidth (also called the critical dimension, CD), the sidewall angle, and the resist thickness of the feature (which is useful for lines or islands, but not spaces or contacts). In effect, the resist profile is modeled as a trapezoid, as shown in Figure 1. Usually it is more convenient to talk about resist loss (the difference between the original resist thickness and the final resist thickness), possibly as a percentage of the original resist thickness.

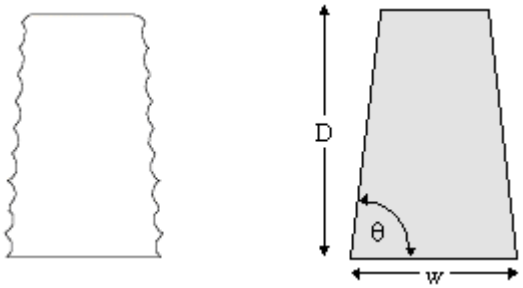

Figure 1: Comparison of an actual, complex photoresist profile (left) with its trapezoidal model (right) used to determine linewidth, sidewall angle, and resist loss.

The variation of linewidth, sidewall angle, or resist loss with focus can be readily determined for any given set of conditions. If these were the only responses of importance, specifications on these responses would lead to a simple definition of the depth of focus: the range of focus which keeps the linewidth, sidewall angle, and resist loss within their stated specifications. There is, however, a second effect of focus that is significantly harder to quantify and of great importance. As an image goes out of focus, the process becomes more sensitive to other errors such as variations in exposure dose. Of these secondary process errors, the most important by far is exposure. To state the issue in another way, focus and exposure are coupled in their effect on the process.

Since the effect of focus is dependent on exposure, the only way to judge the response of the process to focus is to simultaneously vary both focus and exposure in what is known as a Focus-Exposure (FE) matrix. Now that we have stated some definitions of focus and depth of focus it is time to demonstrate these concepts using PROLITH.

Procedure

In PROLITH, start with the default document and set the following input parameters (if the parameters are not listed, use the default values):

Mask:

Mask type: 1D Binary
Feature type: Line
Nominal feature width: 350 nm
Pitch: 3500 nm

Exposure/Focus:

Exposure energy: 185.0 mJ/cm2
Focal position: 0.00
Focal position relative to the middle of the resist.

Numerics:

Image Calculation Mode: High NA Scalar
Speed Factor: 3

Once you have set the parameters above, it is possible to show how focus can directly impact the resist profile. Select the resist profile button on the tool bar. Now, go to the Focus and Exposure input view and change the focal position to –0.40 microns and generate a second resist profile. Figure 2 shows the result: changing the focal position leads to differences in both the resist CD and the sidewall angle.

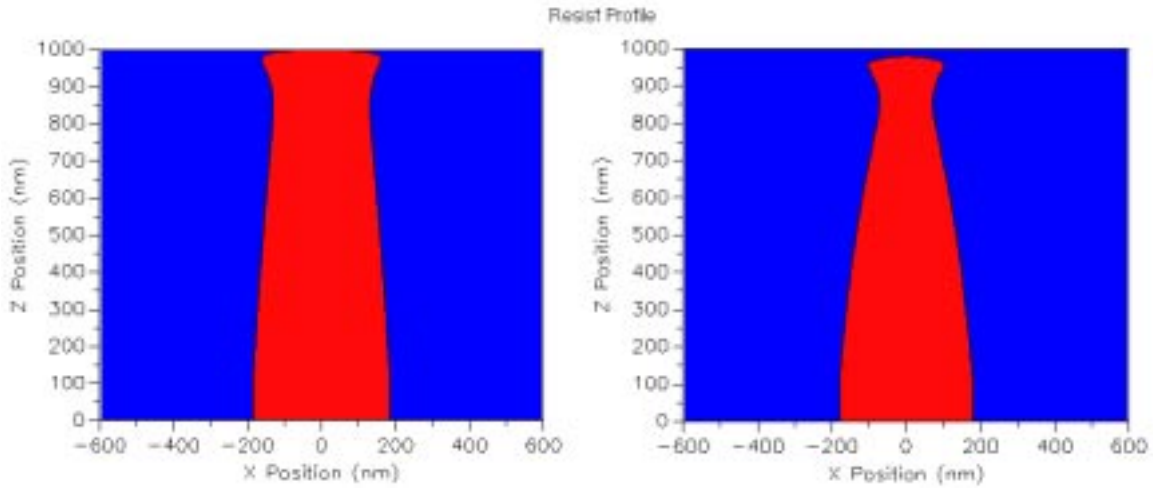

Figure 2: Two resist profiles resulting from a change in focus values.

This simple exercise illustrates the first impact of focus errors described above. A change in focus can directly change the lithographic result.

Now, we will demonstrate how errors in focus change the sensitivity of the lithography process to other errors. Set the focal position back to 0.00. Now, open the metrology window. One section of this window is labeled Process Window Analysis and it is shown in Figure 3 below.

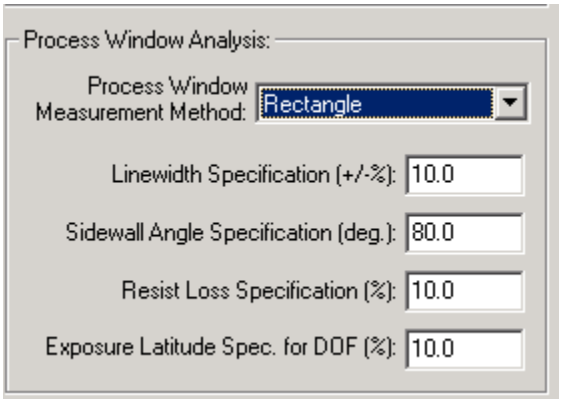

Figure 3: Process Window Analysis section of the Metrology Window.

These settings define the limits of what is "acceptable" for the resist profile results. Leave the settings as they are. Now, run a simulation set to vary focus and exposure over a range of values. Choose the Focus-Exposure Simulation Set. Set the min, max and step of the exposure to 120, 260 and 20 mJ/cm^2, respectively. Set the min, max and step of the Focus to –1.5, 1.5 and 0.2 μm, respectively. Launch the simulation set.

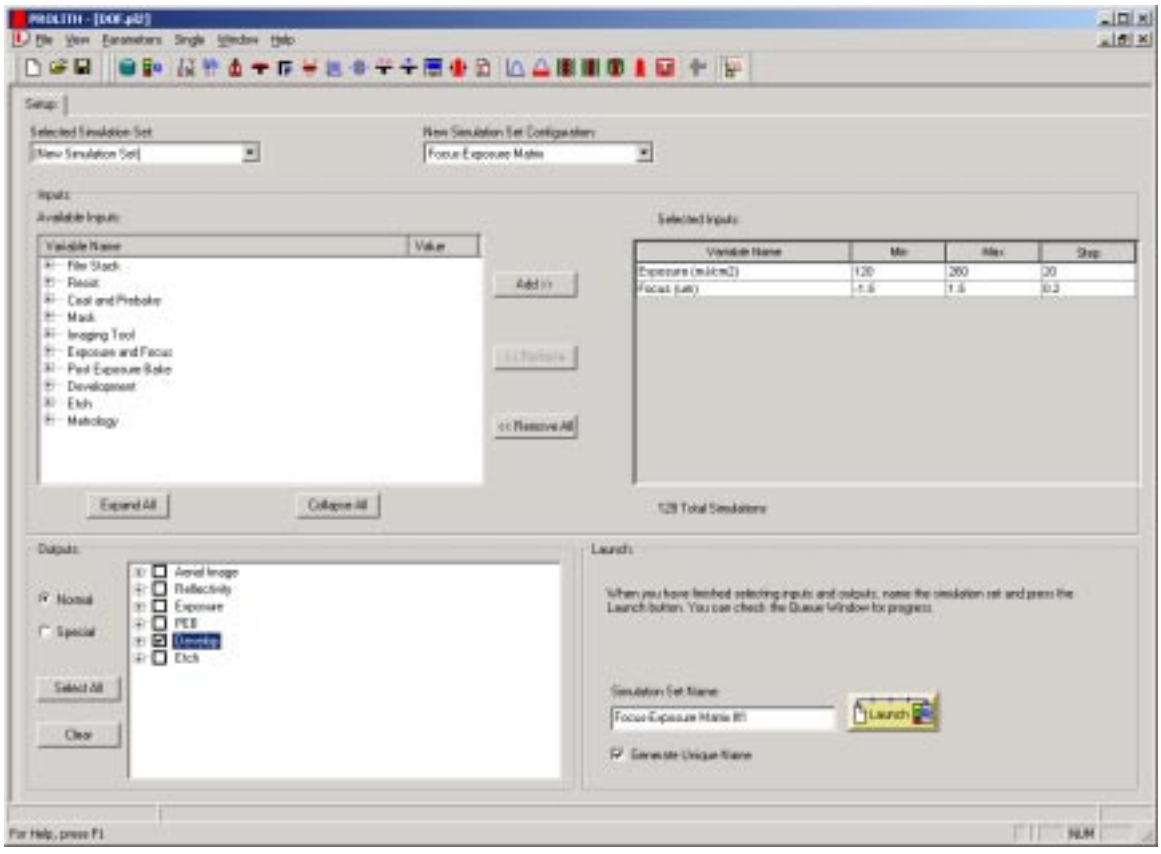

Figure 4: The Simulation Sets Window used to generate a Focus-Exposure matrix for a DOF analysis.

Once the simulation is complete, select the Results Tab. Select a 2D contour plot and change the X-axis to Focus. With some manipulation of the graph controls, the 2D plot

of the results appears as in Figure 5. (Your plot may not look exactly like Figure 5 unless you adjust the number of contour levels.)

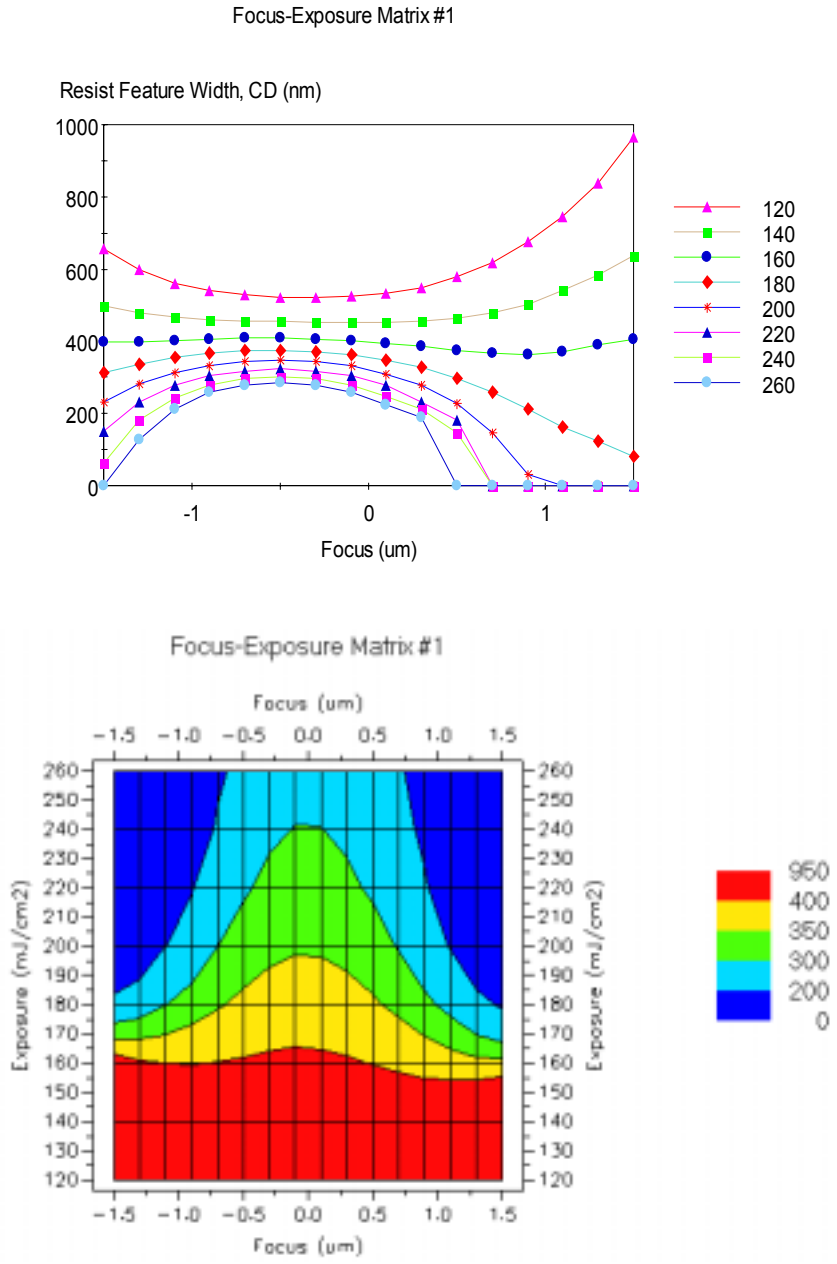

Figure 5 Two representations of the same Focus Exposure matrix data. Graph A is called a Bosong graph and shows resist CD verses focus for various exposure dose values (legend). Graph B shows contours of resist CD (legend) as a function of exposure dose and focus.

Once the simulation is complete, select the Results Tab. Select a MultiLine Graph and change the X Axis to Focus (um), the Y-Axis to Resist Feature Width and the Z-Axis to Exposure (mJ/cm^2). The resulting graph is shown in Figure 5a. This representation of the Focus Exposure data is known as a Bossong plot. Another way to represent the same data is shown in Figure 5B (Select a 2D contour plot and change the X-axis to Focus.

With some manipulation of the graph controls, the 2D plot of the results appears as in Figure 5b. (Your plot may not look exactly like Figure 5B unless you adjust the number of contour levels.)

This plot shows contours of equal resist CD. Regions between two contours represent focus and exposure combinations that result in CDs bounded by the values on the contour. If one uses contours that correspond to the upper and lower acceptable limits of the CD, then the bounded region shows all combinations of focus and exposure that would yield a resist profile within the CD specification. But, this simple analysis does not include the other resist profile specifications, such as resist loss and sidewall angle, that can also be plotted as contour plots.

Next, select the Analysis Tab. The Focus-Exposure (FE) Process Window as displayed as in Figure 6. The three boundaries shown in dashed lines depict the regions of focus and exposure values that are acceptable based on the metrology settings from Figure 3. The boundary shown in solid blue depicts the intersection of these three dashed boundaries and is labeled "Overlap". The Overlap region is the FE Process Window.

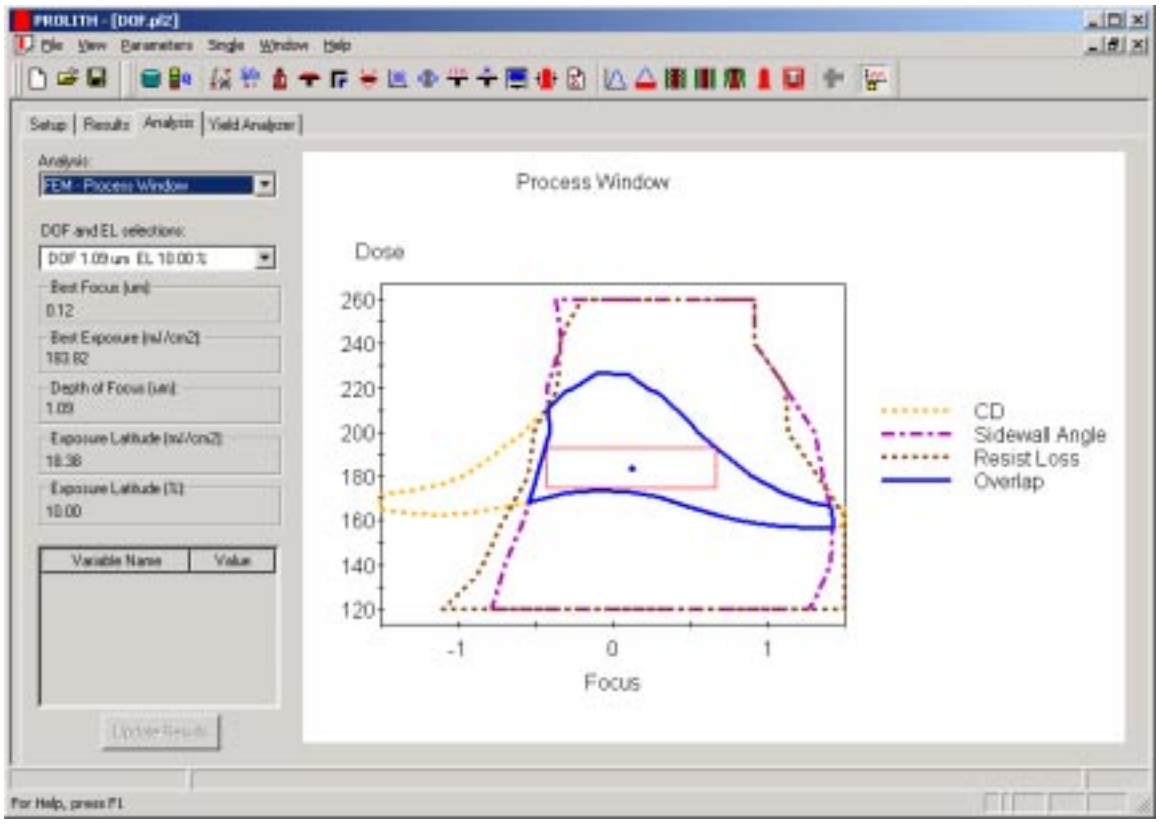

Figure 6: FE Process Window

The rectangle near the center of the process window represents one set of possible systematic errors in the process. The height of the rectangle denotes the systematic error in exposure and the width represents the associated systematic error in focus. On the left hand side of the Analysis Window, the "DOF and EL selection" pull-down shows that this rectangle represents a DOF of 1.09 microns and an Exposure Latitude (EL) of 10%. If the exposure tool were set to operate at the setting shown by the blue dot near the

center of the process window, and the imaging tool had a systematic error in exposure of +/- 10% then the range of focus settings that would still yield acceptable resist profile results would be 1.09 microns.

Using the DOF and EL selection pull-down, select "DOF 1.23 micron EL 6.49%". Notice that the rectangle becomes shorter and wider, but that its boundaries stay within the process window. This indicates that if it were possible to keep the systematic error in exposure to 6.49 %, then the DOF would increase to 1.23. Now, use the DOF and EL selection pull-down, select "DOF 0.79 micron EL 19.35%". The rectangle becomes taller, but less wide. If the systematic error in exposure was 19.35%, then the DOF would be reduced to 0.79 microns. This simple exercise illustrates that exposure and focus are not independent, but rather very closely linked. As the systematic error in one increases, the systematic variation in the other that can be tolerated to keep within the process window is reduced.

Use the DOF and EL selection pull-down to select and view several of the possible rectangles.

Since the allowed systematic errors in focus and exposure are so closely linked, it is helpful to view this relationship in a graph. Using the "Analysis" pull-down, select "FEM – Exposure Latitude vs. DOF". The resulting graph is shown in Figure 7.

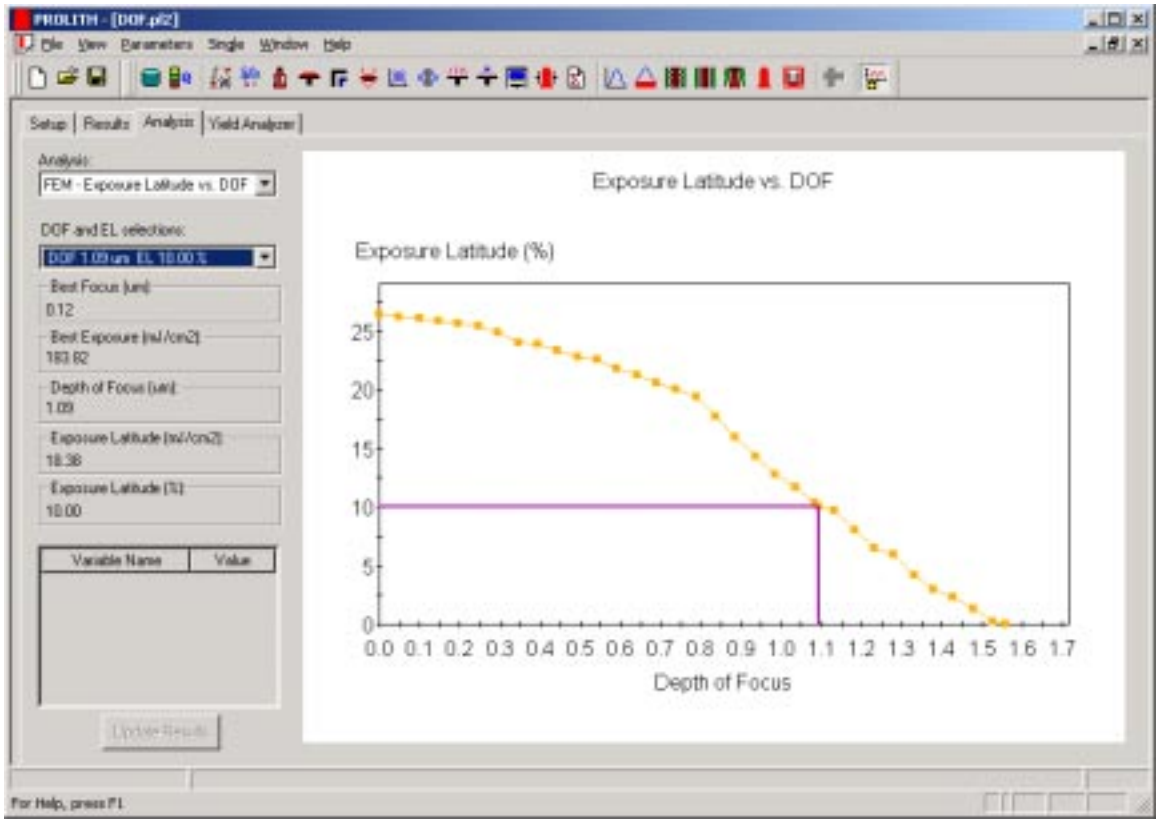

Figure 7: EL vs. DOF

This graph reduces the interdependance of focus and exposure within the process window to a simple function. Now, repeat the last exercise by using the "DOF and EL selection" pull-down to display various combinations of systematic errors.

It is now possible to state a concise definition of DOF:

Depth of Focus is the total range of focus which can be tolerated, that is, the range of focus that keeps the resulting printed feature withing a variety of specifications (such as linewidth, sidewall angle, resist loss, and exposure latitude).

If all focus and exposure errors were systematic, then the proper graphical representation of those errors would be a rectangle. The width and height would represent the total ranges of the respective errors. If, however, the errors were randomly distributed, then a probability distribution function would be needed to describe them. For the completely random case, a gaussian distribution with standard deviations in exposure and focus, σ_E and σ_F respectively, is used to describe the probability of a given set of errors.

$$p(\Delta E, \Delta F) = \frac{1}{2\pi\sigma_E\sigma_F}\exp\left(-\Delta E^2 / 2\sigma_E^2\right)\exp\left(-\Delta F^2 / 2\sigma_F^2\right) \qquad (1)$$

Here, focus errors and exposure errors are assumed to be independent. In order to graphically represent the errors of focus and exposure, one should describe a surface of constant probability of occurrence. All errors in focus and exposure inside the surface would have a probability of occurring which is greater than the established cut-off. What is the shape of such a surface? For fixed systematic errors, the shape is a rectangle. For a Gaussian distribution, the surface can be derived by setting the probability of equation (1) to a constant, p^*.

$$p^* = \frac{1}{2\pi\sigma_E\sigma_F}\exp\left(-\Delta E^2 / 2\sigma_E^2\right)\exp\left(-\Delta F^2 / 2\sigma_F^2\right)$$

$$-\ln\left(2\pi\sigma_E\sigma_F p^*\right) = \frac{\Delta E^2}{2\sigma_E^2} + \frac{\Delta F^2}{2\sigma_F^2} \qquad (2)$$

Equation (2) is that of an ellipse. Suppose, for example, that one wishes to describe a "3-sigma" surface, where p^* corresponds to the probability of having an error equal to 3σ in one variable. The resulting surface would be an ellipse with major and minor axes equal to $3\sigma_E$ and $3\sigma_F$.

$$1 = \frac{\Delta E^2}{\left(3\sigma_E\right)^2} + \frac{\Delta F^2}{\left(3\sigma_F\right)^2} \qquad (3)$$

To illustrate this point, let's reexamine the simulation above with random errors. It is not necessary to rerun the simulation set. Access the metrology input window and change the Process Window Measurement Method from Rectangle (as shown above in Figure 3) to Ellipse. Then, access the simulation set results and the analysis tab. The analysis window will be as shown in Figure 8 below.

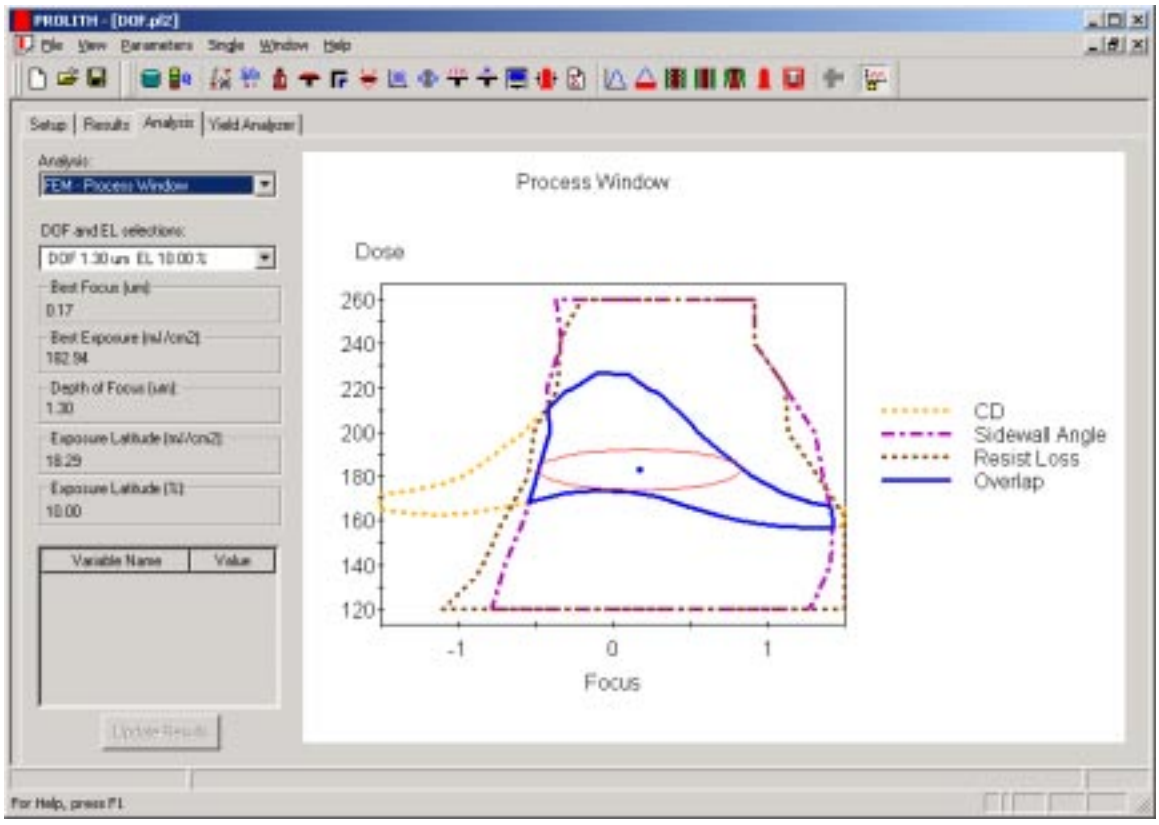

Figure 8: Process window analysis showing random errors.

Let's compare the results from the systematic and random error analyses. Use the DOF and EL selection pull-down, to select "DOF 1.30 micron EL 10.0%". The systematic error analysis yielded a DOF of focus of 1.09 micron for EL of 10%. As one might expect, systematic errors in focus and exposure are more problematic than random errors, leading to a smaller depth of focus. Most actual processes would have a combination of systematic and random errors. Thus, one might consider the rectangle analysis to give a pessimistic value for the DOF, while the ellipse method gives an optimistic view of DOF. The average value of the two will be a more realistic number in some cases.

Summary

In this section we used a simple example of an isolated line to explore the definition of DOF. We generated a FE Process Window by varying exposure and dose and defining some quality metrics. Using this Process Window, we then showed that the tolerable systematic or random errors for focus and exposure are linked – when you increase one the other decreases. Finally, we used this process to come up with an unambiguous definition of DOF.

Questions

See Appendix A for answers.

1. Which of the metrology specifications (CD, Sidewall Angle, and Resist Loss) seems to be constraining the process window?

2. The example used here was an isolated line where the pitch was 3500 nm. How would the process window change if the pitch was reduced to 700 nm and no other variables were changed? Run the simulations and check your intuition.
3. How does the Exposure Latitude vs. DOF curve in Figure 7 change if the Resist Loss specification were relaxed to 20%?

Further Information

For further information on lithographic analyses like these, see chapter 10 of *Inside PROLITH* by Chris Mack. The following technical publications also contain additional relevant information:

Mack, Chris A.; Jug, Sven; Legband, Dale, "Data analysis for Photolithography," Proc. SPIE **3677,** 415-34, (1999).

Mack, Chris A., "Resolution and Depth of Focus in Optical Lithography," Proc. SPIE **3183**, 14-27, (1997).

Mack, Chris A., "Understanding Focus Effects in Submicrometer Optical Lithography: A Review," Optical Engineering **32(10)**, 2350-62, (1993).

Mack, Chris A., "Understanding Focus Effects in Submicron Optical Lithography: Part 3--Methods for Depth-of-Focus Improvement" Proc. SPIE **1674**, 272-84, (1992)

Conley, Will; Garza, Cesar M.; Dusa, Mircea V.; Socha, Robert J.; Bendik, Joseph J.; Mack, Chris A.; "The MEEF Shall Inherit the Earth," Proc. SPIE **4346,** 251-8, (2001).

Socha, Robert J.; Dusa, Mircea V.; Capodieci, Luigi; Finders, Jo; Chen, Jang Fung; Flagello, Donis G.; Cummings, Kevin D. "Forbidden Pitches for 130-nm Lithography and Below" Proc. SPIE **4000**,1140-55, (2000).

Chapter 3
Optimizing Resist Thickness using a CD Swing Curve

Objective

This workbook problem will explain how to analyze a CD swing curve to optimize the resist thickness used in a given process and to perform some basic analysis of the resist thickness choice.

Introduction

The propagation of light through resist-coated wafers in a stepper environment results in various thin film interference effects including standing waves. Another effect is the existence of swing curves. Generically, a swing curve is the sinusoidal variation of some lithographic parameter with resist thickness. There are several parameters that vary in this way, but the most important is the critical dimension (CD) of the photoresist feature being printed. Swing curves are extremely important in lithography because often it is difficult to control the thickness of the resist as it is coated over the topography of underlying layers. When the resist thickness varies, the feature CD will vary as well, which is undesirable for many reasons.

In this workbook chapter, you'll learn how to:

- Generate reflectivity and CD swing curves
- Interpret the positions along the CD swing curve
- Evaluate the impact of varying resist thickness once the nominal thickness has been selected

Theory

In this section, we will discuss the thin film interference effects that result in swing curves. The background material on thin film interference effects is covered in *Inside PROLITH.*

Generically, a swing curve is the sinusoidal variation of some lithographic parameter with changing resist thickness. There are several parameters that vary in this way, but the most important is the critical dimension (CD) of the photoresist feature being printed. Figure 1 shows a typical CD swing curve for *i*-line exposure of a 500 nm line on silicon. The change in linewidth is quite large (more than the typical 10% tolerance) for relatively small changes in resist thickness.

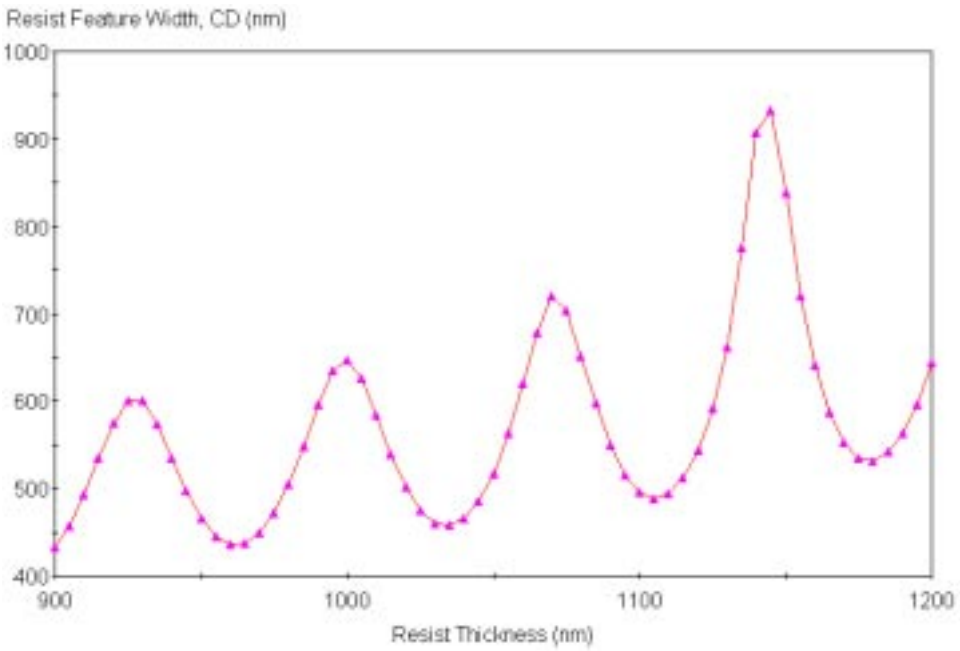

Figure 1: Typical CD swing curve for *i*-line exposure showing that the CD can vary significantly due to thin film interference effects.

Another swing curve is the dose-to-clear or E_0 swing curve, which shows the same sinusoidal swing as the CD swing curve. Figure 2 shows a typical E_0 swing curve using the same resist and stepper as Figure 1.

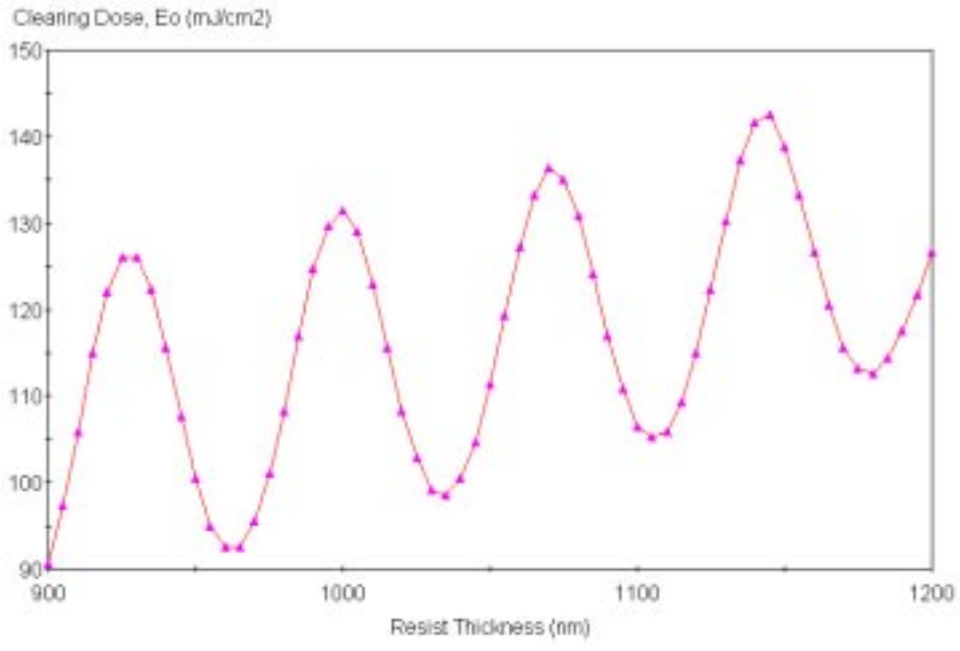

Figure 2: E_0 swing curve corresponding the CD swing curve above.

For a resist thickness that requires a higher dose-to-clear, the photoresist will also require a higher dose to achieve the desired line size. If the exposure dose is fixed (as it was for

the CD swing curve), the result will be an underexposed or over exposed line. Thus, it follows that the E_0 and CD swing curves result from the same effect. The final swing curve measures the reflectivity of the resist coated wafer as a function of resist thickness (Figure 3).

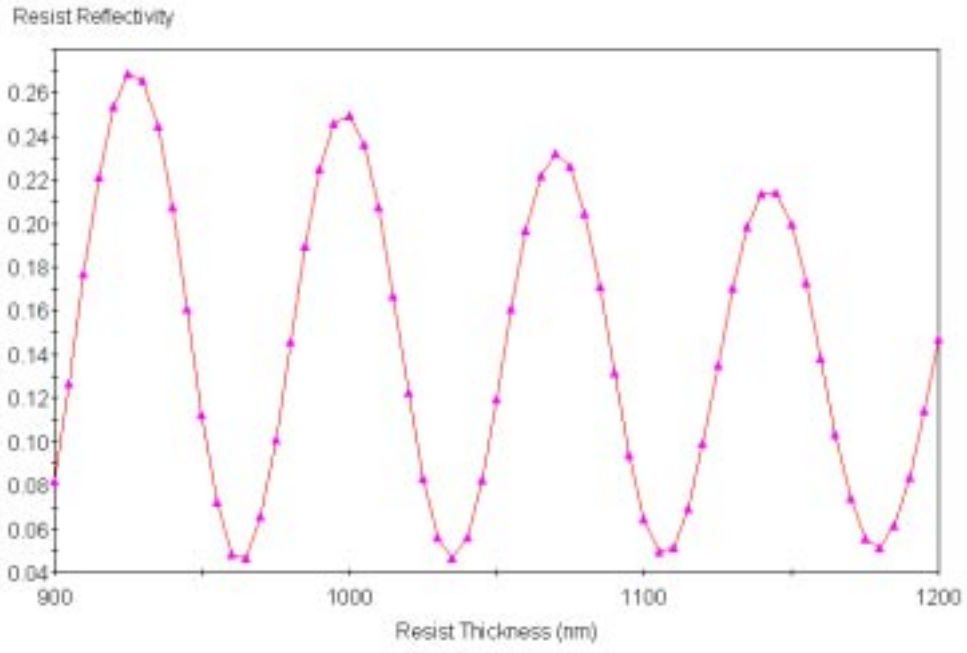

Figure 3: Reflectivity swing curve corresponding to the CD and E_0 swing curves above.

Although reflectivity is further removed from lithographic metrics such as E_o or CD, it is the reflectivity swing curve that provides the most insight into the origin of the phenomenon.

The reflectivity swing curve shows that variations in resist thickness result in a sinusoidal variation in the reflectivity of the resist coated wafer. Since the definition of reflectivity is the total reflected light intensity divided by the total incident intensity, an increase in reflectivity results in less light that makes it into the resist. Less light being coupled into the resist means that a higher dose is required to affect a certain chemical change in the resist, resulting in a larger E_o. Thus, the E_o and CD swing curves both originate from the reflectivity swing curve.

What causes the reflectivity swing curve of Figure 3? Of course, the answer lies in the thin film interference effects. Using the same simple geometry shown in Figure 4, a thin photoresist (layer 2) rests on a thick substrate (layer 3) in air (layer 1).

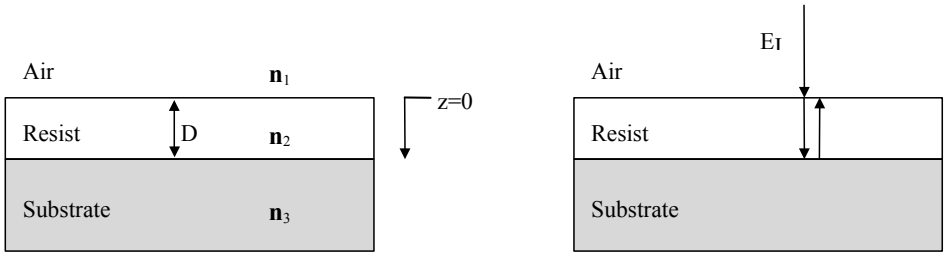

Figure 4: Diagram used to explain thin film interference effects. The diagram on the left defines the three layers: air (layer 1), resist (layer 2), and the substrate (layer 3). The diagram on the right shows "incoming" light within the resist interfering with light reflected off the resist-substrate interface.

Each material has optical properties governed by its complex index of refraction, $\boldsymbol{n} = n - i\kappa$ If we illuminate this film stack with a monochromatic plane wave normally incident on the resist, we can determine the standing wave intensity within the resist. However, our goal here is to determine the total light reflected by the film stack. As shown in Figure 4, the total reflected light is made up of the incident beam reflecting off the air-resist interface and beams that have bounced off of the substrate and then were transmitted by the air-resist interface.

Let's begin by writing an expression for the electric field of the ray which is directly reflected by the air-resist interface.

$$E_{r0} = \rho_{12} E_I \tag{1}$$

where E_I is the incident electric field and ρ_{12} is the reflection coefficient of the air-resist interface. The next "reflected" beam is transmitted into the resist, reflected off the substrate, and transmitted into the air. The result, denoted as E_{r1}, is given by

$$E_{r1} = T_{12} E_I \rho_{23} \tau_D^2 \tag{2}$$

where T_{12} is the transmittance of the air-resist interface ($= \tau_{12}\ \tau_{21}$), ρ_{23} is the reflection coefficient of the substrate, and τ_D is the internal transmittance of the resist. The next reflected beam makes two bounces inside the resist before being transmitted out, resulting in an additional $\rho_{21}\ \rho_{23}\ \tau_D^2$ term.

The total reflection coefficient can be computed by totaling up all the reflected electric fields and then dividing by the incident field.

$$\rho_{total} = \frac{\sum E_{ri}}{E_I} = \rho_{12} + \frac{T_{12}\rho_{23}\tau_D^2}{1 + \rho_{12}\rho_{23}\tau_D^2} = \frac{\rho_{12} + \rho_{23}\tau_D^2}{1 + \rho_{12}\rho_{23}\tau_D^2} \tag{3}$$

The reflectivity of the film stack is the square of the magnitude of the reflection coefficient. At first glance, the sinusoidal dependence of reflectivity with resist thickness is not obvious from equation (3). The dependence is contained in the internal transmittance:

$$\tau_D = e^{-i2\pi \boldsymbol{n}_2 D/\lambda} \tag{4}$$

where $\boldsymbol{n}_2$ is the complex index of refraction of the resist, λ is the wavelength, and D is the resist thickness. Carrying out the calculation of reflectivity is simplified for the case when ρ_{12} and ρ_{23} are real, giving

$$R = \frac{|\rho_{12}|^2 + |\rho_{23}|^2 e^{-\alpha 2D} + 2|\rho_{12}\rho_{23}|e^{-\alpha D}\cos(4\pi n_2 D/\lambda)}{1 + |\rho_{12}\rho_{23}|^2 e^{-\alpha 2D} + 2|\rho_{12}\rho_{23}|e^{-\alpha D}\cos(4\pi n_2 D/\lambda)} \tag{5}$$

where,

$\alpha = 4\pi\kappa_2/\lambda$ the resist absorption coefficient

κ_2 is the imaginary part of $\boldsymbol{n}_2$

The discussion so far has been mostly mathematical. Equation (3) gives a rigorous result which, when expressed as equation (5), leads to an understanding of the reflectivity swing curve. Physically, the reflectance swing curve is the result of interference among the reflected rays. As pictured in Figure 4, the total reflected field is the sum of the various rays. How the initially reflected ray E_{ro} adds to the first transmitted and reflected ray E_{r1} depends on the phase of E_{r1}, which in turn depends on the resist thickness. At some thickness E_{r1} will be in phase with E_{ro}, resulting in a maximum reflectivity. At another thickness E_{r1} will be out of phase with E_{ro}, resulting in a minimum reflectivity.

Equation (5) can also lead to a better understanding of swing curves. The period of all of the swing curves can be easily obtained from equation (5) and is the same as the period of the standing waves in the photoresist:

$$Period = \lambda / 2n_2 \tag{6}$$

Likewise, the effects of increasing or reducing the reflectivities can be seen. If the substrate is non-reflective ($\rho_{23} = 0$), the film stack reflectivity becomes constant. Thus, a bottom antireflection coating can reduce or eliminate the swing curve. Less obviously, if $\rho_{12} = 0$ the reflectivity will also become constant, eliminating the swing curve. This can be achieved by using a top antireflection coating. Physically, if the swing curve results from interference between E_{ro} and E_{r1}, eliminating E_{ro} will eliminate the interference and the swing. Finally, absorption in the resist will reduce the coefficients of the cosines in equation (5), reducing the swing curve as well.

Procedure

In PROLITH, set up the following input parameters. If a parameter is not listed, use the default value.

Numerics:

Image Model: High NA Scalar
Speed Factor: 5

Mask:

Mask Type: 1D Binary
Feature Type: Line
Nominal Feature Width: 250 nm
Pitch: 500 nm
Mask Bias: 0 nm

Imaging Tool:

Source Shape: Partially Coherent
Partial Coherence: 0.5
Wavelength: 248 nm
Numerical Aperture: 0.63

Filmstack/Resist:

Resist File: KrF Shipley UV5
Resist Thickness: 775 nm
Material Layer #2: Brewer ARC DUV18 55 nm
Substrate: Silicon

Exposure:

Exposure Energy: 14 mJ/cm^2

Post Exposure Bake:

PEB Time: 90 sec
PEB Temperature: 130 C

Run a custom simulation set. Select Resist Thickness as the input, setting the Min. to 650, the Max. to 800, and the Step to 2. Select the Reflectivity Group and Developer Group as the outputs. The simulation sets window is shown in Figure 5. Launch the simulation.

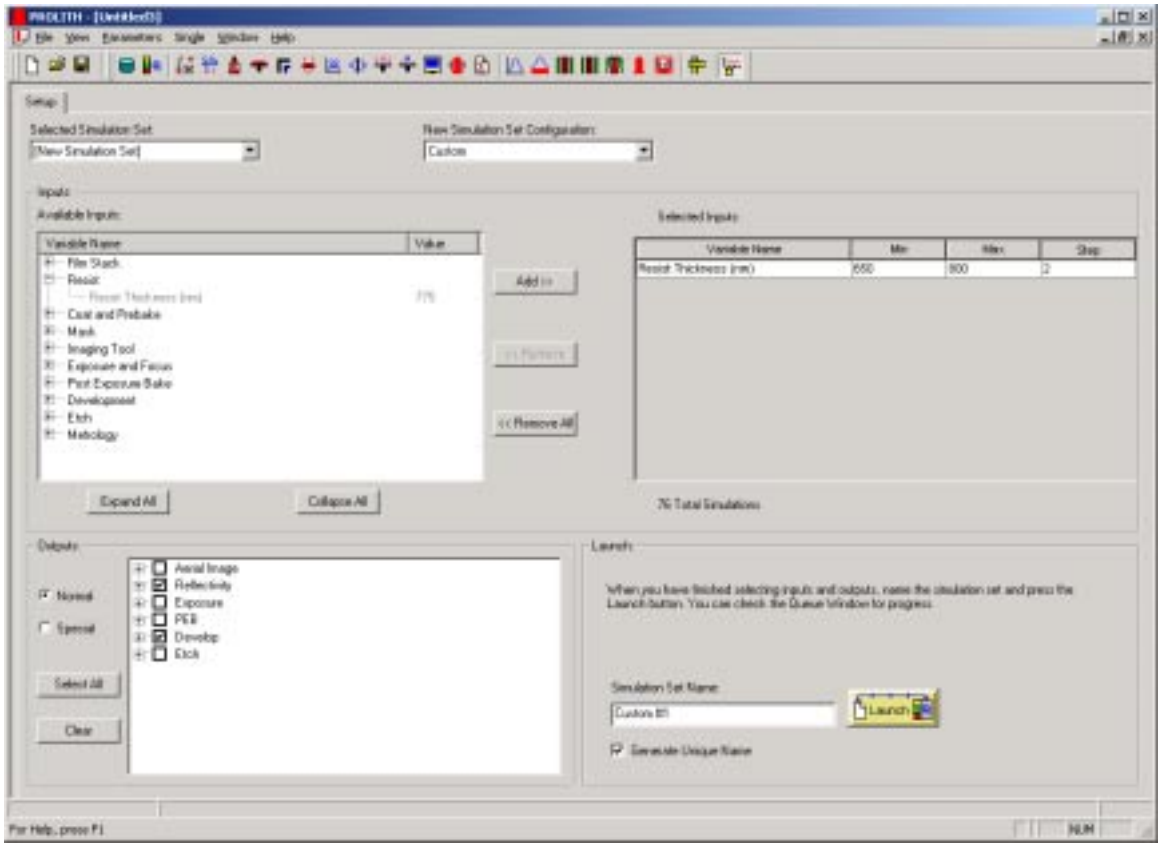

Figure 5: The simulation sets window configured for the simulation.

When the simulation is finished, select the results tab. The X-axis is the resist thickness. Change the Y-axis to Resist Reflectivity. Figure 6 shows the resultant graph.

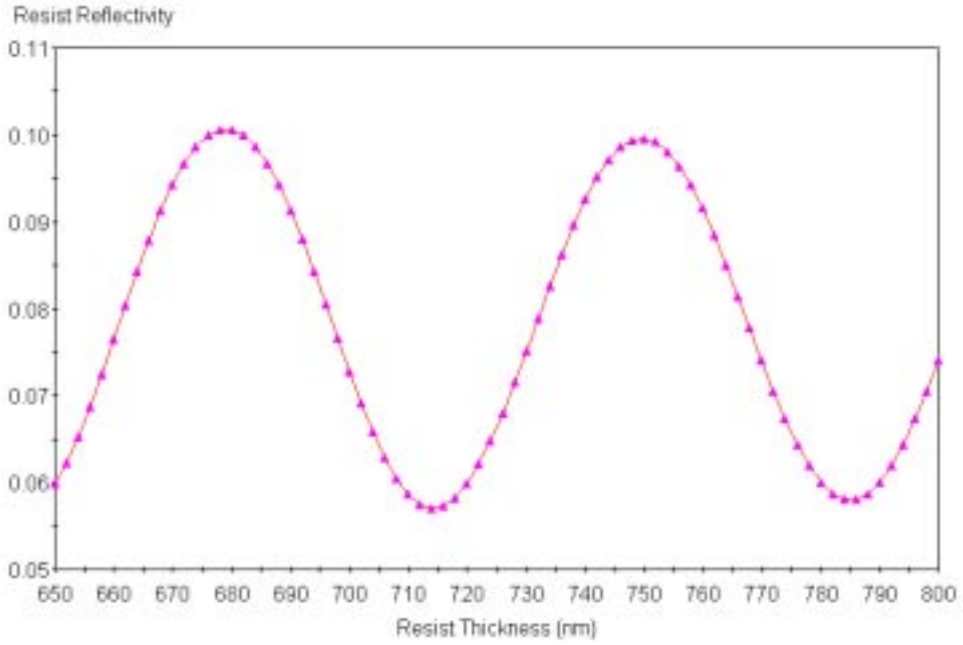

Figure 6: Resist reflectivity as a function of resist thickness.

Looking at the plot in Figure 6 note the horizontal location of the minima/maxima of the reflectivity swing curve. For example, if other process considerations limited the choice of resist thickness to the range 700-770 nm, there would be two such points: a minima at 714 nm and a maxima at 750 nm. Now, set the Y-axis of the graph to be Resist Feature Width. Figure 7 shows the expected output.

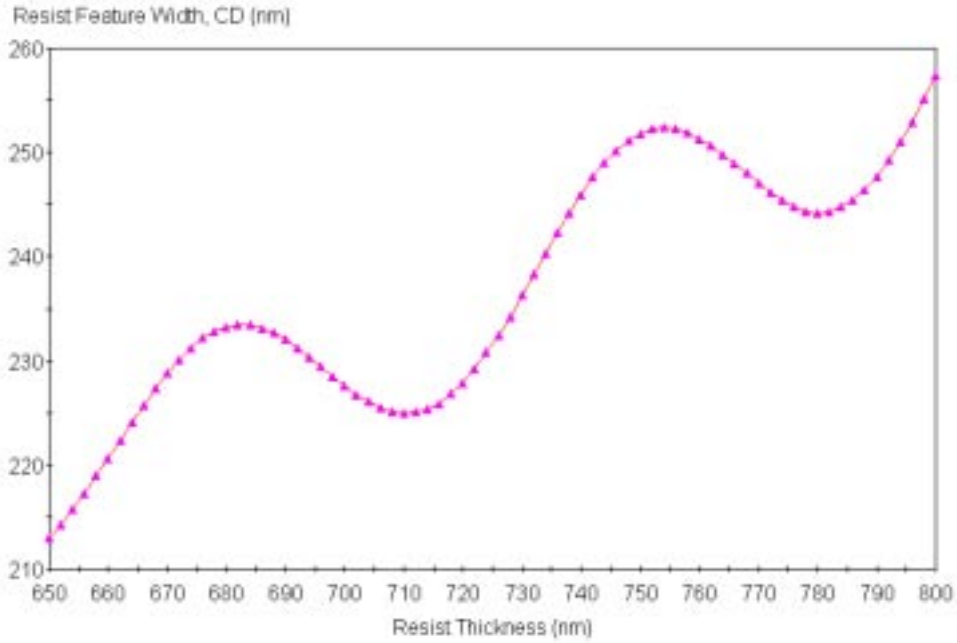

Figure 7: CD swing curve for 250 nm lines using UV5 resist model. You'll notice that the horizontal location of the minima for the CD swing curve closely match although not exactly those from the Reflectivity swing curve.

Using a resist thickness which corresponds with either a minima or a maxima on the CD swing curve provides a buffer to the slight errors in thickness that occur during the coat process. Consider three values that might be used as the nominal resist thickness: 710 nm, 732 nm and 754 nm. If 710 nm were chosen two observations can be made. First, if the actual resist thickness, due to variations in the resist deposition process, is less or more than the nominal by a small amount, the resultant CD will be larger than the expected CD. Second, for small changes in resist thickness (say, ±6 nm), the resultant change in CD is quite small. The same is true for the nominal choice of 754 nm except that any variations cause the feature to print smaller. In contrast, if 732 nm is chosen for the nominal thickness, the CD will be smaller or larger than expected depending on the variation in resist thickness and the relative CD change will be much larger. Let's quantify the results in Table 1. Shown is the variation of resist CD due to ± 6 nm resist thickness variations.

Nominal resist thickness	Change in resist CD caused by + 6 nm resist thickness variation	Change in resist CD caused by – 6 nm resist thickness variation	Total range in resist CD caused by ± 6 nm resist thickness variation
710 nm	1.2 nm	1.1 nm	1.2 nm
732 nm	6.0 nm	-6.0 nm	12 nm
754 nm	-0.7 nm	-1.0 nm	1.0 nm

Table 1: Resist CD values for cases where the resist thickness varies from possible nominal choices.

So, you can see that operating at a relative maxima or minima results in two advantages. First, variations in CD caused by resist non-uniformity are more predictable, and second, the variations are small. Now that we know that it is best to operate at local minima/maxima, which of the two should be chosen? That decision would be greatly influenced by the level of the device. If, for example, this is a poly gate level, it might be best to operate at a local minima since all variations in resist thickness will make the gate larger. [Larger gates may cause the device to be slower. Smaller gates might cause the device to fail due to increased leakage current.] If the level of interest is for contact holes or isolated spaces then the best choice is often the E_0 max location so that any variations in thickness result in larger contact holes or spaces and not in scumming of the resist features. Or for any level the E_0 min location may be chosen to increase the stepper throughput.

Summary

The resist CD swing curve's cyclical nature is controlled by the reflections of light at the air-resist and the resist-substrate boundaries. Defining a resist process where the chosen resist thickness is at a minima or maxima of the CD or reflectivity swing curve makes the process less sensitive to slight changes in resist thickness that can occur. The specific minima chosen is dependent on the limits of the coat process, subsequent etch requirements, and possibly a desired exposure energy.

Questions

See Appendix A for answers.

1. If a gate level process was implemented using the UV5 data shown in the examples and a coating uniformity of ± 3.0 nm, how much across-wafer CD uniformity would one expect to lose operating at 732 nm thickness compared to 754 nm?
2. For resist lines the CD swing curves and E0 swing curves have the same phase (CD_{max} and E_0 max appear at roughly the same thickness). What major difference would you expect for the swing curve behavior of contact holes or spaces?

3. For the resist CD swing curves of a line shown for UV5 the general trend is for the CD to increase as the thickness increases from one CD min or CD max to the next. There is an overall upwards slope as well as a sinusoidal swing. What resist parameter may be causing this trend (see equation 5)? Vary this parameter and repeat the swing curve experiment. What is the result?

Further Information

For further information, see *Inside PROLITH* Chapter 3 pages 38-47 for an in-depth discussion of the theory of standing waves and film stack reflectivity. Also, Workbook Chapter 4 provides additional information on optimizing a bottom anti-reflection coating.

Chapter 4
Optimizing a Bottom Antireflective Coating

Objective

This workbook problem will show how to optimize the thickness of a bottom antireflection coating (BARC) to minimize standing waves and resist thickness swing effects. The simple case of a single layer BARC will be addressed.

Introduction

Thin film interference effects are observed in optical lithography and can have a significant impact on lithographic quality. One of the main effects is the existence of standing waves in the resist. These standing waves are created when various transmitted and reflected electric field components interfere. The standing waves can cause a severe ripple in the resist profile that is undesirable. Standing waves also lead to CD variations (swings) with resist thickness. There are a few common ways to reduce standing waves and swing curves including the use of a bottom anti-reflective coating or BARC.

In this workbook chapter, you'll learn how to:

- Simulate the standing waves in the absence of a BARC
- Evaluate the substrate reflectivity and determine possible BARC thickness values
- Evaluate the reduction in standing waves due to inclusion of a BARC

Theory

When a thin dielectric film placed between two semi-infinite media (e.g., a thin coating on a thick substrate in air) is exposed to monochromatic light, standing waves are produced in the film. This section presents an analytical expression for the standing wave intensity within a thin film.

Consider a thin film of thickness D and complex index of refraction $\boldsymbol{n}_2$ deposited on a thick substrate with complex index of refraction $\boldsymbol{n}_3$ in an ambient environment of index $\boldsymbol{n}_1$, as shown in Figure 1.

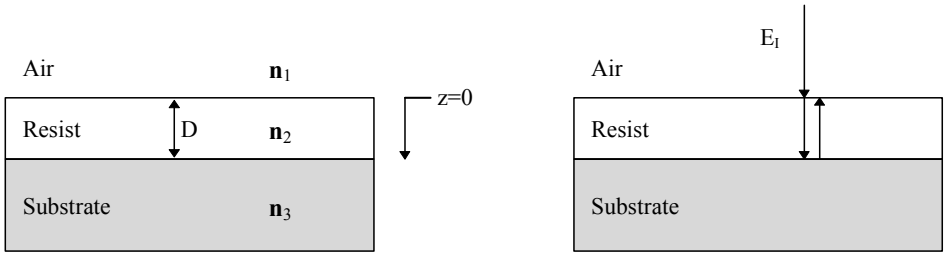

Figure 1: Geometry for standing wave calculation.

An electromagnetic plane wave is normally incident on this film. Let E_1, E_2, and E_3 be the electric fields in the ambient, thin film, and substrate, respectively. Assuming monochromatic illumination by a normally incident plane wave, the electric field in each region is a plane wave or the sum of two plane waves traveling in opposite directions (i.e., a standing wave). Maxwell's equations require certain boundary conditions to be met at each interface: specifically, E_j and the magnetic field H_j are continuous across the boundaries $z = 0$ and $z = D$. Solving the resulting equations simultaneously, the electric field in region 2 can be shown to be

$$E_2(x,y,z) = E_1(x,y)\frac{\tau_{12}\left(e^{-i2\pi n_2 z/\lambda} + \rho_{23}\tau_D^2 e^{i2\pi n_2 z/\lambda}\right)}{1+\rho_{12}\rho_{23}\tau_D^2} \qquad (1)$$

where,

$E_1(x,y)$ = the incident plane wave at $z = 0$,

$\rho_{ij} = (n_i - n_j)/(n_i + n_j)$, the reflection coefficient,

$\tau_{ij} = 2n_i/(n_i + n_j)$, the transmission coefficient,

$\tau_D = \exp(-ik_2 D)$, the internal transmittance of the film,

$k_j = 2\pi n_j/\lambda$, the propagation constant,

$n_j = n_j - i\kappa_j$, the complex index of refraction, and

λ = vacuum wavelength of the incident light.

Equation 1 is the basic standing wave expression where film 2 represents the photoresist.

Although we have determined an expression for the standing wave electric field, it is the intensity of the light which causes exposure. Squaring the magnitude of the electric field gives the standing wave intensity. Calculation of intensity from Equation 1 leads to a fairly messy result, but some simplifications allow for a reasonably useful form by assuming that the imaginary part of ρ_{12} is small:

$$I(z) \approx \left(e^{-\alpha z} + \left|\rho_{23}\right|^2 e^{-\alpha(2D-z)} \right) - 2\left|\rho_{23}\right| e^{-\alpha D} \cos(4\pi n_2 (D-z)/\lambda + \phi_{23}) \qquad (2)$$

where,

$\alpha = 4\pi\kappa_2/\lambda$ the resist absorption coefficient

κ_2 is the imaginary part of $\boldsymbol{n}_2$

ϕ_{23} is the phase of ρ_{23}

This equation is graphed in Figure 2 for a photoresist with typical properties on a silicon dioxide substrate.

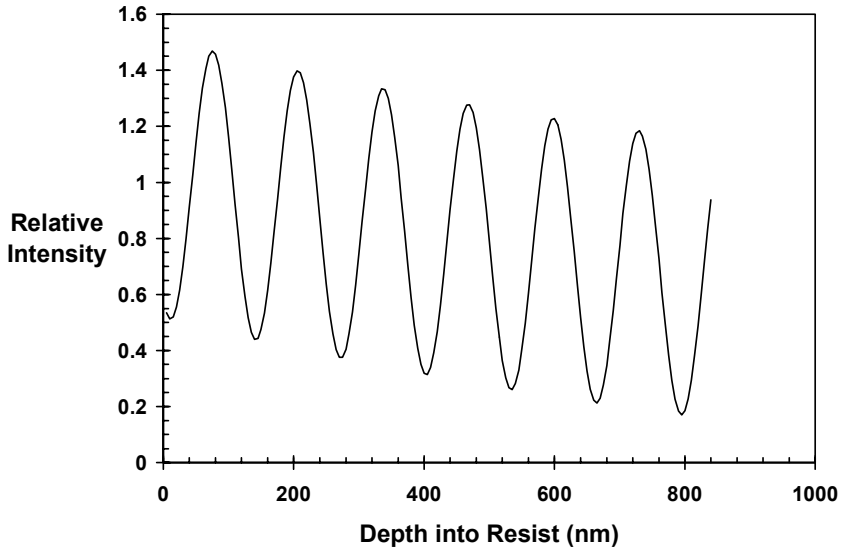

Figure 2. Standing wave intensity for 436 nm wavelength light in 850 nm of photoresist on a SiO_2/Si substrate.

By comparing the equation to the graph, many important aspects of the standing wave effect become apparent. The most striking feature of the standing wave plot is its sinusoidal variation. The cosine term in Equation 2 shows that the period of the standing wave is given by

$$Period = \lambda / 2n_2 \qquad (3)$$

The amplitude of the standing waves is given by the multiplier of the cosine in Equation 2. It is quite apparent that there are two ways to reduce the amplitude of the standing wave intensity. The first is to reduce the reflectivity of the substrate (reduce ρ_{23}). Of course, the use of a BARC is one of the most common methods of reducing standing waves. The second method for reducing the standing wave intensity that Equation 2 suggests is to increase absorption in the resist (reduce the $e^{-\alpha D}$ term). This is accomplished by adding a dye to the photoresist (increasing α). We will pursue the first

method in this workbook example by using PROLITH to design a BARC to minimize standing waves in the resist.

Procedure

To see how you can optimize a BARC, start by opening a default document in PROLITH. Select the *Image in Resist* output view. The output plot, shown in Figure 3, now shows the aerial image intensity contours both vertically and horizontally in the resist. As you go from top to bottom in the bright field region (outside edge) the intensity varies from high (red) to low (blue) intensity ~ 9 times. These are the standing waves within the resist.

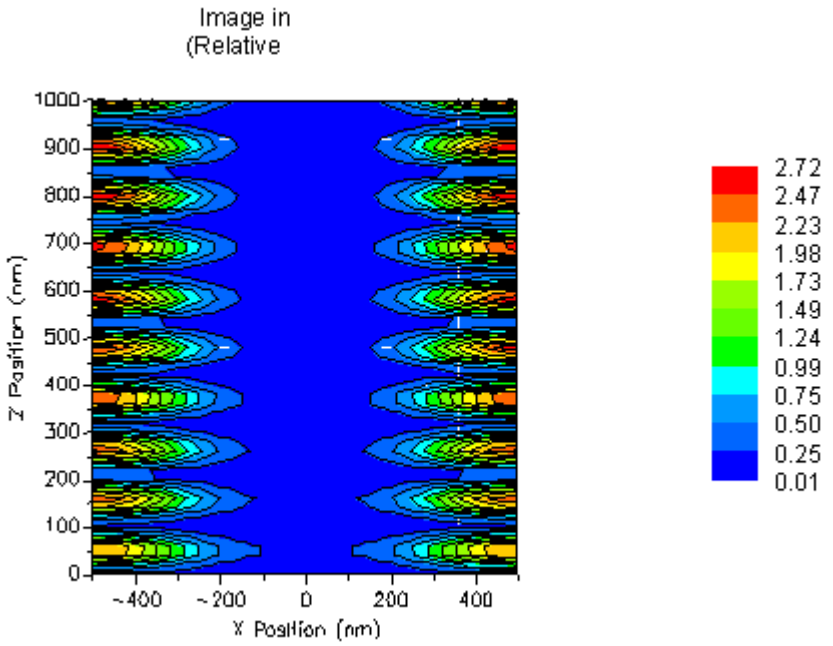

Figure 3: Standing waves within the resist film for exposure on reflective substrates.

Now, display the resist profile (Figure 4a). Notice that the Post Exposure Bake (PEB) process has eliminated the standing waves by thermal diffusion. Shorten the PEB time to only ten seconds and show the final *Resist Profile* (Figure 4b). Although PEB can be used to reduce or remove the standing waves, there are other wave interference effects that remain. This can be seen by simulating a *CD swing curve* using the existing conditions, as shown in Figure 5. The resulting swing in resist CD as a function of resist thickness is an effect of the reflectivity change with resist thickness. Both issues can be solved by using a BARC layer.

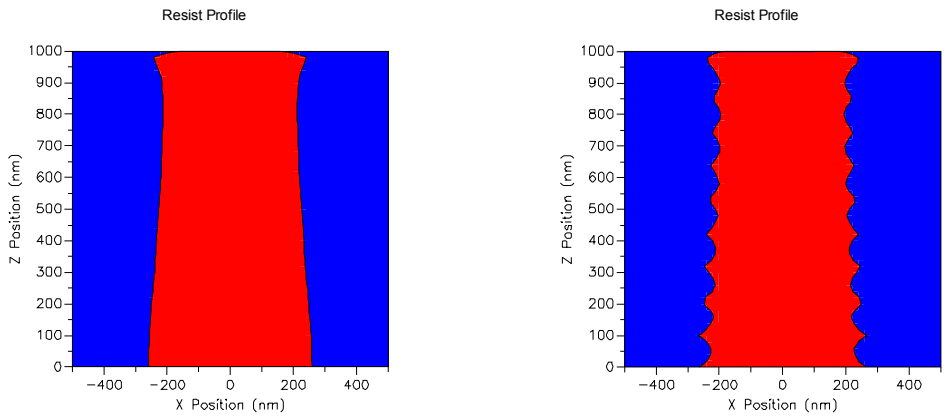

Figure 4: Resist Profile with long PEB time (left) and short PEB time (right).

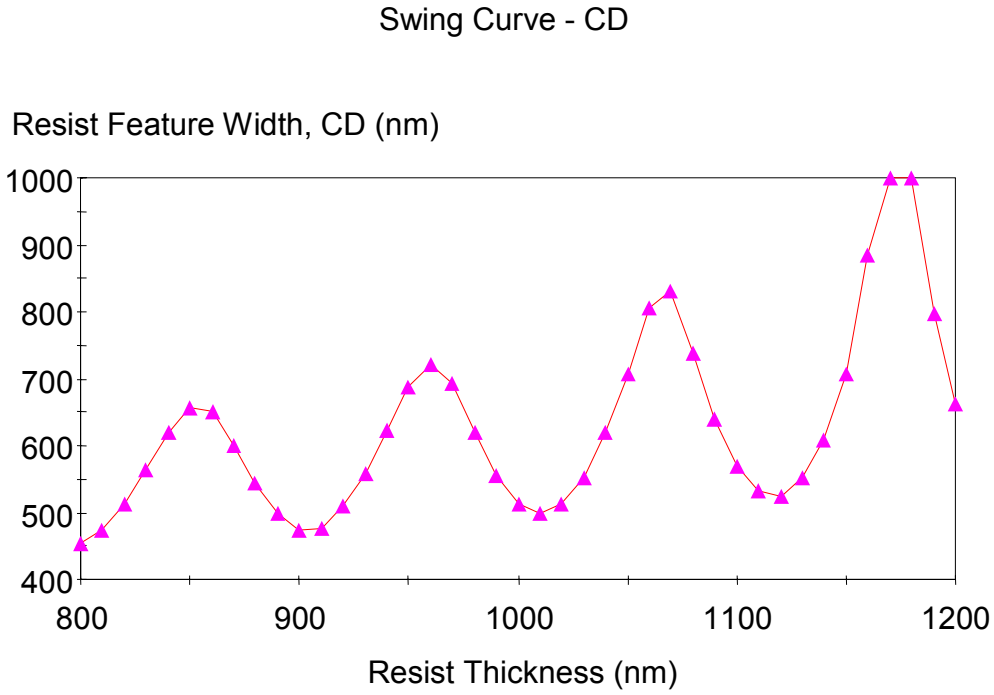

Figure 5: Resist CD swing curve when no BARC is used.

As mentioned earlier, the thickness of an existing BARC material is most easily optimized by minimizing the substrate reflectivity. Using PROLITH, the substrate reflectivity can be minimized as a function of BARC thickness using a custom simulation set. Change the following parameters in the PROLITH document:

Film stack:

Layer #1: SPR 500, Thickness = 1000 nm
Layer #2: AZ BARLi Thickness = 100 nm
Substrate: Silicon

From the Simulation Set Setup page, select *Custom* simulation and add *Film Stack*/*AZ BARLi*/*thickness layer #2* as a custom simulation input. Set the *Min, Max* and *Step* values for the Layer #2 thickness to 0.0, 250.0 and 5.0 nm respectively. Now select the *Reflectivity Output Group* and start the simulation set calculation by clicking the *Launch* button. In the results view, select *Substrate Reflectivity* for the Y-axis. The results are shown in Figure 6. Across this range of BARLi thicknesses there are two minima for substrate reflectivity: one near 90 nm thickness and the other near 195 nm. The 195 nm BARLi thickness has the lowest substrate reflectivity and will be the optimal BARC thickness in this range.

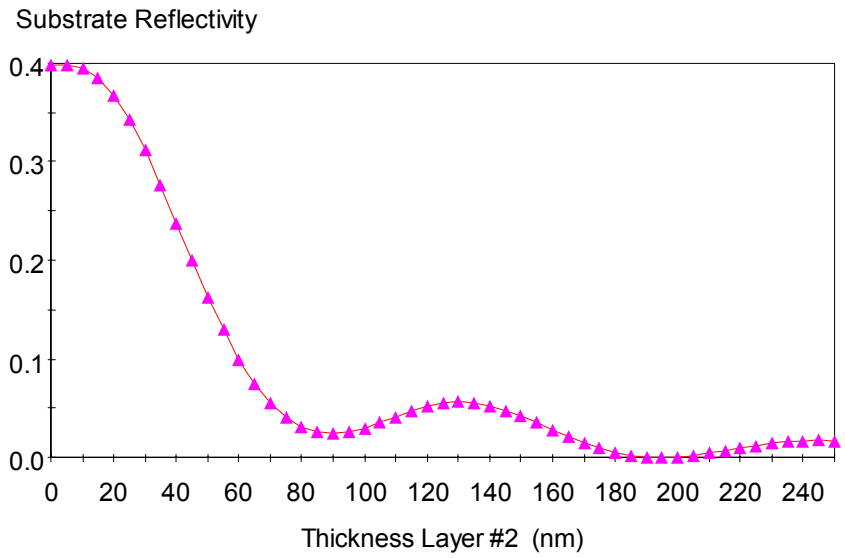

Figure 6: Substrate reflectivity as a function of BARC thickness.

The improved CD swing curve performance can be observed by setting the Layer # 2 thickness to 195 nm under the Film Stack input view and rerunning the CD Swing Curve simulation set. A better picture of the improvement gained is to plot both "with BARC" and "without BARC" swing curve data on the same graph. This can also be performed from the *Custom* simulation set window.

Clear all inputs from the custom simulation window. Setup a new custom simulation set. Select Thickness Layer #2 as an input. Change the *Min, Max* and *Step* values to 0.0, 195.0 and 97.5 nm respectively. This will simulate "no ARC" a mediocre ARC and the optimal ARC case. Add the *Film Stack/Resist/Thickness* as a custom simulation input. Set the *Min, Max* and *Step* values for the resist thickness to 800, 1200 and 10 nm respectively. Now select *Develop Group* as the output. When the simulation is completed, the results are best viewed as a *Multi-Line Graph* with Resist Thickness on the X Axis, Resist Feature Width on the Y Axis and Thickness Layer #2 on the Z axis. The result shown in Figure 7 demonstrates the complete reduction of the CD swing as the BARC thickness is optimized.

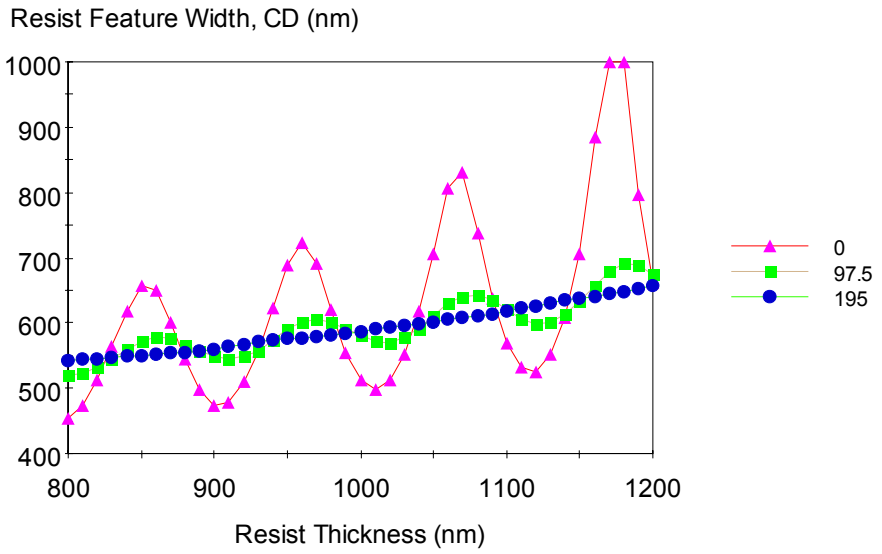

Figure 7: CD swing curve with optimal (195 nm), mediocre (97.5 nm) and zero BARC thickness.

Next, go to the film stack input view, and choose the BARC thickness as the optimized value, 195 nm. Calculate the standing wave intensity by clicking on the image in resist output view icon. The resulting graph is shown in Figure 8.

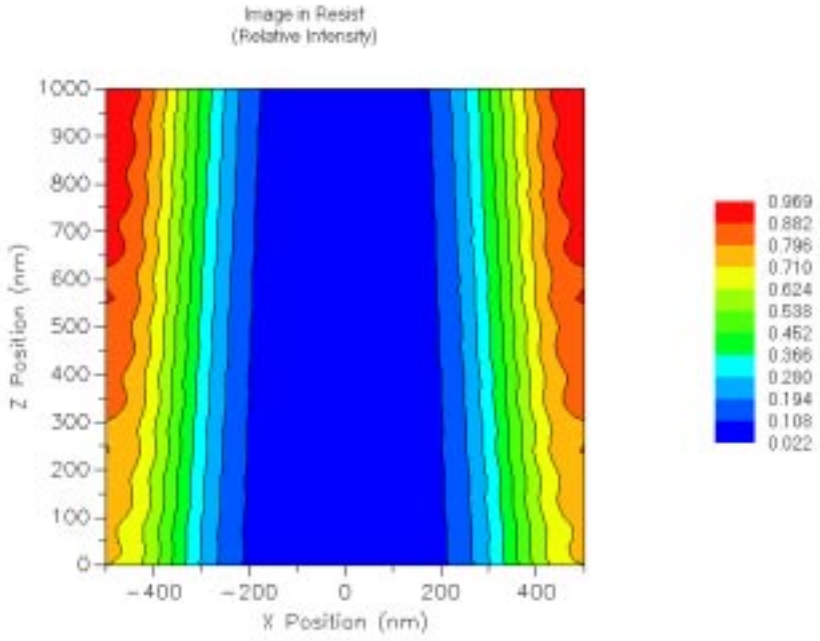

Figure 8: Image in Resist with the optimized BARC.

Here we see that the standing waves have been greatly reduced, as compared with the result without a BARC, shown in Figure 3. If the PEB time is reduced to 10 seconds, the

resulting resist profile is free of standing waves, as shown in Figure 9. Contrast this result with the profile shown in Figure 4b. Reducing standing waves with a BARC is especially important for chemically amplified resists, where the PEB process cannot be easily modified without changing the thermal dose.

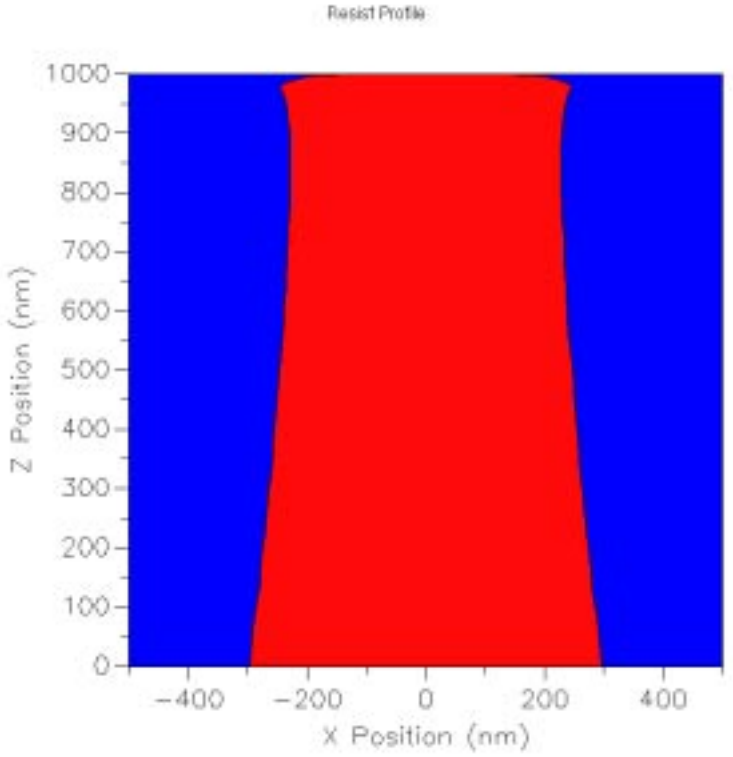

Figure 9: Resist profile for a short PEB time and an optimized BARC.

Summary

In this chapter we have seen that an optimal BARC thickness can be chosen based on the substrate reflectivity. An optical BARC thickness will reduce the standing wave effects and the swing curve, and remove the need for diffusion at the post-exposure bake step.

Questions

See Appendix A for answers.

1. In this workbook example, we optimized the BARC thickness based on the "Substrate Reflectivity". We made this choice because the amplitude of the standing waves depends on the reflectivity of the resist-substrate interface, as outlined in the theory section. However, it is very common to measure the reflectivity of uncoated wafers. PROLITH can simulate the reflectivity of a BARC coated wafer without photoresist by selecting the resist to be "Air". Go to the film stack view, change the resist to "Air", and repeat the reflectivity calculation as a function of BARC thickness. Compare your results with Figure 9. Are the "optimal" BARC thicknesses the same?

2. Use the “Optimal” BARC thickness determined in Question 1 with the “Air” resist. Change the resist back to “SPR500” and calculate an Image in Resist and a CD swing curve. How do your results compare to Figures 7 and 8?

Further information

For further information, see Inside PROLITH Chapter 3 pages 38-47 for an in-depth discussion of the theory of standing waves and film stack reflectivity.

Chapter 5
Optimizing a Film Stack for Reflectivity Control

Objective

This workbook problem will show how to optimize a complex film stack to control reflectivities that lead to process variations (CD swing). First a single film antireflection coating (ARC) with variable optical parameters will be optimized. Then a multiple layer ARC will be optimized to correct for topographic thickness variations.

Introduction

Film thickness variations lead to variations (swings) in the observed resist CD across a wafer. This resist CD swing is caused by thin film interference effects, which alter the resist and substrate reflectivity as a function of thickness. Either resist or substrate thickness variations can produce large CD swing. To minimize the CD variations across a wafer, the reflectivity from both the substrate and the resist must be controlled. Unfortunately, the film thickness of both resist and substrate layers often can not be maintained simultaneously as is the case when coating over topography. A bottom ARC (or BARC) between the resist and substrate is sometimes used to maintain reflectivity control (and CD stability). Chapter 4 "Optimizing a Bottom Antireflective Coating" covered the basics of choosing the thickness of a single layer BARC material with fixed optical properties.

In this workbook chapter, you'll learn how to:

- Evaluate a film stack for substrate reflection control and resist swing.
- Choose the optimal optical properties for a variable inorganic ARC.
- Choose the optimal thickness values for a multiple layer substrate coated over topography.

Theory

The variability in film thickness in semiconductor processing can originate from several sources. First the resist coating process can be non-uniform as a result of poor setup conditions. This situation is often correctable by adjusting the exhaust rate and spin chuck acceleration rate for the coating process. Coating uniformities of less then 3 nm are easily achievable on planar substrates. The most common source of film thickness variations is the inevitable nature of coating over a growing topography as the device is manufactured. This is illustrated in Figure 1 where the resist is coated over a gate and

dielectric structure. The resist thickness varies from d_{min} over the gate to d_{max}. When imaging contact holes over both the poly and the active area a swing effect results. This is illustrated in Figure 2.

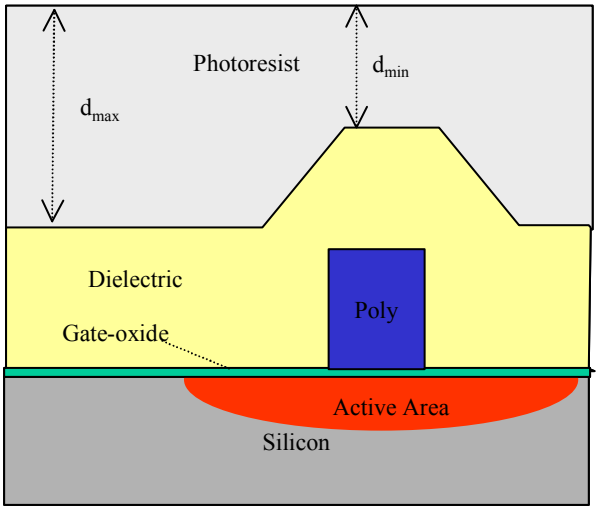

Figure 1: Schematic of resist thickness non-uniformity for resist coated over topography.

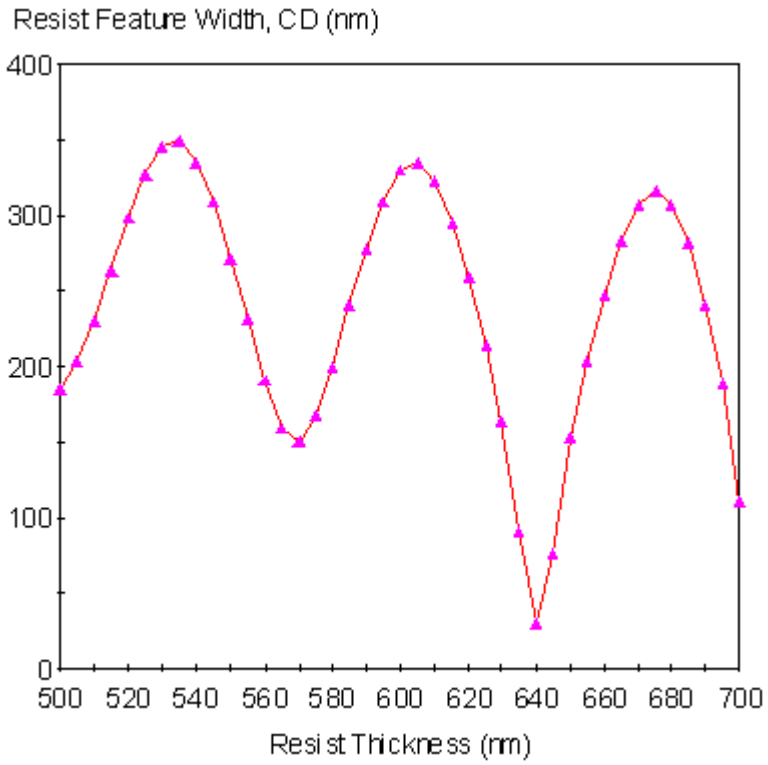

Figure 2. UV 6 resist CD swing for contact holes.

As discussed in Chapter 4, the use of a BARC will help eliminate this CD swing. For spin-on organic BARCs the optical constants are essentially fixed (determined when the BARC was designed by the supplier). The end user can change only the desired

thickness to achieve the best performance. A second approach is to use chemical vapor deposited (CVD) inorganic films as BARC materials.

Inorganic films can be coated using a chemical vapor deposition (CVD) process. By adjusting the process conditions the optical (and other) properties of the film can be modified. This is most certainly true for non-stoichiometric films, which are blends or "alloys" of two or more materials. One material of this type, which is often used as a BARC material, is SiO_xN_y. SiO_xN_y is a combination of silicon nitride (SiN) and silicon dioxide (SiO_2). SiO_2 is transparent and SiN is very absorbing at wavelengths below 300 nm. The optical properties of the combined material depend upon how much oxygen and nitrogen are included in the deposited film. Many deposition process parameters control this chemical composition and hence the optical properties of SiO_xN_y. An example is shown in Figure 3 and Table 1. Here the flow rate of one deposition gas (N_2O) is adjusted to yield five different materials. The optical constants at 248 nm were measured and are given in the table and plotted in Figure 3. Many control parameters other than the N_2O flow rate are responsible for the resulting optical properties and the values shown represent only a typical result.

Process #	Flow (sccm)	n	k
1	250	1.73	0.23
2	200	1.82	0.31
3	150	1.94	0.48
4	100	1.96	0.68
5	50	1.89	0.92

Table 1: The refractive index values for SiO_xN_y deposited as a function of N_2O flow rate.

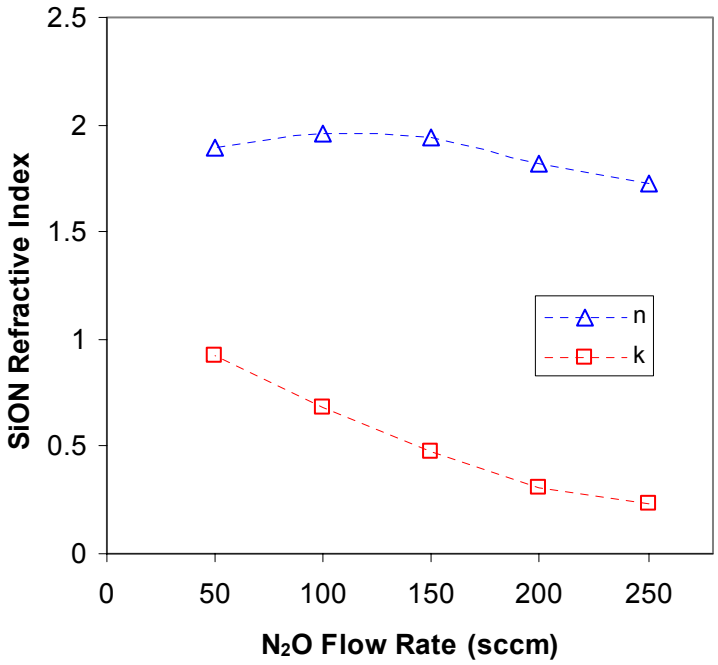

Figure 3: The refractive index of deposited SiO_xN_y as a function of N_2O flow rate

To minimize resist CD swing effects the substrate reflectivity should be as small as possible. The substrate reflectivity is defined as the total fraction of reflected light at the resist/substrate interface. This quantity is impossible to measure but is easy to simulate. A good specification for substrate reflectivity is $\leq$1% (the lower the better). Figure 4 shows a simulation of the substrate reflectivity as a function of SiON thickness and the imaginary refractive index of the SiON material. This simulation assumed a real refractive index of 1.85 (middle of range in Table 1) and a film stack consisting of UV6/SiOxNy/Si. The dark blue areas have acceptable substrate reflectivity below 1%. Two such regions exist: thickness 40 nm, k = 0.64 and thickness = 105 nm, k = 0.38. The choice of which region to use will depend upon other considerations such as the etch requirements. A more detailed evaluation procedure will be demonstrated in the Procedure section below.

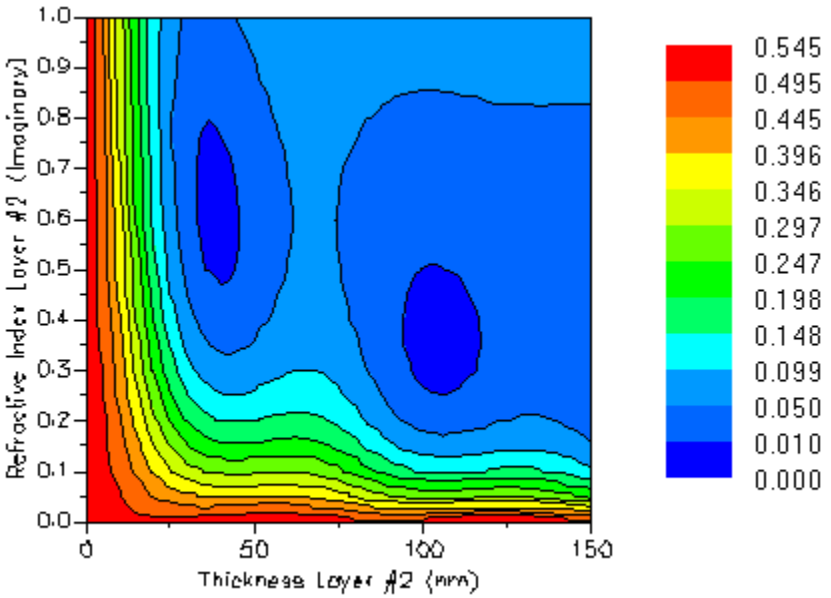

Figure 4: Substrate reflectivity contours for SiON as a function of thickness and imaginary refractive index.

For planarization processes (CMP) the surface under the resist is fairly flat and the resist film thickness will be fairly constant. However, swing curve effects still exist. The planarizing layer under the resist has a varying thickness and this film can induces a CD variation across the wafer. This situation is illustrated in Figure 5 where the resist is coated over a planarizing oxide layer. The resist thickness is constant but the oxide thickness varies from d_{min} over the gate to d_{max}. As before swing curve effects must be considered when imaging this layer. Now two swing curve effects are important: the variation in the resist CD as a function of the oxide thickness, and the variation of the resist CD with resist thickness. The resist CD swing with changing oxide thickness is shown in Figure 6. Here the resist thickness was fixed at 630 nm and the oxide thickness was varied from 400 to 600 nm representing a 200 nm thick polysilicon gate. The swing observed is larger for variation in oxide thickness than that observed for resist thickness variation shown in Figure 2. By choosing an appropriate BARC material to place between the resist and the varying oxide layer both swing curve effects can be reduced. A sample solution is shown in the procedure section below.

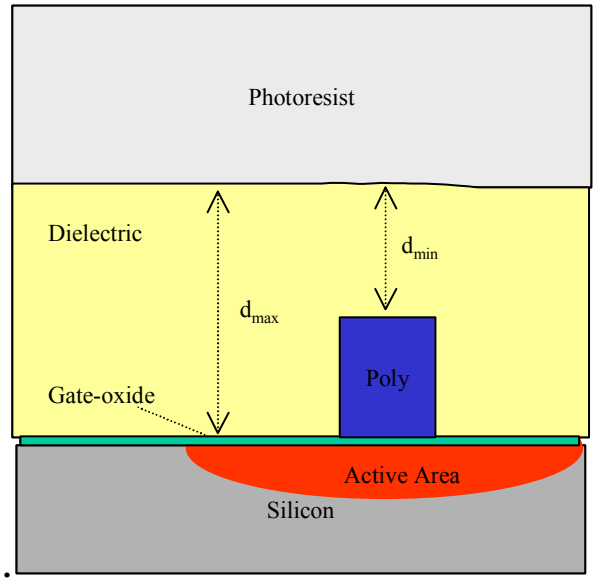

Figure 5: Schematic of oxide thickness non-uniformity for resist coated over a CMP wafer.

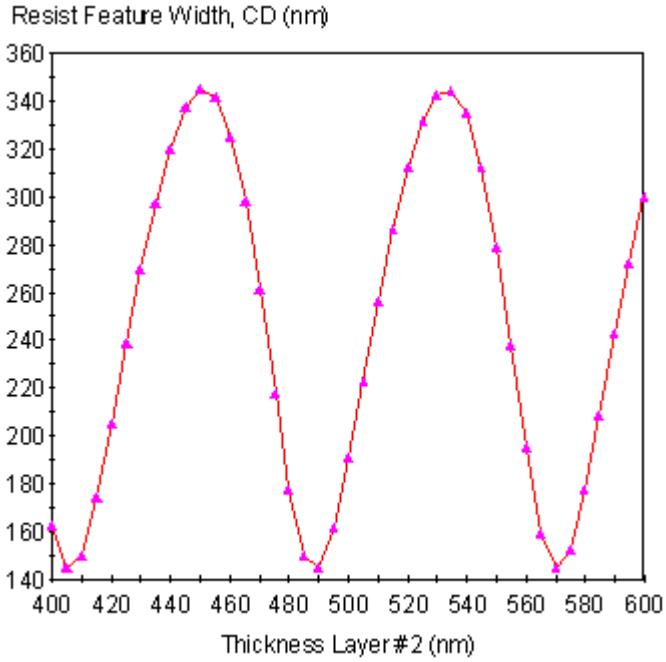

Figure 6. UV 6 resist CD swing as a function of oxide thickness for contact holes and no BARC.

Procedure

First an optimization of both the optical constants and the thickness of a single BARC material will be discussed. The sample case will be based upon the SiO_xN_y deposition processes resulting in the range of optical values given in Table 1. First generate a material file that is a reasonable starting point for the SiO_xN_y material. The n values shown in Table 1 vary slowly with an average of 1.868. The k values vary more rapidly,

with an average of 0.524. Use a text editor to build a simple material file containing the average optical properties as follows

```
[Version]
7.0
[Parameters]
SiOxNy-temp
;data in wavelength (nm), n, k
[Data]
248.0          1.868          0.524
```

Save the file as "SiOxNy-temp.mat" on your desktop (a copy has been provided). Then open PROLITH. Drag the SiOxNy-temp.mat file into the PROLITH window to add the file to the database. Then in a new PROLITH document set up the following input parameters:

Numerics:

Image Model: High NA Scalar
Speed Factor: 5

Mask:

Mask Type: 1D Binary
Feature Type: Contact
Nominal Feature Width: 275 nm
Pitch: 600 nm

Imaging Tool:

Source Shape: Annular
Outer Sigma: 0.8
Inner Sigma: 0.4
Wavelength: 248 nm
Numerical Aperture: 0.63

Filmstack/Resist:

Resist File: KrF Shipley UV6
Resist Thickness: 630 nm
Material Layer #2: SiOxNy-temp 60 nm
Material Layer #3: Silicon Dioxide 400 nm
Substrate: Silicon

Exposure:

Exposure Energy: 12.0 mJ/cm^2
Focus = -0.1 μm

Post Exposure Bake:

PEB Time: 90 sec
PEB Temperature: 135 C

Perform a single run and verify that the resist is printing close to sizing with this condition. Go to the *Simulation Sets* view and add *Refractive Index Layer #2 (Imaginary)* min = 0.0, max= 1.0 , step = 0.05. Add *Thickness Layer #2* min = 0.0, max = 150, step = 5. Select the *Reflectivity* output group and click the *Launch* Button. When the simulation is completed go to the output view and select contour plot as the graph type. Set the *X axis* variable as *Thickness Layer #2*, and The *Z Axis* variable as *Substrate Reflectivity*. The default contour plot only shows 10 contours. To add a 1% contour level, right click any place on the graph. A graph setup page should appear. Click the *Levels* tab and *Add* a contour. Enter 0.01 as the new contour level. This contour will define the 1% substrate reflectivity areas for the SiO_xN_y BARC. To remove the grid lines select the *Chart Group* Tab and turn off the *IsMeshed* and *IsShaded* options. The graph should now appear as follows.

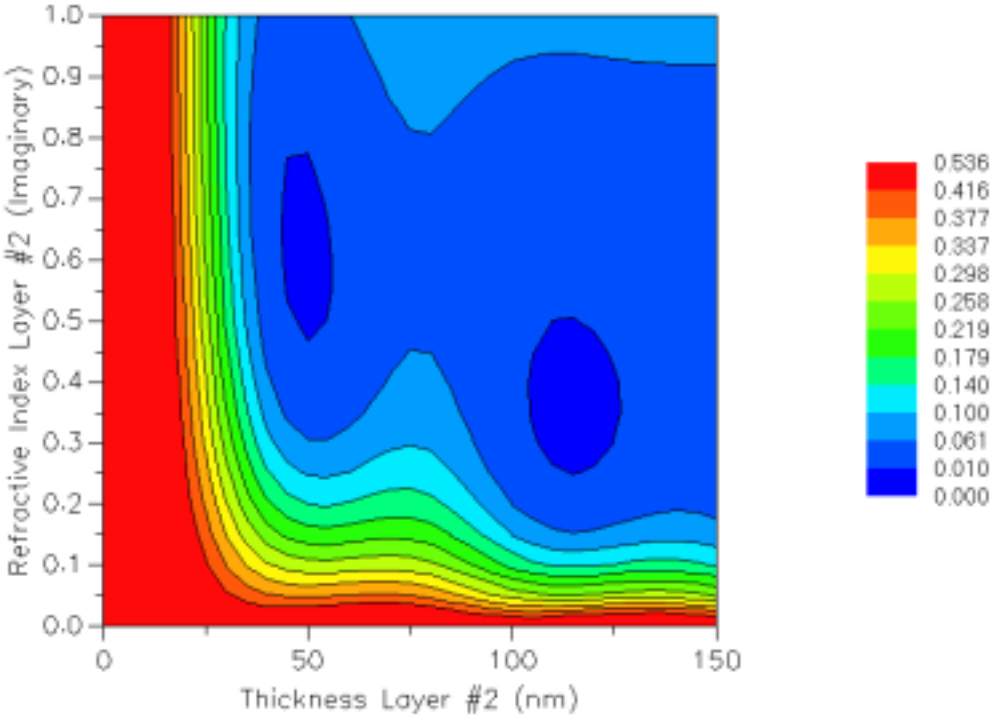

Figure 7: Substrate reflectivity contours for SiON as a function of thickness and imaginary refractive index.

Note the location of the two regions of ideal substrate reflectivity. These areas are centered at imaginary refractive index values: k=0.35 and k=0.60.

From Table 1 the lower k value corresponds to a process conditions of ~175 sccm N_2O flow rate and a corresponding n value of approximately 1.85. So, using the same procedure as before, create a second material file called SiOxNy.mat using the n and k values of 1.85 and 0.35, respectively. Now, we will determine the quality of this new SiO_xN_y film that has just been created. Drag the SiOxNy.mat file into PROLITH and use it to replace the SiOxNy-temp entry in the film stack. Set the thickness to 60 nm as before. Then, set up another simulation set with SiO_xN_y thickness and resist thickness as inputs. Set the SiO_xN_y thickness *min* value to 105, the *max* to 125 and the *step* as 10 nm. Set the resist *min*, *max* and *step* to 500, 700, 5 nm. Select the *develop* output group

and *Launch*. In the output view change the graph type to *MultiLine Plot* and select the *X Axis* parameter to be the *Resist Thickness*. The graph should now display the resist swing curve for three ARC thickness values (105, 115, and 125 nm) The ARC thickness of 115 nm shows the lowest swing which matches the substrate reflectivity minimum point shown in Figure 7.

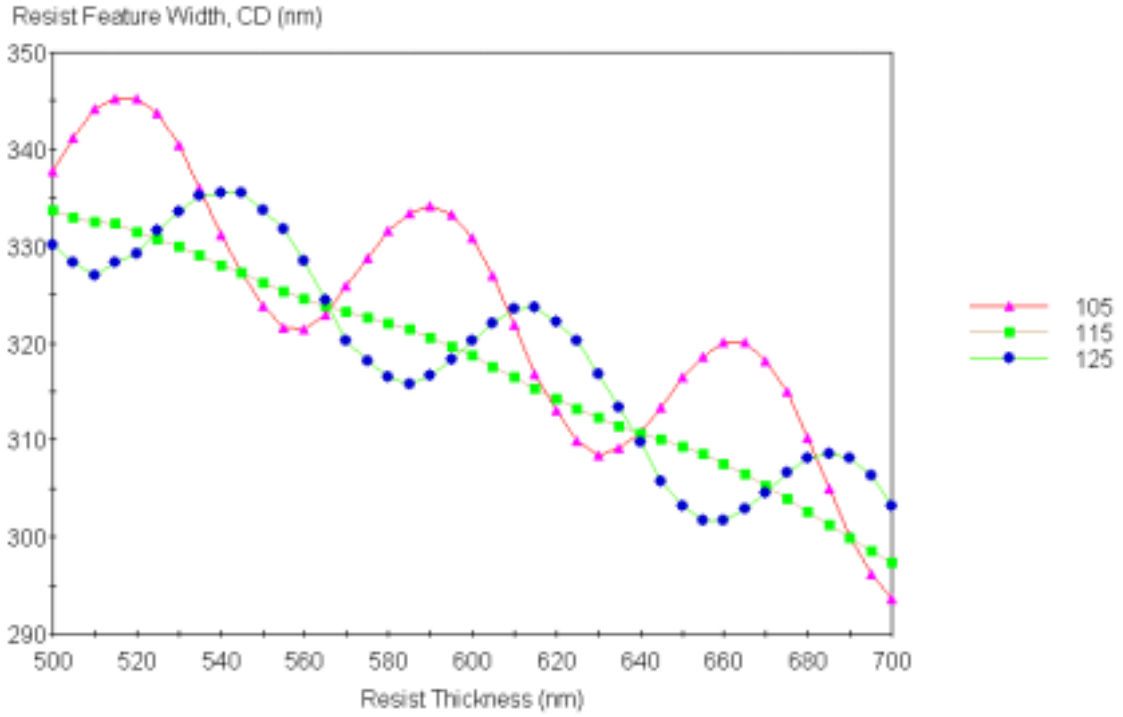

Figure 8: Resist CD swing as a function of resist and SiON thickness using a material corresponding to 175 sccm flow rate deposition condition.

This would be an ideal SiO_xN_y BARC material for the topography model shown in Figure 1 where the resist thickness varies dramatically but the substrate thickness (oxide) is fairly constant. Unfortunately the optimal BARC location chosen was designed to work for only one oxide thickness. To see how the BARC material performs to minimize oxide swing set up a simulation set where the oxide thickness varies but the resist thickness remains constant. First, change the SiOxNy thickness to 115 nm in the film stack. In the simulation sets view, begin a new simulation with the *Thickness Layer #3* (oxide) as the input parameter. Set the *min*, *max* and *step* to 400, 600 and 5 nm respectively. Select *Develop* group output parameters and *Launch*. The resulting oxide swing is shown in Figure 9. To minimize against oxide thickness variations a different ARC material may perform better. This issue is addressed further in question 1 at the end of this chapter.

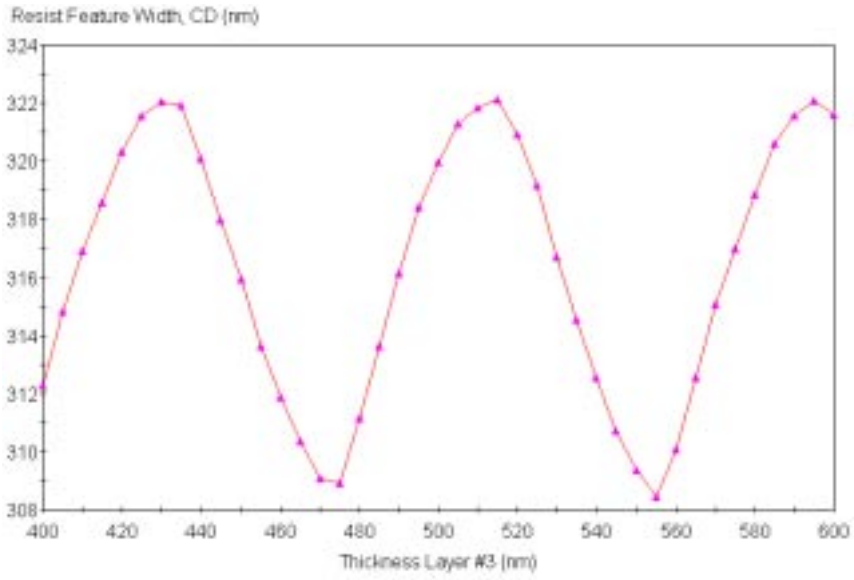

Figure 9: Resist CD swing as a function of oxide thickness using a material corresponding to 175sccm flow rate deposition condition and 115 nm SiO_xN_y thickness 115 nm.

Summary

In this chapter we have seen that the optimal BARC optical properties can be chosen based upon the substrate reflectivity. With a variable inorganic material (e.g., SiO_xN_y) there are several regions (n, k and thickness) that produce a good BARC material. When imaging over topography the film thickness of several layers must be considered to minimize CD variations.

Questions

See Appendix A for answers.

1. From Figure 7 the thicker SiO_xN_y solution was chosen (175 sccm N_2O process). If the thinner solution was desired for etch purposes what values of n, k and thickness would be optimal? What gas flow rate should be used? Generate a material file for this material and simulate the resist swing to verify the reduced CD swing. Which material is better?
2. Typically, with SiON films a thin 5 nm SiO_2 cap layer is placed between the resist film and the SiO_xN_y BARC layer. This cap is used as a barrier to contamination of chemically amplified resists by the basic SiON films. This contamination leads to footing problems. How much would the addition of this cap layer affect the quality of the SiO_xN_y as a BARC? Would a different n and k condition work better?

Further Information

For further information, see *Inside PROLITH* Chapter 3 pages 38-47 for an in-depth discussion of the theory of standing waves and film stack reflectivity. Also, Workbook Chapters 3-4 provide additional information on optimizing the thickness of a resist film and BARC to minimize processing errors from a reflective substrate.

Chapter 6
Influence of PEB on Standing Waves

Objective

In this problem, you will learn how to use PROLITH to examine the influence of post-exposure bake (PEB) on standing waves in the resist profiles for conventional (non-chemically amplified) resists.

Introduction

The Post Exposure Bake (PEB) process for conventional resists was originally designed to remove the impact of standing waves in the resist profiles. However, the same process that reduces the standing wave corrugations in the resist profile (diffusion of the photoactive compound) can also degrade the quality of the image projected into the resist. The PEB model in PROLITH can be used to choose an optimal PEB process that removes standing waves without having a detrimental impact on the lithography process.

In this workbook chapter, you'll learn how to:

- Use PROLITH to learn about the relationship between post-exposure bake, the diffusion length, and the amplitude of standing waves in the resist profile for conventional resists.
- Run a basic simulation
- Use Raw Threshold or Weighted Threshold metrology.
- Run a simulation set to examine trends.

Theory

The Post-Exposure Bake (PEB) process was originally developed to reduce the amplitude of standing wave corrugations in the resist profiles for conventional (non-chemically amplified) resists. Figure 1 shows a simulated resist profile with a typical PEB and Figure 2 shows a simulated resist profile a very short PEB.

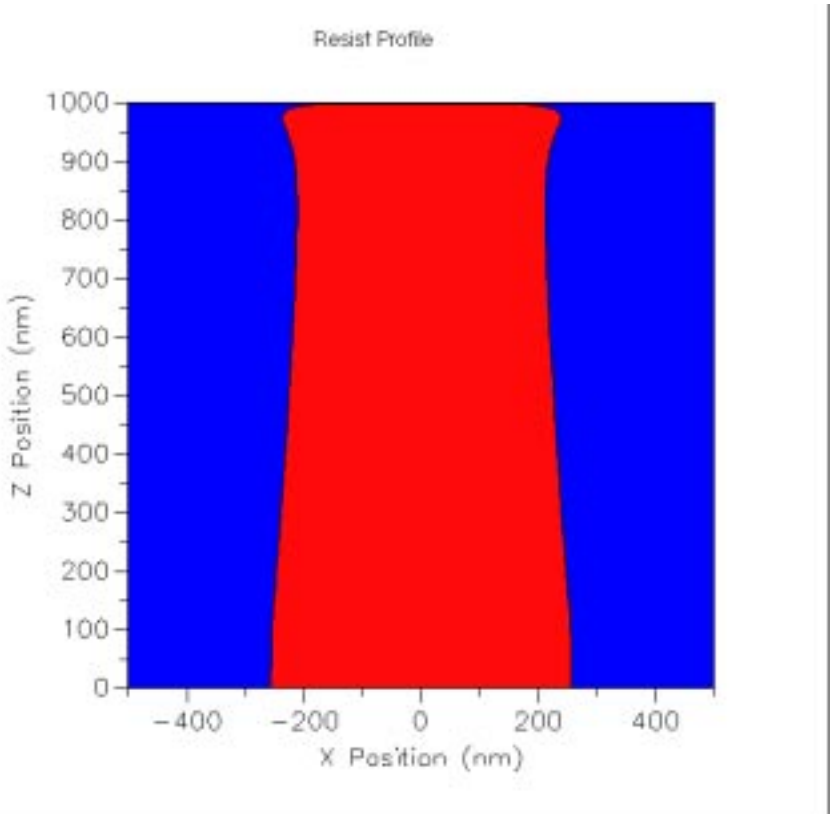

Figure 1. Simulated resist profile with PEB for 60 seconds at 110°C. The CD of this feature is 509.7 nm for the Weighted Threshold CD measurement method, and is 509.8 nm for the Raw Threshold measurement method with a CD Measurement Threshold of 10%.

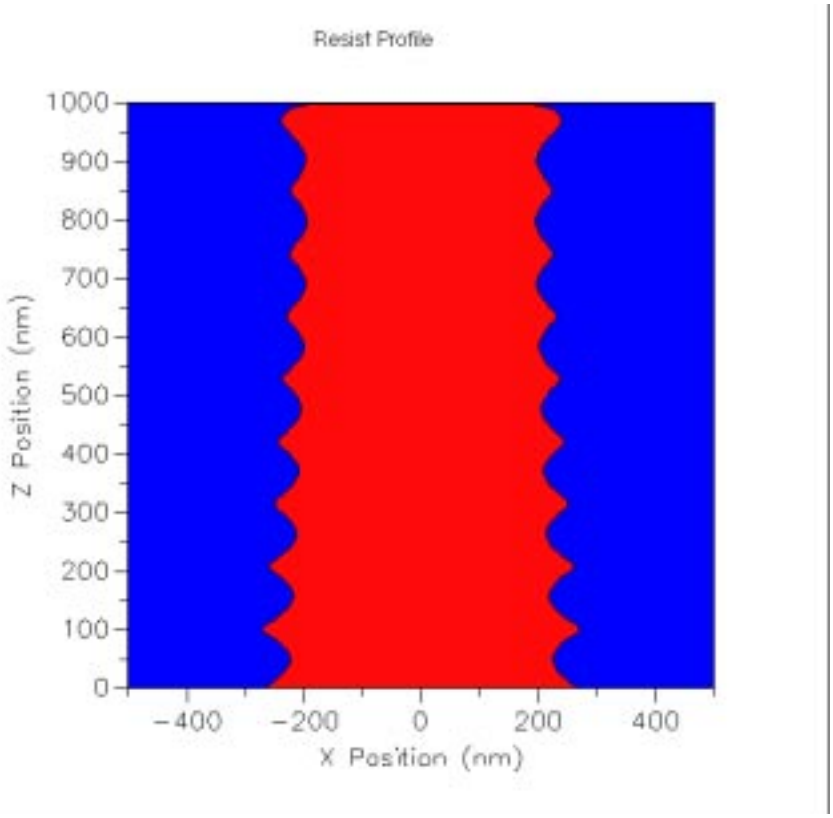

Figure 2: Simulated resist profile with PEB for 10 seconds at 110 °C. The CD of this feature is 492.5 nm for the Weighted Threshold CD measurement method, and is 543.6 nm for the Raw Threshold measurement method with a CD Measurement Threshold of 10%.

Standing waves are caused by thin-film interference of the light within the resist layer during exposure. The standing waves in the light intensity are converted into standing waves in the latent image through reaction of the photoactive compound (PAC). For a conventional resist, the solubility of the resist in the developer solution is dependent on the PAC concentration. If the standing waves in the PAC latent image are not removed, standing wave corrugations will appear in the final resist profile. During PEB, the PAC diffuses through the resist and smoothes out sharp gradients in the PAC concentration. The goal of PEB for a conventional resist is to diffuse the PAC enough to reduce the standing waves without significantly degrading the desired resist pattern on the wafer. This condition can be written in terms of the diffusion length, which is the average distance a PAC molecule will diffuse during the PEB process:

$$\sigma = \sqrt{2Dt} \qquad (1)$$

where σ is the PAC diffusion length, D is the diffusivity of the PAC, and t is the duration of the bake. From the equation, you can see that the average distance a PAC molecule will diffuse increases if the diffusivity is increased (by increasing the bake temperature) and also increases if the bake time is increased. Our goal during PEB is to choose the bake conditions so that σ is larger than the standing waves and smaller than the features on the wafer.

Standing wave corrugations also can appear with chemically amplified (CA) resists, but for this case the relationship between diffusion and standing waves is more complicated. For a CA resist, the PAC is a photoacid generator (PAG), so an acid is generated on exposure to light. During PEB, the acid diffuses through the resist and reacts with developer-insoluble chemical groups in the resist and converts them into chemical groups that are soluble in the developer solution. This chemical reaction is called the "deblocking reaction" because the chemical groups that prevent (or block) dissolution in the developer solution are removed by a reaction with the acid. The relationship between diffusion and standing waves is more complicated because even if the standing wave pattern in the acid has diffused away by the end of the bake, it is possible that the acid caused a large number of deblocking reactions at the beginning of PEB, when the standing wave pattern was still present. The impact of the duration of PEB for chemically amplified resists is described in Workbook Chapter 7 which addresses the trade-off between exposure dose and thermal dose. In the current chapter, we will only examine conventional resists.

Procedure

Open a new document. Use the default settings with the following exceptions:

Numerics:

Speed Factor: 4

Go to the PEB input view and notice that the PAC Diffusion Length is 65.0 nm. Next, go to the Exposed Latent Image output view and examine the Latent Image Before PEB, shown in Figure 3.

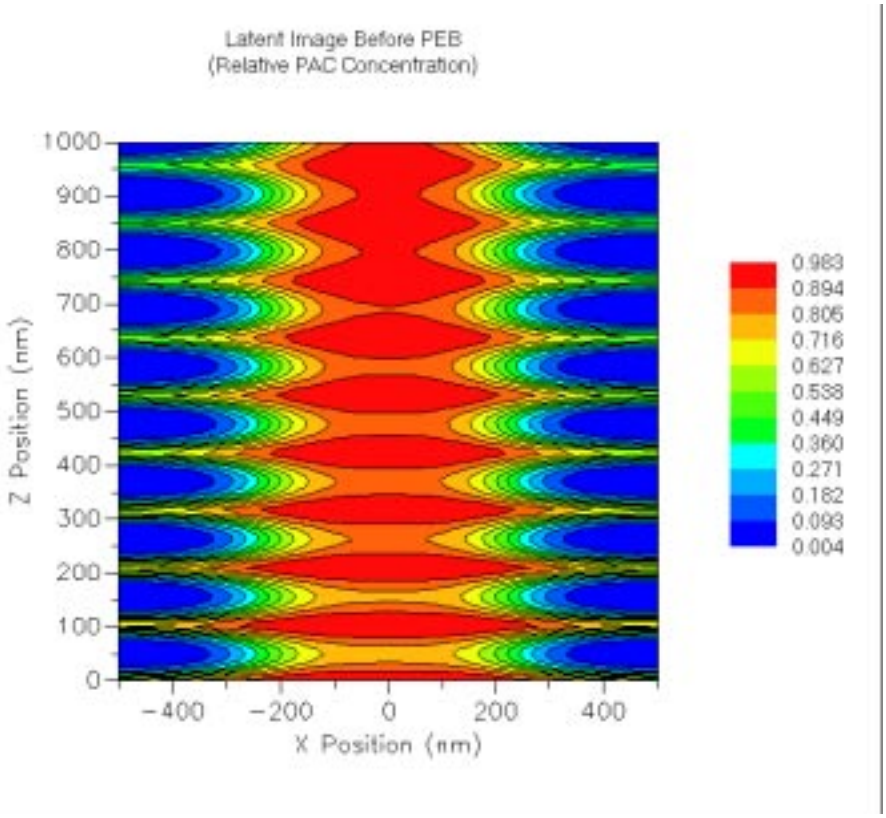

Figure 3: PAC concentration before PEB.

The standing waves in the latent image have a period of about 100 nm, so with a diffusion length of 65 nm, the PAC from the peaks in the latent image should be able to diffuse into the minimums in the latent image. (It should be about 50 nm from a peak to a minimum in the z-direction.) The resulting resist profile is shown in Figure 1. The result shown in Figure 2 can be generated by setting the duration of the bake to ten seconds in the PEB view.

It is also interesting to notice that the CDs of the two resist profiles shown in Figures 1 and 2 are different. Because we chose the Weighted Threshold method for the CD measurement method, PROLITH calculates a weighted profile from the profile shape and then measures the width of the weighted profile at 10% of the resist profile height. The weighted profile is generated by setting the height of the new profile at each point on the wafer equal to the total amount of resist above that point. (See *Inside PROLITH* for more details on how a weighted profile is generated and this analysis is performed.)

With the weighted profile, the standing waves in the resist profile are effectively removed before the CD of the profile is measured, so CD measurements are not as sensitive to the presence of standing waves. Because we want to study standing waves in greater detail, go to the Metrology input view, shown in Figure 4, and switch the CD Measurement Method from "Weighted Threshold" to "Raw Threshold". The Raw Threshold CD metrology method measures the profile directly, without constructing a weighted profile. Next, re-run the simulation where the bake time is ten seconds, and notice that the reported value of the CD changes from 492.5 nm to 543.6 nm! The reason for the

dramatic change is the large amplitude of the corrugations on the resist profile shown in Figure 2. If you change the value of the CD Measurement Threshold from 10% to 15%, then the CD will change to 440.5 nm because the width of the resist profile at this height has changed from a peak in the profile to a valley.

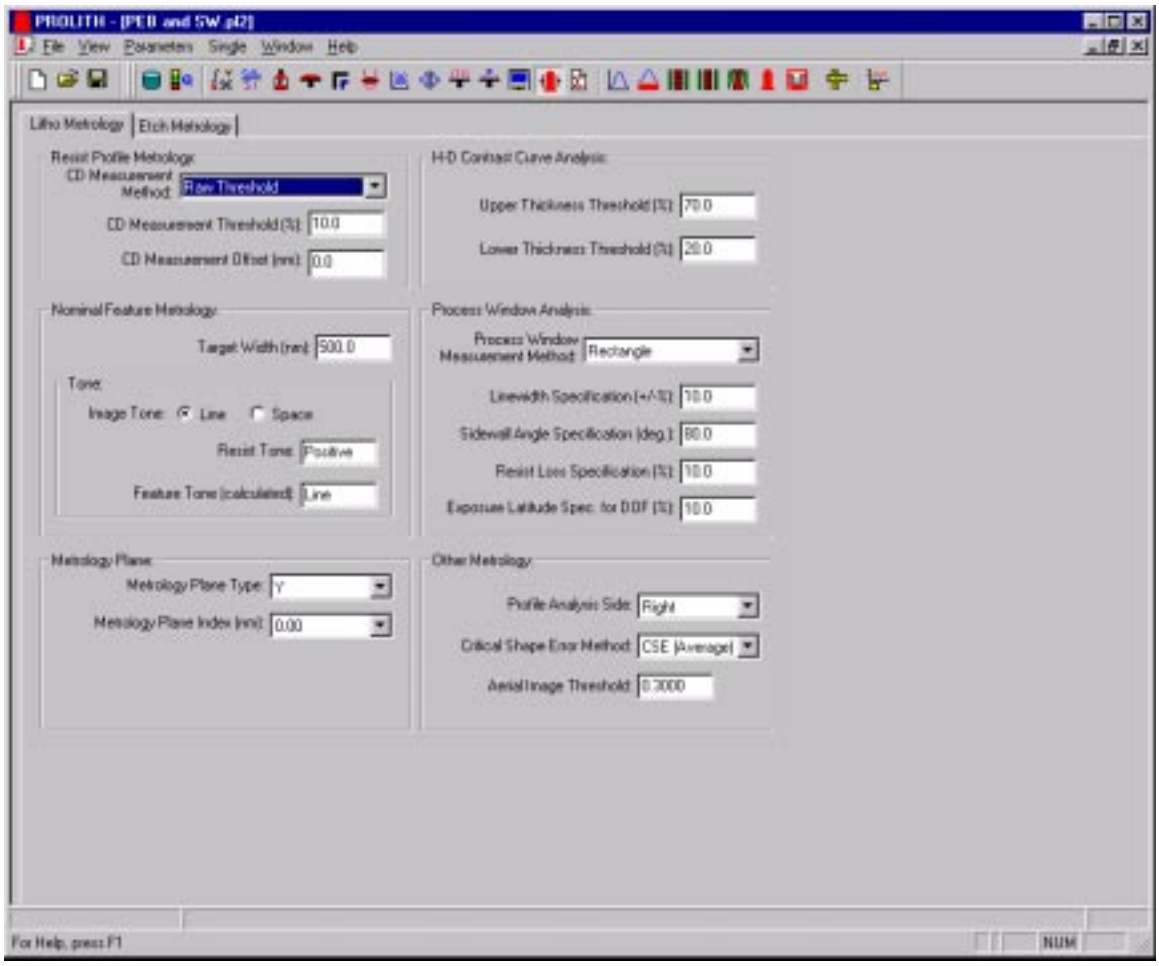

Figure 4: Metrology input view. The Raw Threshold method is chosen for the CD Measurement Method, and the CD Measurement Threshold is set to 10%.

We can use the Raw Threshold CD metrology method to measure directly the amplitude of the standing waves. First, change the CD Measurement Threshold back to 10%. Next, set-up a Simulation Set where the duration of the bake during PEB is an input. The Simulation Set view is shown in Figure 5. Choose the minimum PEB time to be 10 seconds, the maximum to by 240 seconds, and the step to be 5 seconds. Choose the Develop output group and start the simulation set by pressing the Launch button.

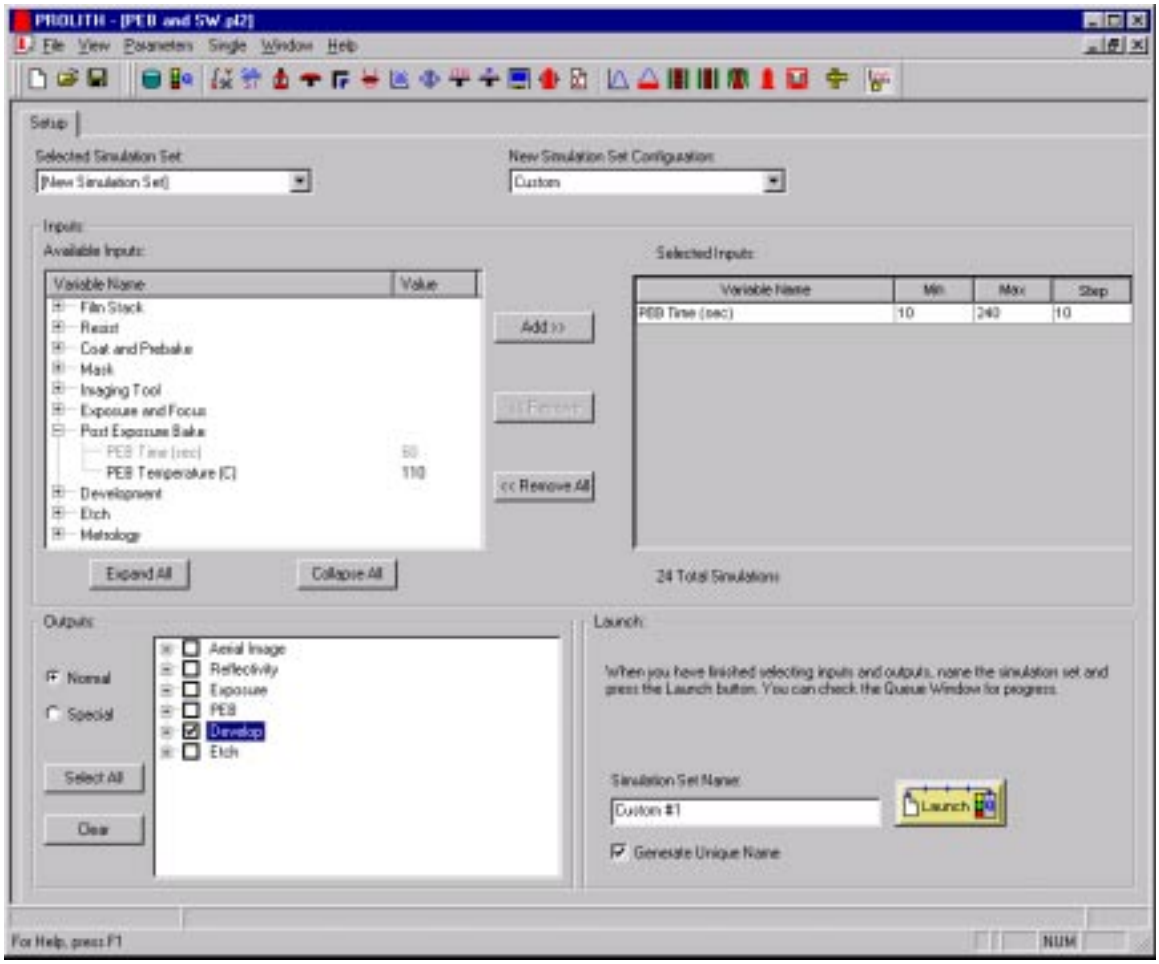

Figure 5: The Simulation Sets view.

If you select the Results tab, you will see a graph similar to the one shown in Figure 6. It is also possible to examine the individual resist profiles. To do this, change the "Y-Axis" from "Resist Feature Width, CD (nm)" to "Resist Profile", as shown in Figure 7. Double-click on the rightmost resist profile to see a close-up of the resist profile for a bake time of 240 seconds. The properties window also reports that the resist CD is now 617.7 nm. Double-click on several of the resist profiles – the standing waves disappear for bake times longer than about 30 seconds, which corresponds to the minimum in the CD in Figure 6.

The question at this point is "Which bake time is best?" Obviously, the resist profile shown in Figure 2 is unacceptable, but the results in Figures 6 and 7 show a large range of PEB times that lead to acceptable resist CDs and resist profile shapes. The optimal bake time will depend on how you want to define "best". One possible criterion for choosing the best bake time is to maximize the size of your focus-exposure process window, subject to the additional requirement that standing wave corrugations are not present in the resist profile.

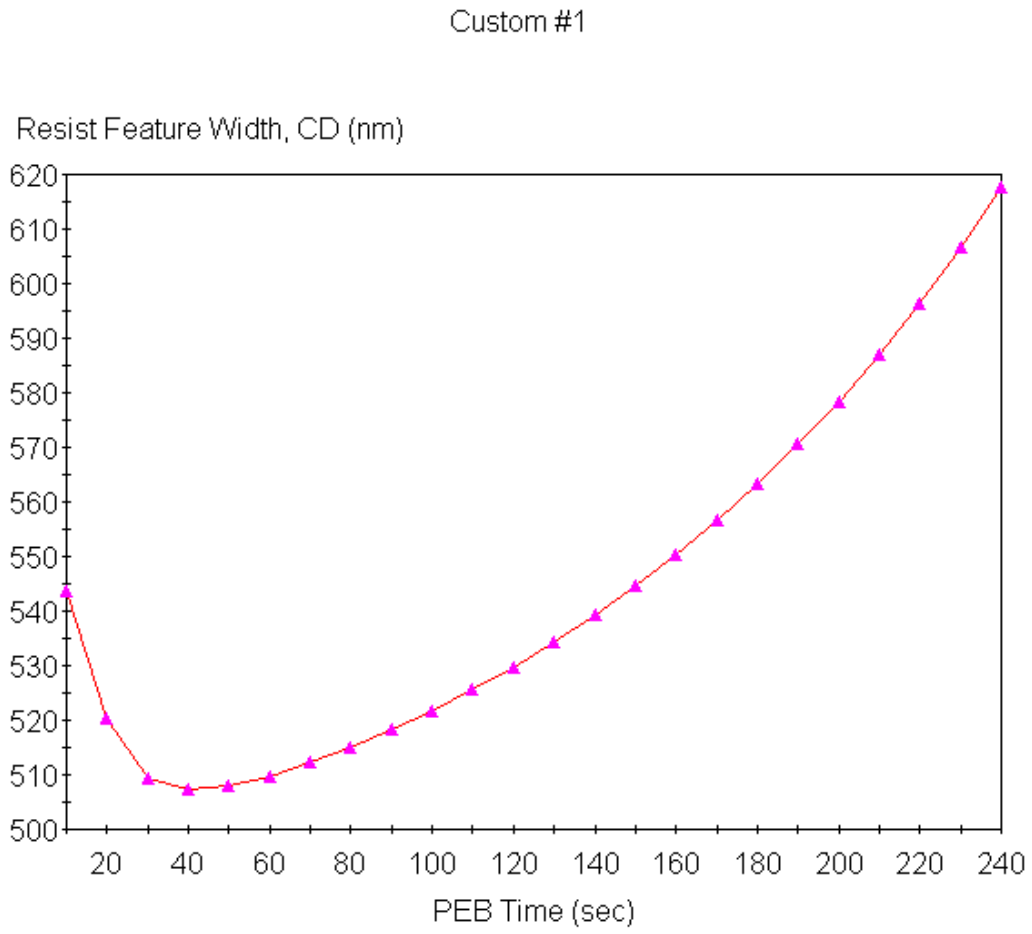

Figure 6: Resist feature with as a function of PEB bake time.

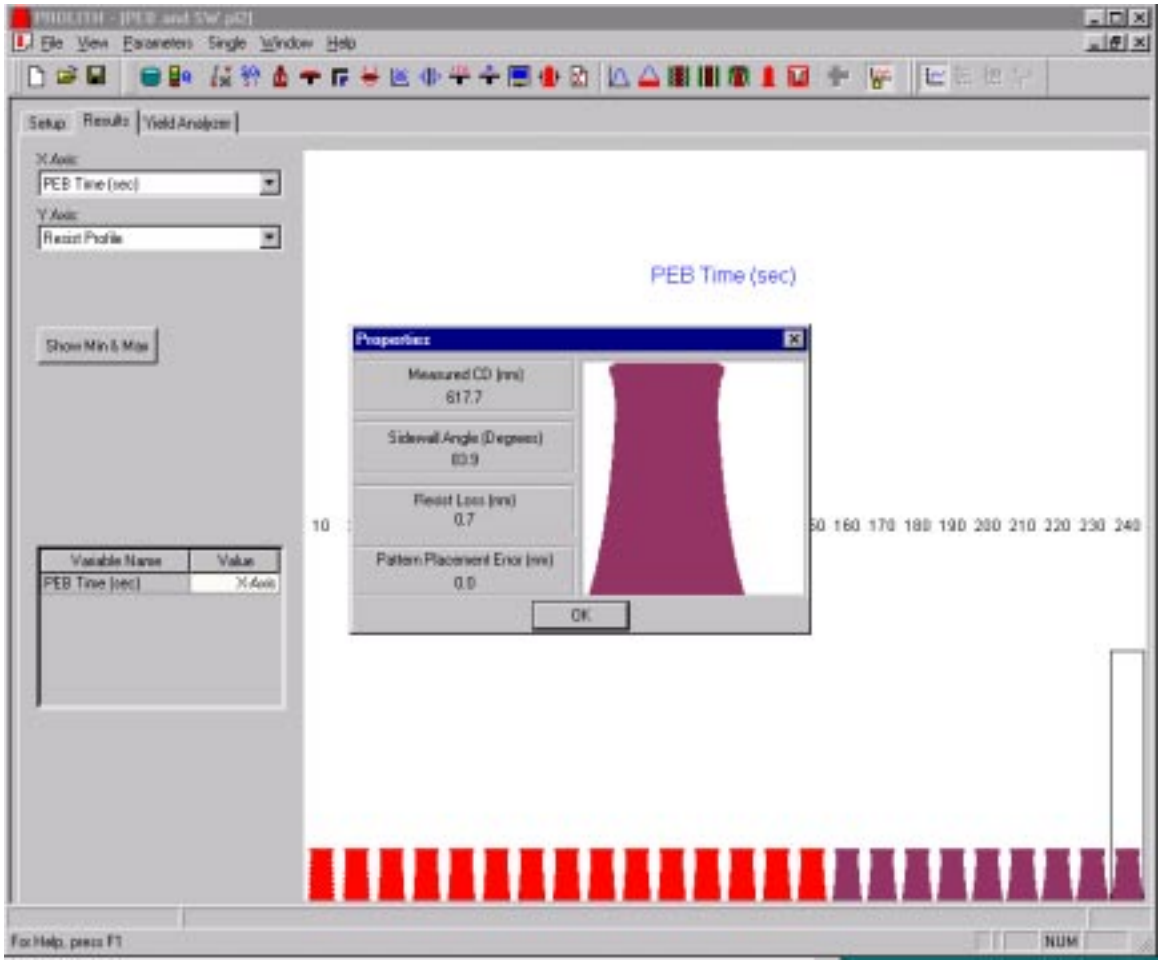

Figure 7. Resist Profile shape as a function of PEB time. Create this view by selecting the Y Axis variable as Resist Profile. Open the properties box by double-clicking on one of the small resist profiles in the graph.

For a given exposure latitude specification, simulation sets can be used to calculate the Depth Of Focus (DOF) for a range of PEB times (see Workbook Chapter 2 for the definition of DOF). First, go to the Metrology view and set the "Exposure Latitude Spec. for DOF". The value selected in Figure 4 is 10% exposure latitude. We will keep this value, but if you wanted to use a different exposure latitude specification, you would change it here. Second, go to the Simulation Sets view and select the PEB Time as an input, with the same range and step as in the previous calculation. Next, click on the "Special" output radio radio button and choose "Depth of Focus". Finally, click on the "Launch" button to start the calculation. This calculation may take a little while, because each data point requires calculation of a focus-exposure matrix.

When the calculation is complete, the results should look like the curve shown in Figure 8. The results in Figure 8 indicate that too much diffusion will hurt depth of focus, and this places an upper bound on the PEB time. Depth of focus slowly decreases for long PEB times because too much diffusion degrades the latent image. For a bake time of 240 seconds, the diffusion length is 130 nm, which is more than 25% of the target CD of 500 nm!

Based on the results in Figures 7 and 8, a bake time between 30 and 60 seconds should remove standing waves and provide sufficient depth of focus. Shorter bake times might be favored over longer times in order to improve throughput.

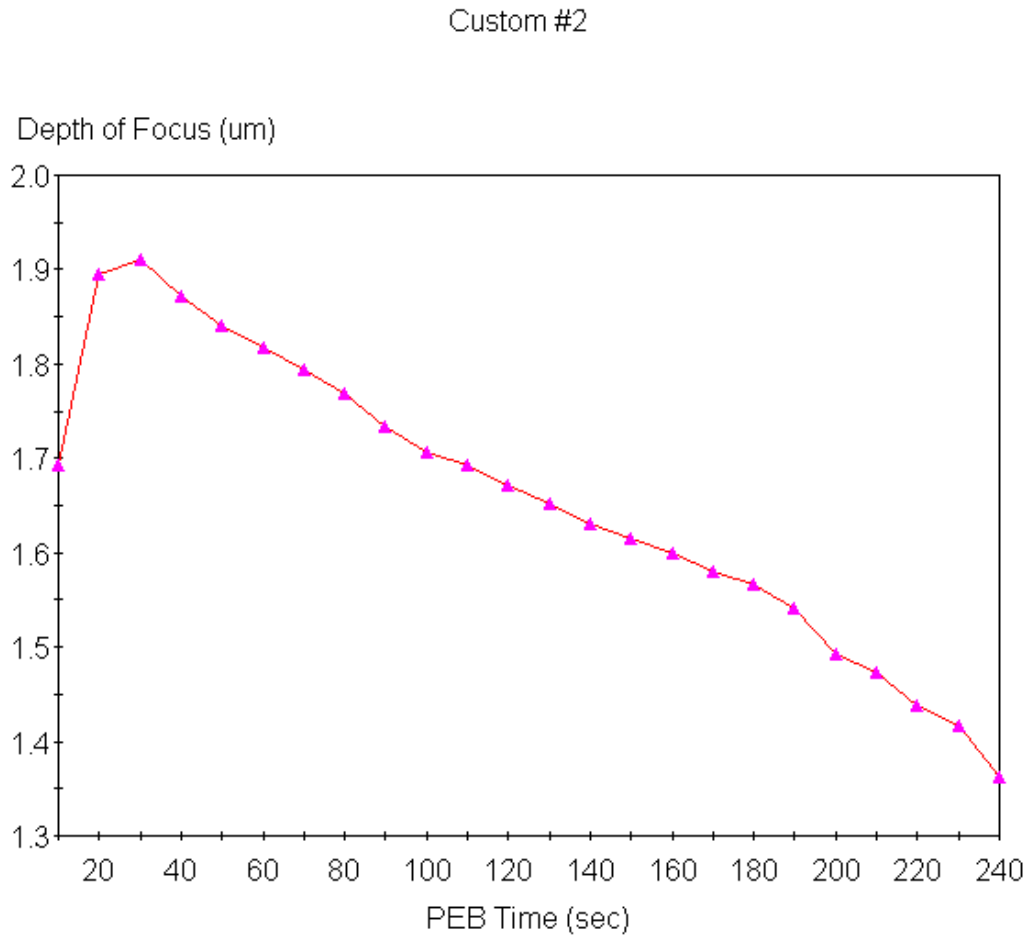

Figure 8: Depth of Focus as a function of PEB Time.

Summary

For conventional resists, PEB is used to remove standing waves from the resist profiles. The simulation set results presented here show that the duration of the PEB must be long enough for the PAC to diffuse out the standing waves in the latent image after exposure, but not so long that the image in resist degrades due to too much diffusion.

Questions

See Appendix A for answers.

1. The results shown in Figures 7 and 8 were for dense features. Repeat the calculations for isolated lines. Do the conclusions about the optimal bake time change? If both isolated and dense features were on the same mask, which type of feature would you analyze to choose a bake time?
2. How does bake time influence iso-dense bias? One way to perform this analysis is to run a simulation set with both the PEB time and the pitch as inputs and with the develop group as the output. Another approach is to calculate the results directly with the special output "Iso-dense print bias".

Further Information

The post exposure bake model is described in Chapter 6 of *Inside PROLITH*. Workbook Chapter 7 discusses the trade-off between exposure dose and thermal dose for chemically amplified resists.

Chapter 7
Exposure vs. Thermal Dose for Chemically Apmplified Resists

Objective

In this workbook example, you will learn to use PROLITH to examine the trade-off between exposure and post-exposure bake for a chemically amplified resist.

Introduction

The solubility of a chemically amplified resist changes in a two-step process. In the first step, an exposure dose is delivered to the resist that results in the generation of acid. In the second step, the post-exposure bake process delivers a thermal dose that causes the acid to react with the resist and change the solubility. When using chemically amplified resists, one must consider and optimize both of these dose components.

In this workbook chapter, you'll learn how to:

- Use PROLITH to learn about the relationship between the exposure dose and the thermal dose for a chemically amplified resist
- Run a custom set to calculate the dependence of dose-to-size on post exposure bake time
- Run a custom set to calculate the dependence of dose-to-size on post exposure bake temperature
- Run a simulation set showing the trade-off between exposure dose and thermal dose

Theory

Chemically amplified resists require both an exposure dose and a thermal dose to change the solubility of the resist in developer. During exposure, light converts the photoacid generator (PAG) molecules in the resist into acid, and during the post-exposure bake (PEB) process, this acid reacts with chemical groups in the resist which are insoluble in developer and converts these insoluble sites into chemical groups which are soluble in the developer. The chemical reaction which converts an insoluble, or "blocked", chemical group into a soluble chemical group is called the "deblocking reaction". Because a single acid molecule can react with many blocking groups during the bake process, the influence of the exposure dose (which may generate only a small number of acid molecules) is "chemically amplified".

The development rate of resist is a strong function of the concentration of deblocked sites in the resist. If enough of the insoluble groups are deblocked, the exposed regions of the resist will completely dissolve during develop. As a rule of thumb, the concentration of deblocked sites is approximately proportional to the product of the exposure dose and the thermal dose. Mathematically, this relationship can be stated as:

$$N_{deblocked} \approx CEK_{amp}t_{bake} \quad (1)$$

where $N_{deblocked}$ is the fraction of deblocked sites, C is the exposure rate constant (cm^2/mJ), E is the exposure dose in mJ/cm^2, K_{amp} is the rate of the deblocking reaction with units 1/sec, and t_{bake} is the duration of the bake in seconds. The product $K_{amp}t_{bake}$ is the equivalent of a thermal dose. Intuitively, the above relationship between the exposure dose and the thermal dose makes sense – if the exposure dose is cut in half, then only half as much acid will be present, and it will take the acid twice as long to deblock the same number of insoluble groups in the resist. The equation above also indicates that increasing t_{bake} is not the only way to increase the thermal dose: the rate of the deblocking reaction K_{amp} is very sensitive to the bake temperature, so a decrease in the exposure dose required can be accommodated by increasing the bake temperature.

More accurate relationships between exposure and the PEB process are described in *Inside PROLITH*, Chapters 5 and 6. For the current workbook example, the simple rule of thumb given above will provide significant insight into the relationship between the exposure dose, the PEB time and the PEB temperature.

Procedure

In PROLITH, start with the default document and set the following input parameters:

Numerics:

Image calculation mode: High NA Scalar
Speed Factor: 4

Film stack:

Layer #1: 750 nm of KrF Shipley APEX E resist
Layer #2: 60 nm of Brewer ARC DUV18
Substrate: Silicon

Mask:

Mask type: 1D Binary
Feature type: Line
Nominal feature width: 350 nm
Pitch: 700 nm
Mask bias: 0 nm

Imaging Tool:

Source shape: Partially Coherent
Partial coherence: 0.50
Wavelength: 248 nm

Wavelength range: 0.0 nm
Numerical aperature: 0.70

Exposure and Focus:

Exposure energy: 14.0 mJ/cm^2
Focal position: 0.0
Focal position relative to the middle of the resist.

Post Exposure Bake:

PEB time: 60 sec
PEB temperature: 90 C

First, we will examine the influence of post exposure bake time on the dose-to-size, *Es*. Run a custom simulation set varying the bake time. To do this, select *Post Exposure Bake/PEB Time (sec)* as an input. Set the *Min, Max* and *Step* to 30, 90 and 5 sec, respectively. Next, choose the output as *Special/Dose-to-size, Es (mJ/cm^2)*. The output from this custom run is shown in Figure 1. The dose-to-size drops from 25 mJ/cm^2 to 10 mJ/cm^2 as the bake time is increased from 30 seconds to 90 seconds. This result is consistent with the rule of thumb described in the Theory section: doubling the bake time from 30 seconds to 60 seconds approximately cuts *Es* in half.

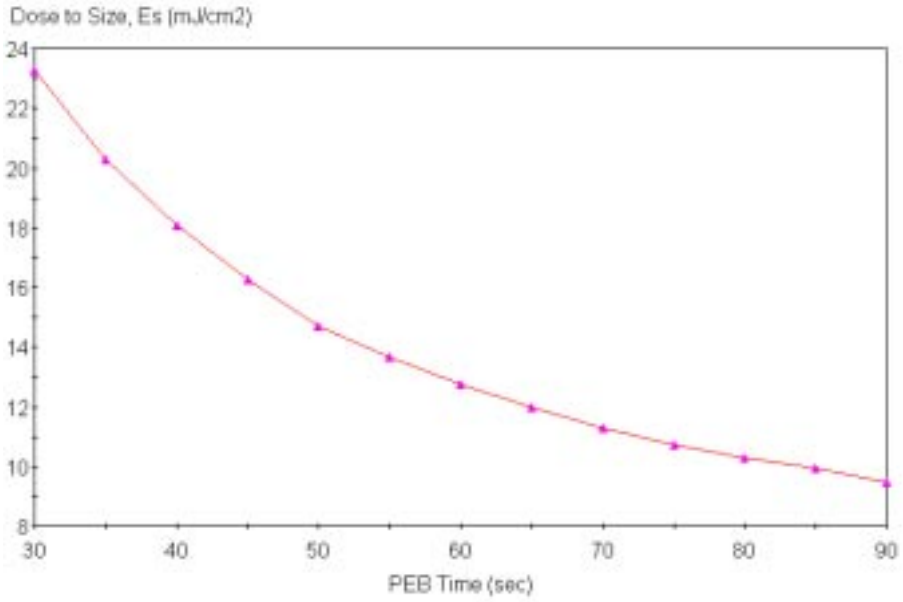

Figure 1. Dose-to-size as a function of PEB time with a bake temperature of 90^{o}C.

Next, we want to investigate the relationship between dose-to-size and the PEB temperature. Before running any new simulations, it is worthwhile to try to anticipate the results by using the relationship between thermal dose and exposure dose. Go to the resist view, and click on the *Chemically Amplified Graph* tab. This should lead to the graph shown in Figure 2, which shows the temperature dependence of the rate of the deblocking reaction, K_{amp}. As the bake temperature is increased from 80^{o}C to 100^{o}C, K_{amp} increases by more than a factor of 10, so we anticipate that the dose-to-size will decrease by about a factor of 10.

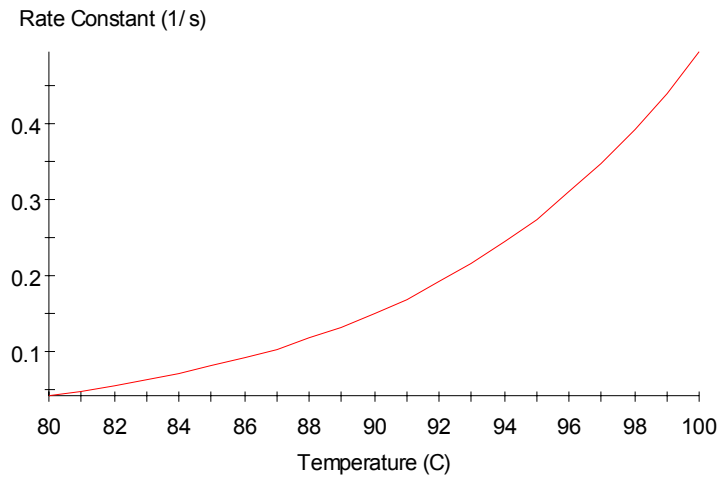

Figure 2. The temperature dependence of the rate constant of the deblocking reaction, K_{amp}.

Run a custom simulation just like the previous one, except choose the input variable as bake temperature. To do this, return to the Simulation Sets view and select *Remove All*. Next, select *Post Exposure Bake/PEB Temperature (C)* as an input. Set the *Min, Max* and *Step* as 80, 100 and 5 ^{o} C, respectively. As shown in Figure 3, the dose-to-size drops dramatically as the PEB temperature is increased. Note that the dose for a bake temperature of 80 C is about a factor of 10 larger than the dose for a bake temperature of 100 C, which was exactly what we expected.

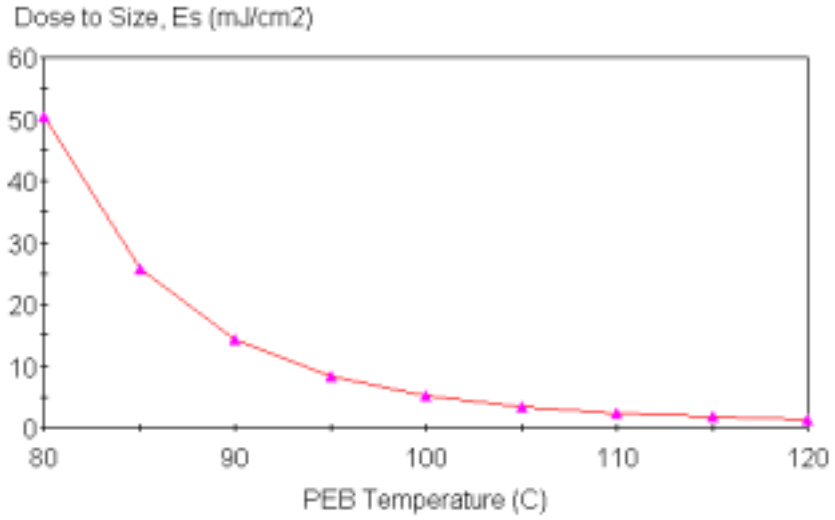

Figure 3. Dose-to-size as a function of PEB bake temperature for a bake time of 60 seconds.

So, as these first simulations have shown, the exposure dose required to size a feature is reduced by an increasing thermal dose. This leads to a trade-off between thermal and exposure dose. If a chemically amplified resist (CAR) is used, there is a continuum of values for exposure and PEB temperature that, combined, will yield the correct feature size. For example, as exposure is increased, the PEB temperature must decrease.

However, since the various operating points are not equivalent for all metrics, it is necessary to evaluate the range of effects caused by the variation of these two parameters. The resulting data are used to choose the correct combination based on process and manufacturing considerations.

To see these effects, run a new custom simulation set. Vary PEB temperature from 85-100^{o} C in steps of 1^{o} C. Vary Exposure from 8-18 mJ/cm^{2} in steps of 1 mJ/cm^{2}. Select "Normal – Develop" for output and launch the simulation set calculation. Graph CD error as a function of the two input parameters.

To see the data most clearly, first select the contour plot button. Then, use the right mouse button and click on the graph to bring up the 3D Chart Control Properties window.

Select the Levels tab as shown in Figure 4. The contour levels are not very rounded, so we will reset them. Select the Remove button several times until the contour levels have been deleted. Then select the Add button and add 0. Repeat and add the following: 10, -10, 20, -20.

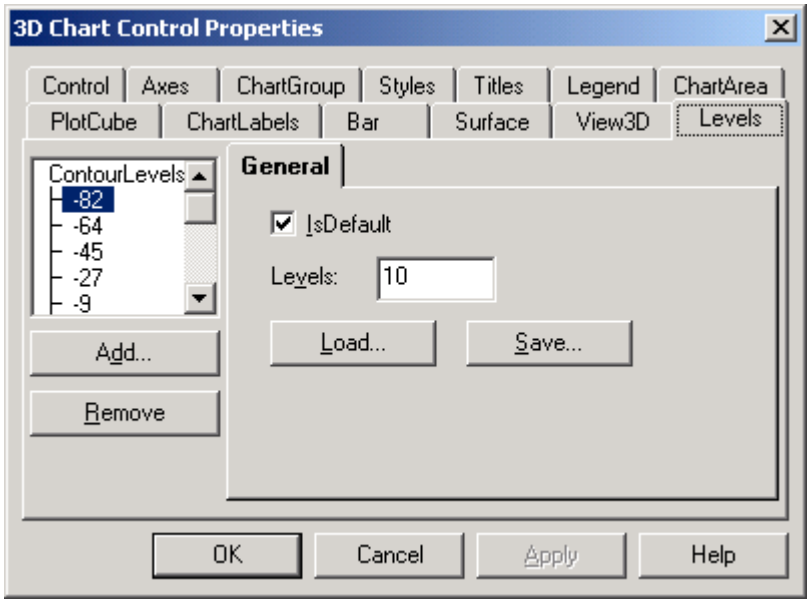

Figure 4: Levels tab of the Chart Control Properties dialog

When you have done this, you should see the contour plot shown in Figure 5.

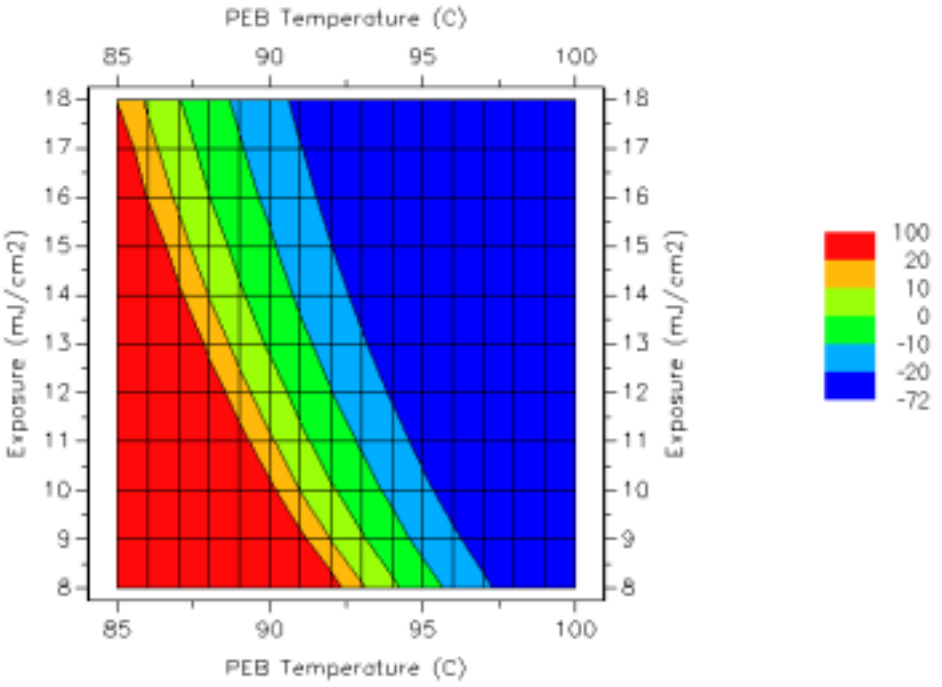

Figure 5: Contour plot of CD error as a function of PEB Temperature and Exposure.

From Figure 5, you can see that there is a range (shown in green) of operating parameters that keeps the CD error within +/- 10%. This is only one of the process metrics, but Figure 5 does show the tradeoff – as PEB temperature is increased, the thermal dose increases, and the exposure dose must decrease to keep the CD within the specification.

Summary

In this workbook example, we examined the relationship between exposure dose and thermal dose. The exposure dose is the amount of energy put into the resist during exposure – this is the same concept as in conventional resists. The thermal dose is required for the deblocking reaction to occur in the resist. The solubility of the resist in developer is approximately proportional to the product of the thermal dose and the exposure dose, so there are many trade-offs which can be made between exposure dose, PEB temperature, and PEB time.

Questions

See Appendix A for answers.

1. The examples above used dense lines, but all of the trends should be the same for isolated lines. Generate Figure 5 by using an isolated line (set the pitch equal to 3500 nm). What observations can you make about the results compared to the dense line case?

Further Information

For further information, see *Inside PROLITH* Chapter 5.

Chapter 8
Effects of the Aberration Coma

Objective

This workbook example will explain the meaning of lens aberrations and demonstrate how one type of aberration (coma) affects the resist profile.

Introduction

Lens aberrations are present in all lithography systems and their impact on image quality can be significant. Aberrations are described as a wavefront deviation, the difference in phase (or path difference) of the actual wavefront emerging from the lens compared to the ideal wavefront as predicted from Fourier optics. The wavefront deviation is most often expressed as a special polynomial series called a Zernike polynomial. One of the most useful properties of the Zernike polynomial is the fact that individual terms in the polynomial can be related to common aberration behavior such as tilt, spherical aberration, coma and astigmatism. Although a complete understanding of the aberration effects must take into account the entire Zernike polynomial, it is common to examine the components individually and identify the dominant term(s). This workbook example will define aberrations in the context of Fourier optics and, using the example of coma, demonstrate how PROLITH can be used to evaluate the impact of lens aberrations.

In this workbook chapter, you'll learn how to:

- Visualize the lens aberration
- Simulate the resist profile of a feature with and without coma and compare the two.
- Quantitatively evaluate the impact of coma.

Theory

A convenient starting point for the discussion of aberrations is a review of the aerial image formation. The immediate goal is to review the mathematical expression for the aerial image with and without aberrations for coherent and partially coherent illumination. A more detailed derivation, including a more complete treatment of partial coherence, is found in Chapter 2 of Inside PROLITH.

Figure 1 below shows a generic projection system with light source, photomask, objective lens and wafer.

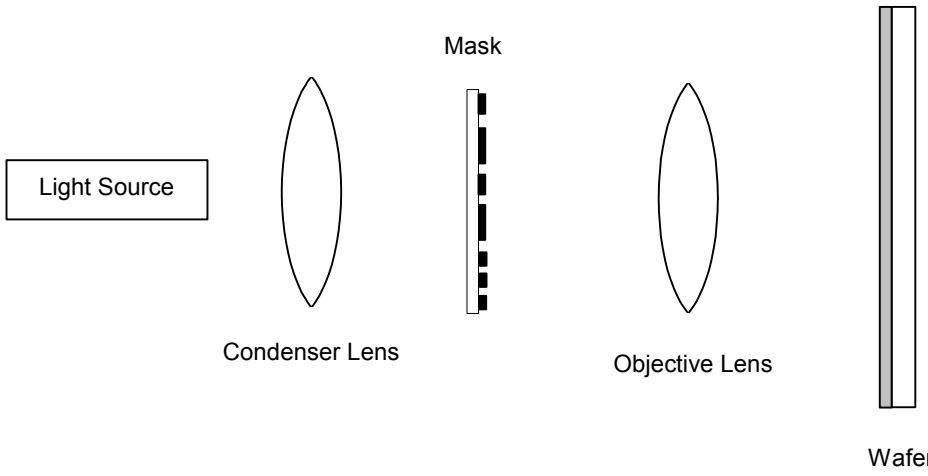

Figure 1: Block diagram of a generic projection system.

Light originates at the source, passes through the condenser lens, and is diffracted by the photomask. The diffracted light is collected by the objective lens that focuses the light onto the wafer plane. The aerial image is defined as the intensity distribution of the light at the plane of the wafer.

The Fourier optics approach is used to mathematically model the projection system. The mask is described by its electric field transmission *m(x,y)* where the function *m(x,y)* is often assumed to be zero where chrome is present (no light passes through) and one where the mask is transparent. The electric field that enters the objective lens is the diffraction pattern generated by the mask, $M(f_x, f_y)$. Mathematically, for coherent illumination, the diffraction pattern $M(f_x, f_y)$ is the Fourier transform of *m(x,y)*.

$$M(f_x, f_y) = \mathcal{F}\{m(x,y)\} \qquad (1)$$

Here, f_x and f_y are the spatial frequencies or scaled coordinates of the x'- y' plane (the plane of the objective lens). The diffraction patterns for two common mask patterns are shown in Figure 2.

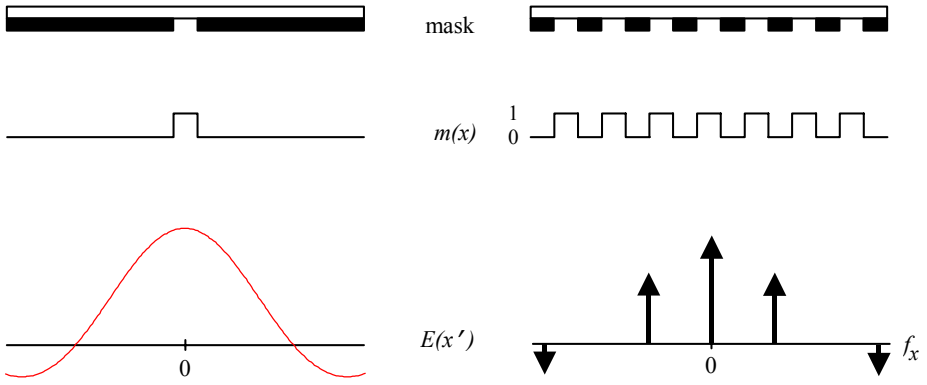

Figure 2: The diffraction pattern for two common masks: an isolated space (left) and a line-space pattern (right). The mask, the mask transmission function *m(x)*, and the diffraction patterns are shown for each case.

The objective lens takes the diffraction pattern and forms an image on the wafer. This is described mathematically by taking the inverse Fourier transform of the diffraction pattern in the objective lens. However, the objective lens cannot collect all the diffracted light. The maximum spatial frequency that can enter the objective lens is given by NA/λ. To account for this high frequency cut-off, we define the objective lens *pupil function P* (a pupil is just another name for an aperture). The pupil function of an ideal lens simply describes what portion of light enters the lens: it is one inside the aperture and zero outside.

$$P(f_x, f_y) = \begin{cases} 1, & \sqrt{f_x^2 + f_y^2} < NA / \lambda \\ 0, & \sqrt{f_x^2 + f_y^2} > NA / \lambda \end{cases} \tag{2}$$

Thus, the product of the pupil function and the diffraction pattern describes the light entering the objective lens. Combining this with our description of how a lens behaves gives us the expression for the electric field, at the image plane (that is, at the wafer):

$$E(x,y) = \mathcal{F}^{-1}\{M(f_X, f_Y)P(f_X, f_Y)\} \tag{3}$$

where the symbol $\mathcal{F}^{-1}$ represents the inverse Fourier transform. The *aerial image* is defined as the intensity distribution at the wafer and is simply the square of the magnitude of the electric field.

$$I(x, y) = |E(x, y)|^2 \tag{4}$$

Although we have completely described the behavior of a simple ideal imaging system, we must add one more complication before we have described the operation of a projection system for lithography. So far, we have assumed that the mask is illuminated by *spatially coherent* light. Coherent illumination means simply that the light striking the mask arrives from only one direction. We have further assumed that the coherent illumination on the mask is normally incident. If light strikes the mask from another direction, the effect is simply to shift the position of the diffraction pattern with respect to the lens aperture. This is shown in Figure 3 (See *Inside PROLITH* chapter 2 for more information)

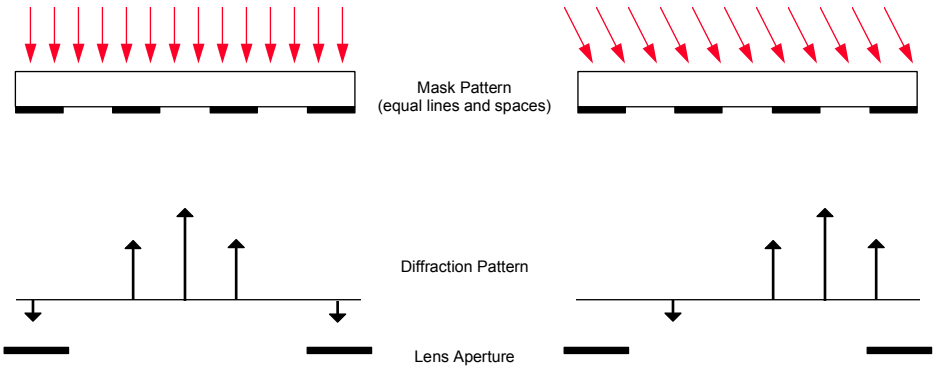

Figure 3: The effect of changing the angle of incidence of plane wave illumination on the diffraction pattern is simply to shift its position in the lens aperture.

Now we are ready to include the effects of aberrations in our model. Mathematically, aberrations are described as a *wavefront deviation*, the difference in phase (or path difference) of the actual wavefront emerging from the lens compared to the ideal wavefront as predicted from Fourier optics. This phase difference is a function of the position within the lens pupil, most conveniently described in polar coordinates. This wavefront deviation is in general quite complicated, so the mathematical form used to describe it is also quite complicated. The most common model for describing the phase error across the pupil is the *Zernike polynomial*, an infinite polynomial series, usually cut off at 36 terms, with powers of the radial pupil position *R* and trigonometric functions of the polar angle θ. The Zernike polynomial can be arranged in many ways, but most lens design software and lens measuring equipment in use today employ the fringe or circle Zernike polynomial. The first four terms of the polynomial are listed below:

$$W(R,\theta) = Z1*R*\cos\theta + Z2*R*\sin\theta + Z3*(2*R*R-1) + Z4*R*R*\cos 2\theta \qquad (5)$$

$W(R,\theta)$ is the optical path difference relative to the wavelength and Zi is called the ith Zernike coefficient. It is the magnitude of the Zernike coefficients that determine the aberration behavior of a lens. They have units of optical path length relative to the wavelength. The impact of aberrations on the aerial image can be calculated by modifying the pupil function of the lens to include the aberration phase error given by equation (5) (or its more complete form):

$$P(f_x, f_y) = P_{ideal}(f_x, f_y)e^{i2\pi W(R,\theta)} \qquad (6)$$

So, we have found that lens aberrations distort the image relative to the ideal case and the distortion can be accounted for by modifying the pupil function by a factor containing the Zernike polynomial expression of the phase error. For partially coherent sources, each broadened diffraction order will sample a range of positions within the lens. Now, we will use PROLITH to visualize these effects and examine how one type of aberration, coma, can affect image quality.

Procedure

To see how aberrations affect the image quality, open PROLITH with the default document template and modify or confirm the following parameters:

Mask:

Mask Type: 2D Parametric Five Bar
Nominal Feature Width: 400 nm
Pitch: 800 nm
Simulation Region Top: 0 nm
Simulation Region Bottom: -200 nm
Simulation Region Left: -2200 nm
Simulation Region Right: 2200 nm

Focus and Exposure:

Exposure 160 mJ/cm^2
Focus: 0.0 micron relative to middle of resist

Numeric View:

Speed Factor: 2

Run a simulation to generate the resist profile. In the Resist Profile window, change the following metrology parameters (this is a good time to experiment with these controls and learn what each of them alters):

ResistProfile:

Metrology Type: Y
Metrology Index: -100 nm
Start Position: -2200 nm
End Position: 2200 nm

Select the *Exchange Graphs* button and observe that the resist profile for the set of five bars as shown in Figure 4.

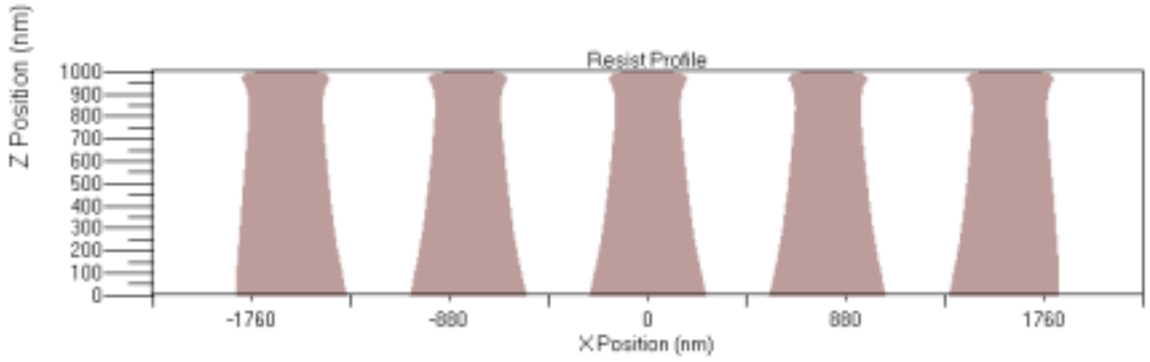

Figure 4: Slice showing resist profiles for all five bars without lens aberrations.

Note that only the center bar is symmetric. For the other four, the left and right sides of the resist profiles are different with the first and fifth bars showing the most asymmetry.

This asymmetry is caused by the proximity effect of the other bars and is not associated with any illumination system asymmetry or aberration.

Now, look at the first bar alone. To do this, change the following.

ResistProfile:

Metrology Type: Y
Metrology Index: -100 nm
Start Position: -2200 nm
End Position: -1100 nm

The first of the five bars is shown in Figure 5. It is easier now to see that the sidewall angle is different on the left and right sides. Make a note of the resist feature width.

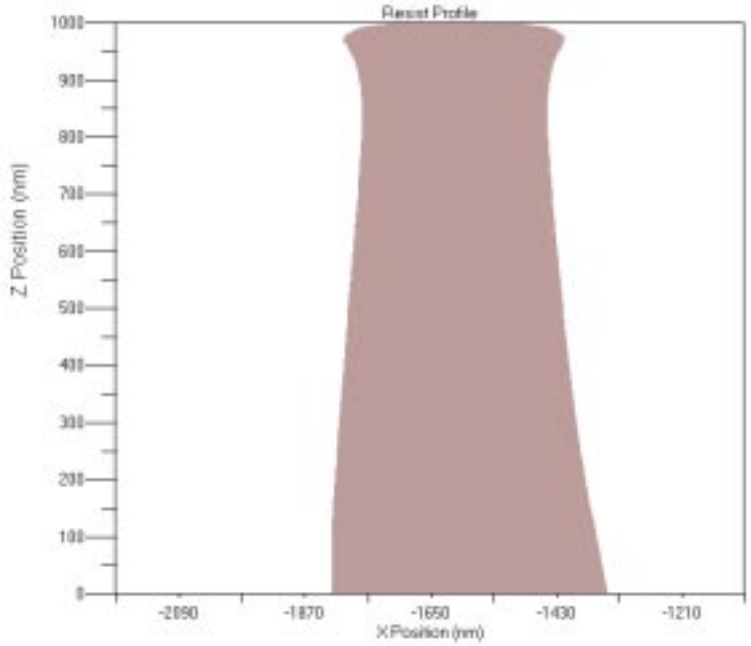

Figure 5: First bar of the five-bar pattern without lens aberrations.

Now, to examine the fifth bar, change the metrology parameters to the following:

ResistProfile:

Metrology Type: Y
Metrology Index: -100 nm
Start Position: 1100 nm
End Position: 2200 nm

Note the resist feature width. It should be identical to that of the first bar. Without aberrations, the imaging system itself is symmetric about the Y axis. As we have seen, other factors, such as proximity effects, can introduce asymmetries. Now we will introduce coma to the lens.

In the Imaging Tool window, change the following:

Imaging Tool:

Aberrations: Coma_20

When you do this, the graph portion of the window automatically changes to display the objective lens aberrations as shown in Figure 6 below.

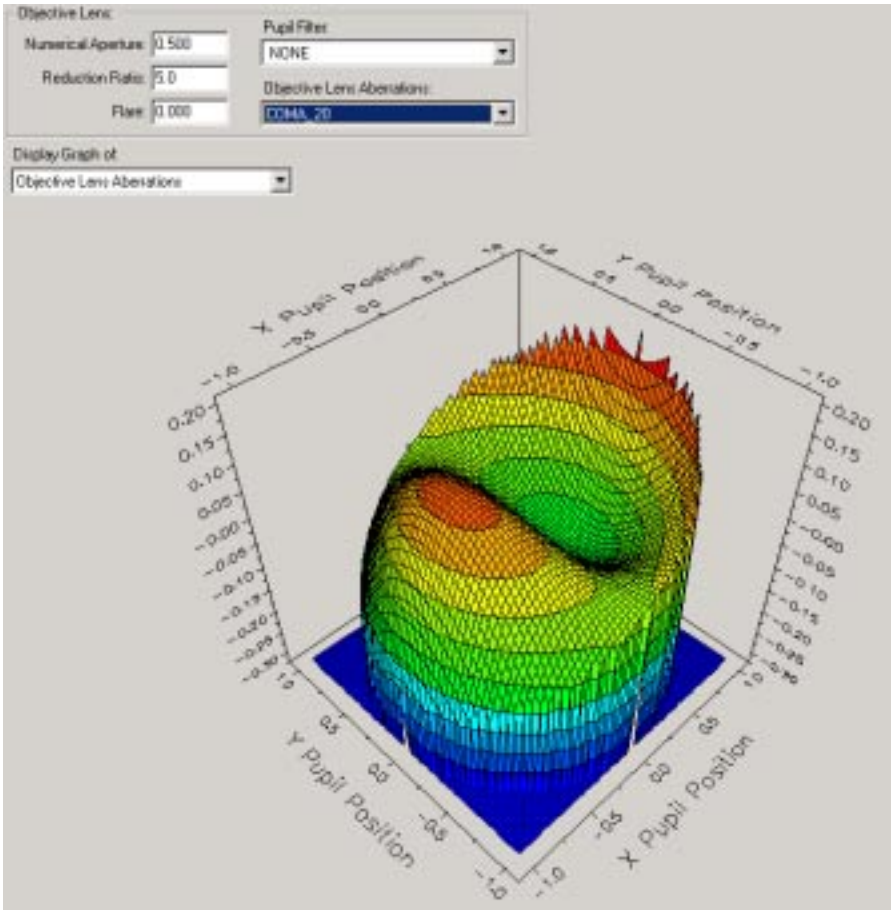

Figure 6: Graph showing the Optical Path Difference as a function of pupil position.

First observe that we have now introduced asymmetry into the lens system (in particular, a strong left/right asymmetry). We expect that the five bar pattern will now be asymmetric as well. Only the relative phase is important, so the differences in values (not the values themselves) should be noted. Note that along the Y axis (X=0) the phase is relatively constant. Along the X axis (Y=0) the phase varies greatly from a large positive value to a large negative value then back to positive. This is an indication that we would expect to see more of an effect with features oriented along the Y-axis and less of an effect with features along the X-axis. Let's now check these expectations by running simulations with coma. First, change the Exposure to 180 mJ/cm^2 (this will make the results a little easier to visualize).

Select the Resist Profile button and view a slice of the five-bar pattern by using the following metrology settings in the Resist Profile window:

ResistProfile:

Metrology Type: Y
Metrology Index: -100 nm
Start Position: -2200 nm
End Position: 2200 nm

Select the Exchange Graphs button and you will see the graph of Figure 7. The asymmetry is now very obvious. Note how the first and fifth bars are quite different. Even the center bar is asymmetrical. Now repeat the procedure above to view the first and fifth bars individually and record their resist feature widths. Note that the Resist Feature Width is no longer the same for the two bars (something that is obvious from Figure 7). This difference in CD between the leftmost and rightmost bars is a common effect of coma and can, in fact, be used as a measurement of coma.

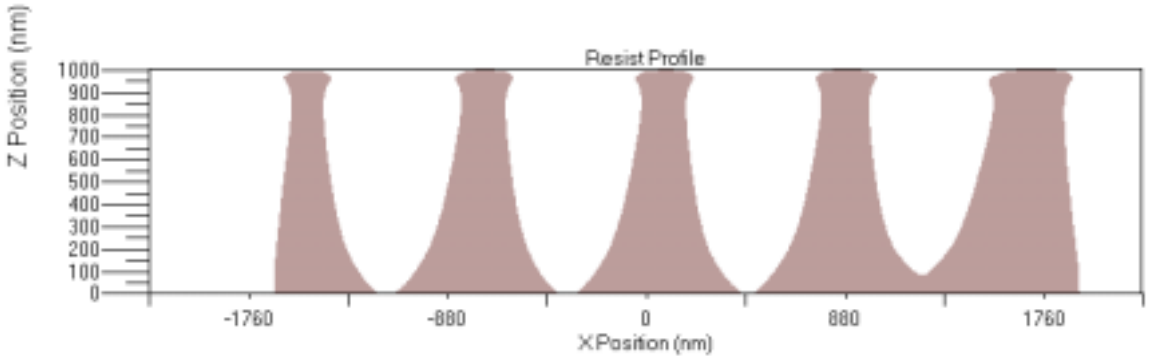

Figure 7: Cross section showing asymmetry caused by coma.

Now, let's check our expectation that the aberration effect will be less significant for features oriented in the X-direction. In the Mask window, select the checkbox labeled Rotate 90 degrees. Now, we have the same pattern but it is oriented along the X-axis. Use the Resist Profile button to complete the simulation. View a slice of the five-bar pattern by using the following metrology settings in the Resist Profile window:

ResistProfile:

Metrology Type: X
Metrology Index: 100 nm
Start Position: -2200 nm
End Position: 2200 nm

The result is shown in Figure 8. Note the difference between Figures 7 and 8.

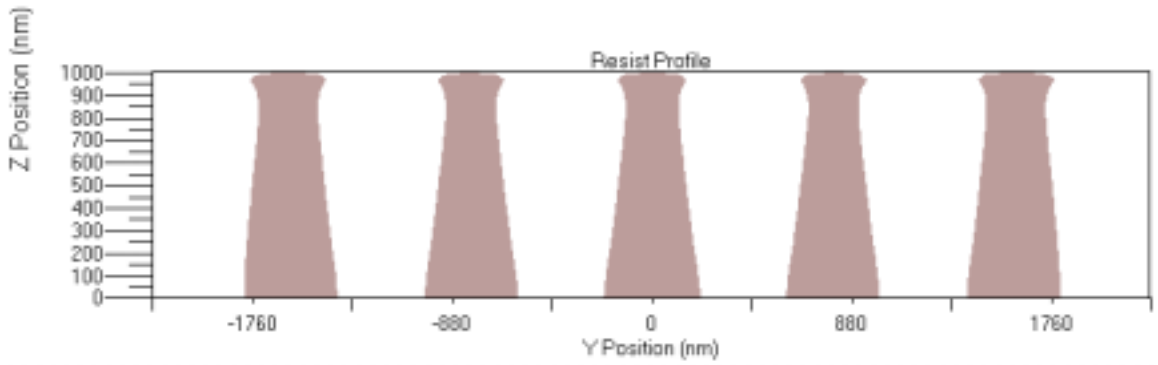

Figure 8: Five bar pattern oriented along the X-axis with coma.

Finally, let's look at the effect of coma on pattern placement. Set the following parameters for the simulation. ***Note: Remember to deselect the Rotate 90 degrees checkbox in the Mask window so the feature is oriented along the Y-axis***

Mask:

Mask Type: 1D Binary Parametric Line
Nominal Feature Width: 500 nm
Pitch: 1000 nm

Imaging Tool:

Aberrations: None

Use the Resist Profile button to complete the simulation. Since there are no aberrations, the image is symmetrical. Access the Metrology Results window and look for the Resist Placement Error at the bottom right of the results listing. It should be 0.00 nm. Now, repeat the above simulation with the following single change:

Imaging Tool:

Aberrations: Coma_20

Before you run the simulation, it is interesting to examine some of the graphs available on the imaging tool view. When you change the aberration to Coma_20, the graph on the imaging tool view should display the lens aberration shown in Figure 6. Change the graph from "Objective Lens Aberrations" to "Diffraction Pattern (Amplitude)". You should now see a graph displaying a diffraction pattern similar to the one shown on the left side of Figure 9.

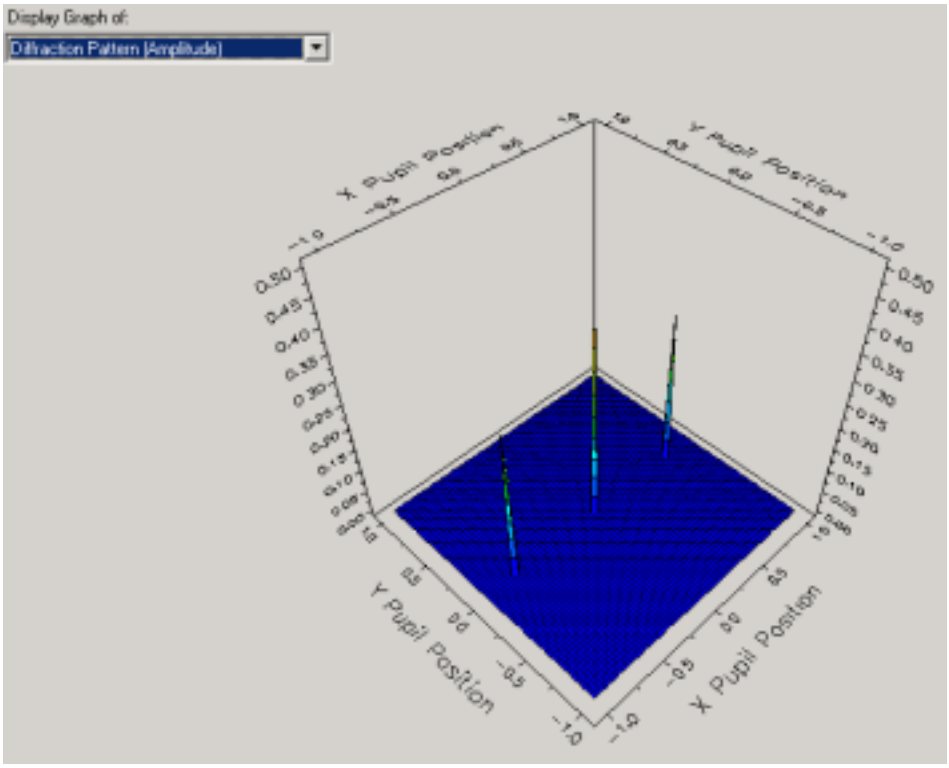

Figure 9: Amplitude of the diffraction pattern.

From the diffraction pattern and the graph of the objective lens aberrations, it should be apparent that the +/- 1 diffraction orders pass through the lens precisely where the lens aberrations are the largest. However, the partially coherent source shape broadens each diffraction order. This can be graphed on the imaging tool view by changing from the "Diffraction Pattern (Amplitude)" graph to the "Diffraction Pattern (Amp w/Source Shape)" graph, as shown in Figure 10.

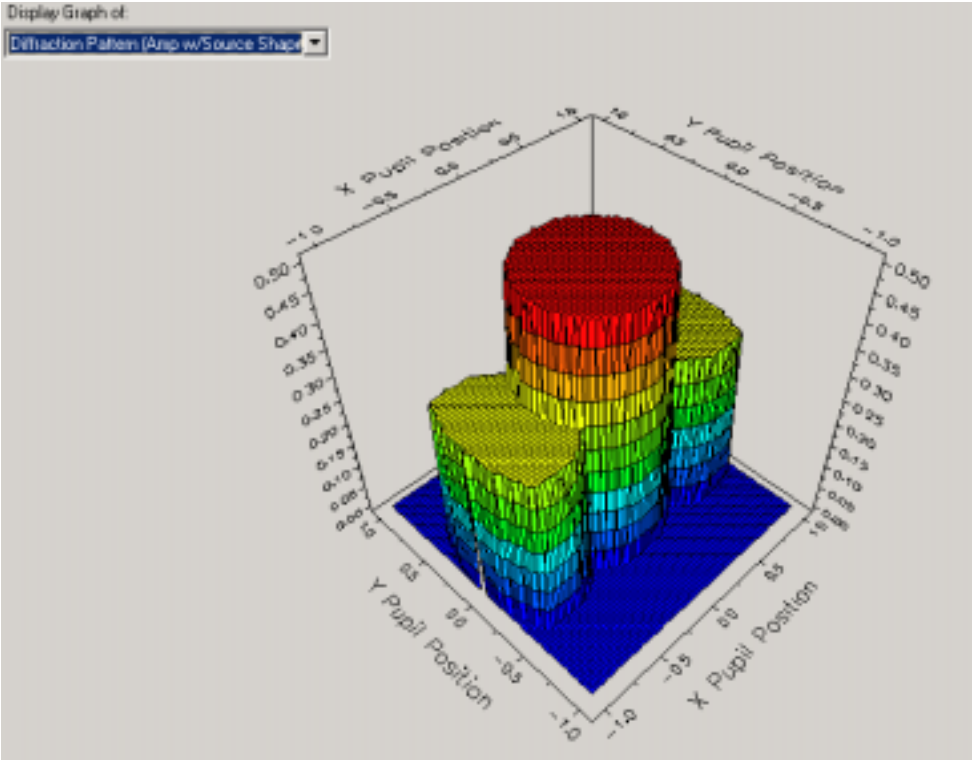

Figure 10: Diffraction pattern amplitude with source shape.

From this graph, you can see that much more of the lens is sampled by the diffraction orders, and that the resulting aerial image will reflect some "average" amount of coma since each diffraction order is spread over a region of the lens. Increasing the partial coherence can make the impact of aberrations better if the new regions of the lens have less wavefront deviation, but on the other hand, if the new regions have greater wavefront deviation, an increased value of the partial coherence might make the impact of aberrations worse (see Question 1 below).

View the resist profile. Can you see that it is shifted off axis? Record the Resist Placement Error. Coma introduces a pattern placement error that is pitch dependant. To see this, change the following parameter:

Mask:

Pitch: 1200 nm

Repeat the simulation and record the Resist Placement Error. The pitch changes the location of the diffraction orders going through the objective lens. By changing the pitch, the diffraction orders "sample" different areas of the lens and experience different phase shifts due to the varying coma aberration.

Summary

Lens aberrations are present in all systems and can affect image quality. They are modeled using the Zernike polynomial approach that allows us to look at individual aberration components. Coma can affect image placement and the can cause

asymmetries in resist images such as those observed in the five-bar pattern. The effects of coma depend on many variables including pitch and feature orientation.

Questions

See Appendix A for answers.

1. If increasing partial coherence causes the diffraction orders to spread out and sample more of the lens, would you expect that the effects of coma are exaggerated or reduced when partial coherence is increased? Can you explain this?
2. How would the introduction of the coma used in this workbook chapter affect the process window of a single feature oriented along the Y-axis? How would this change for the X-axis? Since masks generally have features in both orientations, how would one account for this using process window analysis?

Further Information

For further information, Chapter 2 of Inside PROLITH.

Chapter 9
Using the Yield Analyzer Option to Predict CD Distributions

Objective

This workbook example will explain how to calculate CD distributions with the Yield Analyzer Option in PROLITH, and how to use the results from this calculation to optimize a lithographic process.

Introduction

As the critical dimensions (CDs) of photolithographic processes continue to shrink, the processing of wafers becomes much more expensive and difficult. A result of these higher costs is the increased need to understand and control the CD distribution of lithography processes. Better control of the CD distribution will lead to higher yields and more favorable bin sorting of the final product.

It is possible to accurately predict the parametric CD yield of a photolithographic process using well-established lithography modeling tools. This workbook chapter describes the methodology and benefits of using the PROLITH Yield Analyzer Option to predict and analyze the CD distribution for a process. This methodology has proven to be an accurate and effective way to optimize a lithographic process. There are hundreds of types of optimizations that are possible using this methodology, a few of which are offered as examples in this chapter.

In this workbook chapter, you'll learn how to:

- Calculate a CD and reflectivity histogram for various errors in process parameters
- Define the CD limited yield of a process
- Evaluate the robustness of a process based on the C_{pk} of the CD distribution
- Use CD distributions to optimize a process and maximize yield.

Theory

To predict the parametric CD yield of a photolithographic process using the Yield Analyzer option, a simple three-step process is used, as shown in Figure 1. First, an analysis of a lithographic process must be performed to determine the error distributions of the input parameters. For example, it may be determined that exposure varies in a normal distribution with a mean at the nominal setting and a standard deviation of 5%. Second, PROLITH is used to create a multi-variable process response space (for

example, final resist critical dimension (CD) versus focus, exposure, resist thickness, etc.). Using a Simulation Set, the range of each input variable is chosen to completely cover the range of possible set points plus their errors. Third, by correlating the input error distribution with the process response space, a final CD distribution is generated. Analysis of the output distribution produces a predicted parametric CD yield using some acceptance criterion for CD. This number can be used to help optimize the yield of a given process.

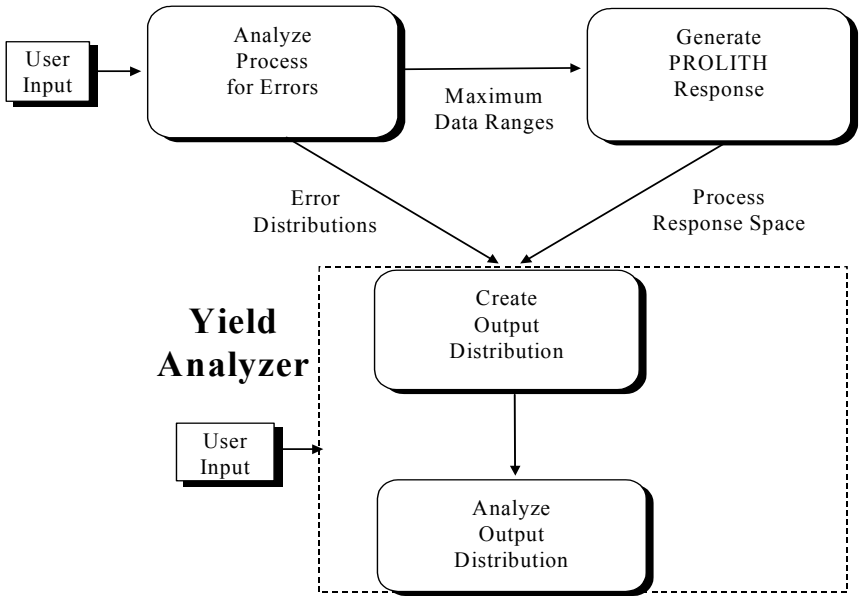

Figure 1: Methodology for using Yield Analyzer to predict and analyze lithographic distributions.

Consider a simple example to illustrate the method – the effect of exposure errors on line width. The process response in this case is the well-known exposure latitude curve. If the input error distribution is known, correlation of the input error probability with the process response function gives the output error distribution. For this example let us assume that the exposure errors are normally distributed about the mean with a 3σ of 10% (Figure 2).

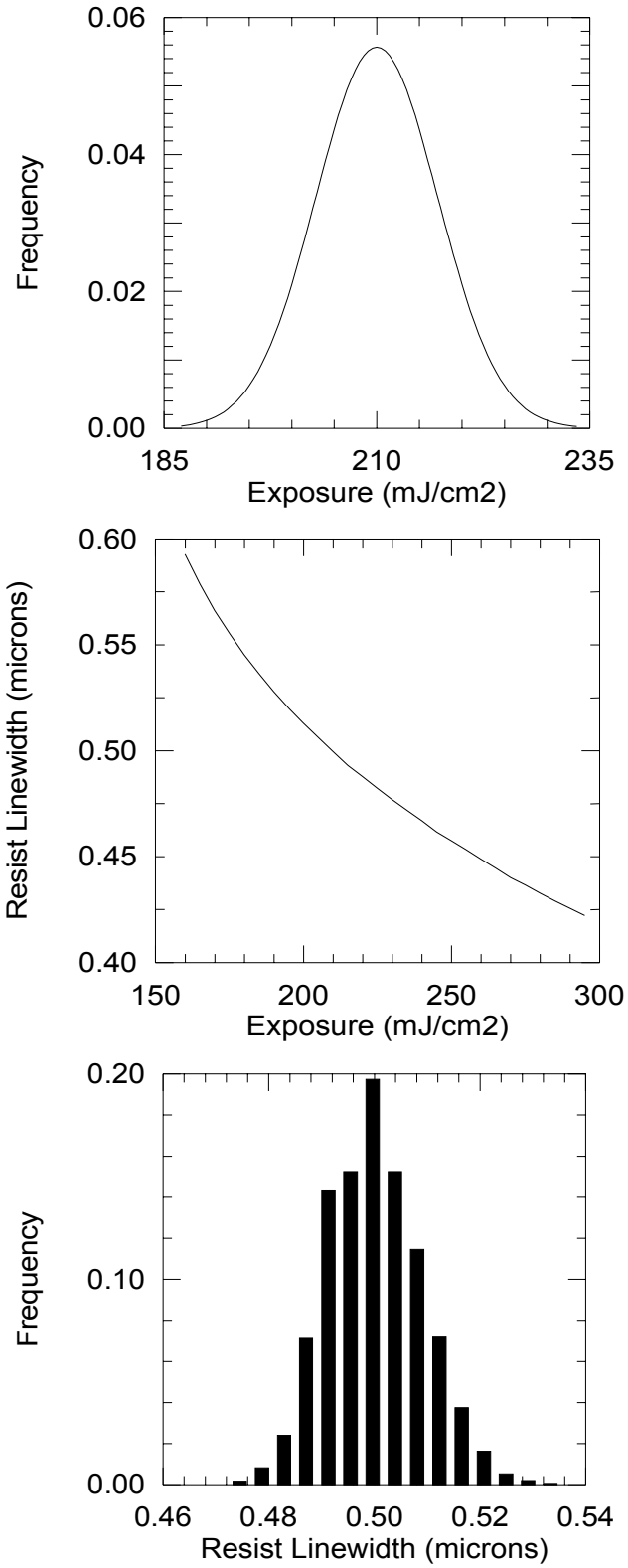

Figure 2: (Top) Input error function (Normally distributed exposure error determined by user) (Middle) Process response (Exposure latitude as determined by PROLITH) (Bottom) Output error (Resulting line width distribution calculated with Yield Analyzer)

The error distribution is plotted as the frequency of occurrence (or probability of occurrence) versus exposure energy with arbitrary units for frequency. The process response is line width versus exposure energy as predicted using PROLITH. For any given exposure energy, there is a probability that this energy will occur (for example, 200 mJ/cm^2 has a probability of 0.021 in Figure 2). From the process response curve, an exposure energy corresponds to a specific CD (for example, 0.513 μm for an energy of 200 mJ/cm^2) and thus must have the probability of occurrence corresponding to the probability of the exposure energy. Correlation of the input error distribution with the process response results in a list of line width values with corresponding frequencies of occurrence. The line width can then be divided up into equal size bins (for Figure 2, the bin size is 0.004 μm) and all of the probabilities with CDs within a given bin are summed. The result is plotted as a histogram of frequency versus CD and represents the resulting output CD error distribution.

Once a CD distribution has been predicted, the calculation of CD limited yield used here is straightforward. Given some CD specification (for example, the mean ±10%), the frequencies of all CDs within spec are summed and divided by the sum of the frequencies for all CDs to give the yield. Thus, CD limited yield is defined as:

CD Limited Yield = The fraction of CDs in the CD distribution that meets the CD specification.

The procedure described above and illustrated in Figure 2 is not limited to one input error variable. What if resist thickness and exposure energy were varying independently, but at the same time? For such a case, the 1-D analysis method can be easily extended to two dimensions. If the two input errors are independent (as is usually the case), their individual 1-D probability functions can be multiplied together to obtain a 2-D probability function. Figure 3 shows such a 2-D input error function assuming both exposure energy and resist thickness errors are normally distributed. Figure 3 illustrates the following equation:

2-D input error function * 2-D process response = Output error (1)

Where Figure 3a is the 2-D input error function, Figure 3b is the 2-D process response and Figure 3c is the Output error (Resulting Line width Distribution)

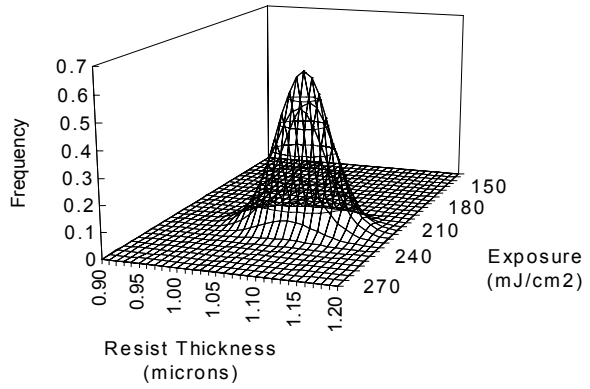

(a)

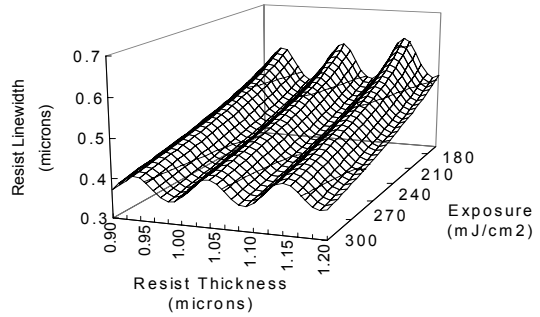

(b)

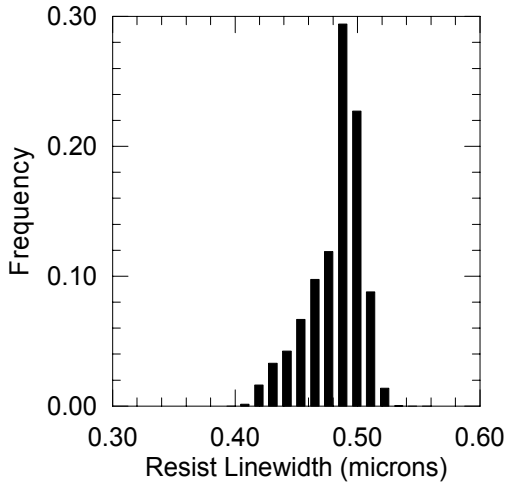

(c)

Figure 3. Two-dimensional error distribution taking into account both exposure energy and resist thickness errors.

Looking at the result (Figure 3), the distribution is skewed due to the swing curve, but is somewhat smoothed out due to the exposure errors. One extremely important result is that the mean of the CD distribution is not the nominal CD, even though the nominal CD would occur for the mean of the exposure and resist thickness distributions. The reason

for this is the non-linear nature of the process response. Note that we assume that the input error distributions are independent of each other. We do not, however, assume the inputs are independent with respect to the process response. Most inputs, such as exposure and resist thickness, are coupled in their effect on the resulting CD.

The power of the CD distribution method is its ability to investigate CD errors in the presence of multiple error sources. Figure 4(a) shows the results of an investigation of a 0.5 micron i-line process using four input variables: focus, exposure energy, resist thickness, and the development parameter R_{max} where R_{max} is the maximum development rate of the photoresist corresponding to completely exposed positive resist. The mean of the resulting CD distribution is 0.480 μm with a calculated yield of 87.7% based on a ±10% CD specification. The fact that the mean of the CD distribution is less than the nominal line width indicates that the nominal process is not "centered" despite the non-statistical evidence to the contrary.

One advantage to using the automated CD distribution analysis is the ability to easily perform optimizations. In the example in Figure 4, the mean line width of the nominal process is undersized by 4%. Could shifting the process result in an improvement in yield? Such a question can be easily answered using this type of analysis. To find the process that optimizes the CD limited yield, the mean of each of the four input errors was varied, keeping the 3σ values constant. Yield was calculated for each process condition. The best result, shown in Figure 4(b), used the same process as the nominal but with the exposure energy reduced by about 8%. This "under-exposure" shifted the mean line width up to the nominal line width and resulted in a significant increase in yield (to 94.8%).

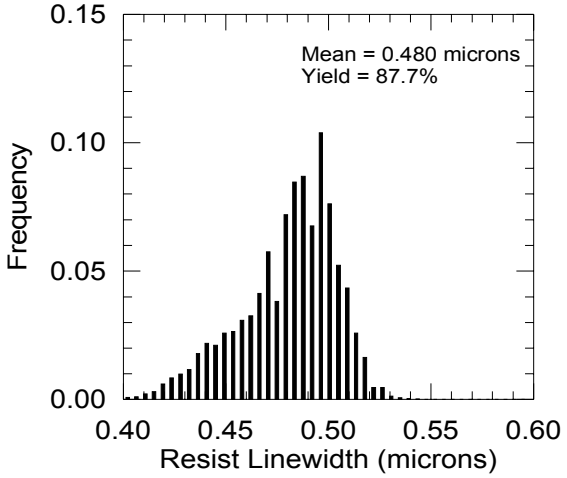

(a)

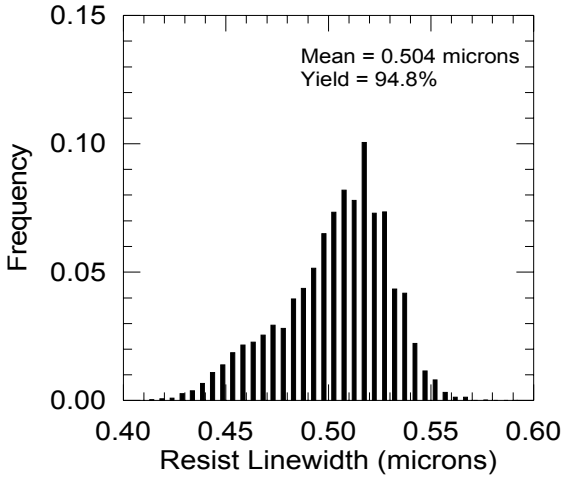

(b)

Figure 4. CD distributions from 4-dimensional process spaces at (a) nominal exposure and (b) nominal exposure minus 8%.

In addition to adjusting the mean of the CD distribution, another goal of distribution analysis is to find ways to make the standard deviation of the distribution smaller. The reason for doing this is obvious: if the process is properly centered, then a tighter distribution will lead to a smaller frequency of CDs falling outside of the CD specification range. This, of course, leads to higher CD limited yield. A convenient metric of the breadth of the distribution is the C_p statistic, which is the ratio of the range of acceptable CD values divided by 6 times the standard deviation of the CD distribution:

$$C_p = \frac{UpperSpecLimit - LowerSpecLimit}{6\sigma} \qquad (2)$$

However, a more commonly used statistic is the C_{pk} value, which incorporates both a measure of the "centeredness" of the process and the breadth of the distribution. The C_{pk} statistic is defined as

$$C_{pk} = (1-k)C_p \tag{3}$$

where the *k* variable describes the "centeredness" of the process:

$$k = \frac{2|TargetCD - \mu|}{UpperSpecLimit - LowerSpecLimit} \tag{4}$$

where μ is the mean of the CD distribution. With this definition, *k* is equal to zero if the process is exactly centered, and when the process is not centered, the factor of (1-*k*) will cause the value of C_{pk} to be less than the value of C_p. A robust process has a C_{pk} of at least 1.0. We will use both the CD limited yield and the C_{pk} statistic as a measure of the robustness of a process.

Procedure

In this example, we will use the Yield Analyzer Option in PROLITH to calculate the impact of variations in film stack thicknesses on the substrate reflectivity and on the resist CD. As outlined in the previous section, there are three steps to calculating output distributions with the Yield Analyzer, but we will skip the first step, where you characterize the errors in your process. Instead, we will make some assumptions about the size of the errors in the process, and then spend more time on the final two steps: setting up the PROLITH calculations and using the Yield Analyzer to calculate a reflectivity distribution and a CD distribution. Finally, we will show how to use the Yield Analyzer to optimize a process.

In PROLITH, set up the following input parameters. If a parameter is not specified, use the default value.

Film Stack:

Layer 1: 500 nm of Shipley UV6 Resist
Layer 2: 45 nm of Shipley AR2
Layer 3: 100 nm of Silicon Dioxide
Layer 4: Silicon substrate

Mask:

Mask type: 1D Binary
Feature type: Line
Nominal Feature Width: 180 nm
Pitch: 450 nm
Mask Bias: 0.0 nm

Imaging Tool:

Source Shape: Partially coherent
Partial Coherence: 0.5
Wavelength: 248 nm
Numerical Aperture: 0.63

Focus and Exposure:

Exposure: 11.3 mJ/cm^2
Focus: -0.2 microns

Post Exposure Bake:

Hotplate model: Ideal
Temperature: 130 degrees
Duration: 60 seconds

The next step is to generate a "response surface" that the Yield Analyzer will use in order to calculate the output distributions. You will be able to analyze errors in all of the input variables in the Simulation Set by calculating output distributions for any of the output variables in the Simulation Set. In this example, we will investigate the impact of errors in film stack thicknesses on the reflectivity of the substrate and the final resist CD.

When generating the response surface, you need to choose a range for the input variables that includes the set point (the mean value in the error distribution) along with any values that might arise due to process errors. For example, we will later describe the error in the oxide thickness with a Gaussian distribution centered at 100 nm with a standard deviation of 10 nm. Therefore, we chose the range for the oxide thickness as the mean minus 3 sigma (70 nm) to the mean plus three sigma (130 nm). In addition, the step size should be less than the standard deviation, so that you can accurately resolve the shape of the error distribution on the response surface. For the BARC thickness, we will choose a larger range so that we can use the Yield Analyzer to optimize the BARC thickness over a wide range of values. Set up the Simulation Set as follows:

Input Variables:

BARC thickness (layer #2): Min = 5, Max = 250, Step = 5
Oxide thickness (layer #3): Min = 70, Max = 130, Step = 5

Output Variables:

Reflectivity and Develop Groups

After you have launched and completed the calculation, go to the results tab and make a contour plot of the Substrate Reflectivity versus the thickness of layer #2 (BARC) and layer #3 (oxide), as shown in Figure 5. Notice that this plot can tell you which film stack layer thicknesses will minimize the substrate reflectivity. Suppose that the thickness of the SiO_2 layer is 100 nm. From the figure, the value of the BARC thickness (layer #2) that minimizes reflectivity is around 45 nm – if you examine the film stack settings listed above, you will see that this is what we have chosen as our nominal process. However, while this BARC thickness will minimize the reflectivity, it is not necessarily the thickness that is the least sensitive to errors in the oxide thickness and errors in the BARC thickness.

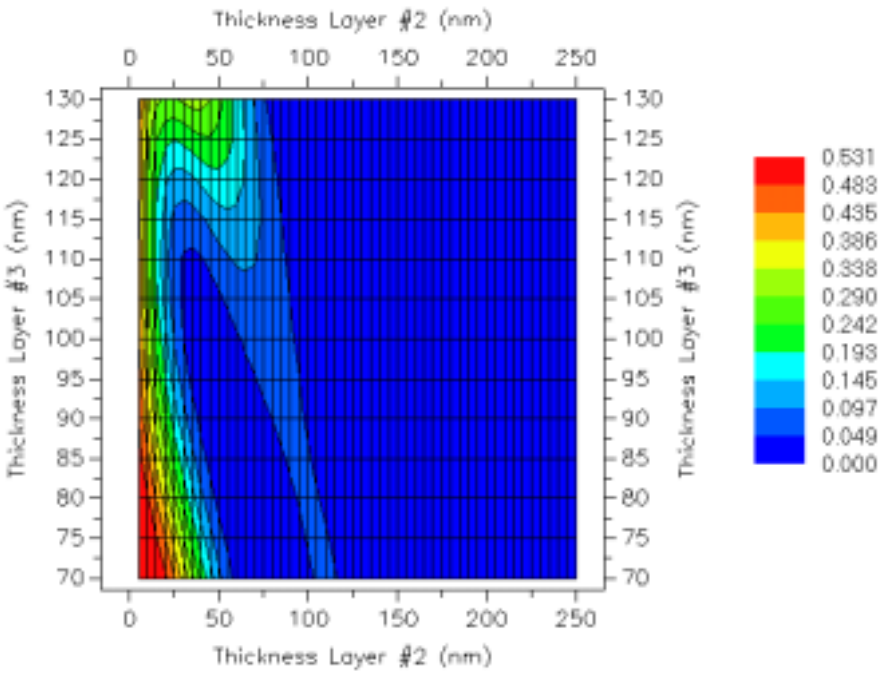

Figure 5: Substrate reflectivity as a function of AR2 BARC thickness (layer #2) and the SiO_2 thickness (layer #3).

The final step in using the Yield Analyzer to calculate output distributions is to choose the output variables that you want to study, and to describe the errors in those input variables. We will examine the impact of errors in Oxide thickness and BARC thickness on the substrate reflectivity and the resist CD, and then use these results to determine the optimal BARC thickness. As we will see, this optimized thickness is not necessarily the value that minimizes the reflectivity.

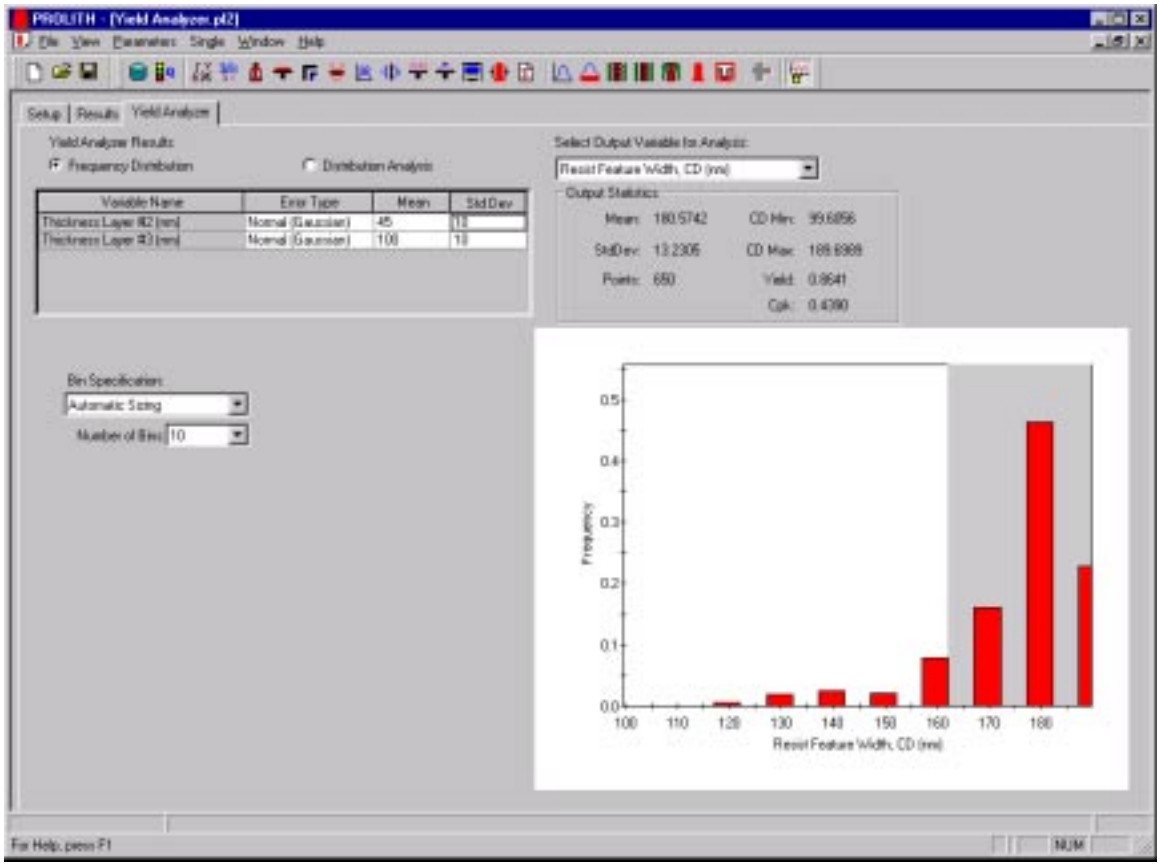

Figure 6: The Yield Analyzer tab, with Gaussian error distributions selected for the BARC and oxide thicknesses. Also shown is a predicted histogram for the resist feature CD that results from the BARC and oxide thickness input distributions.

Go to the Yield Analyzer tab, as shown in Figure 6. At the top of the tab is a spreadsheet-like table where you can describe the errors in each of the input variables to your simulation set. In this example, we can look at errors in BARC thickness and Oxide thickness. Set the entries as follows:

Variable	Error Type	Mean	Std Dev
Thickness Layer #2	Normal (Gaussian)	45	10
Thickness Layer #3	Normal (Gaussian)	100	10

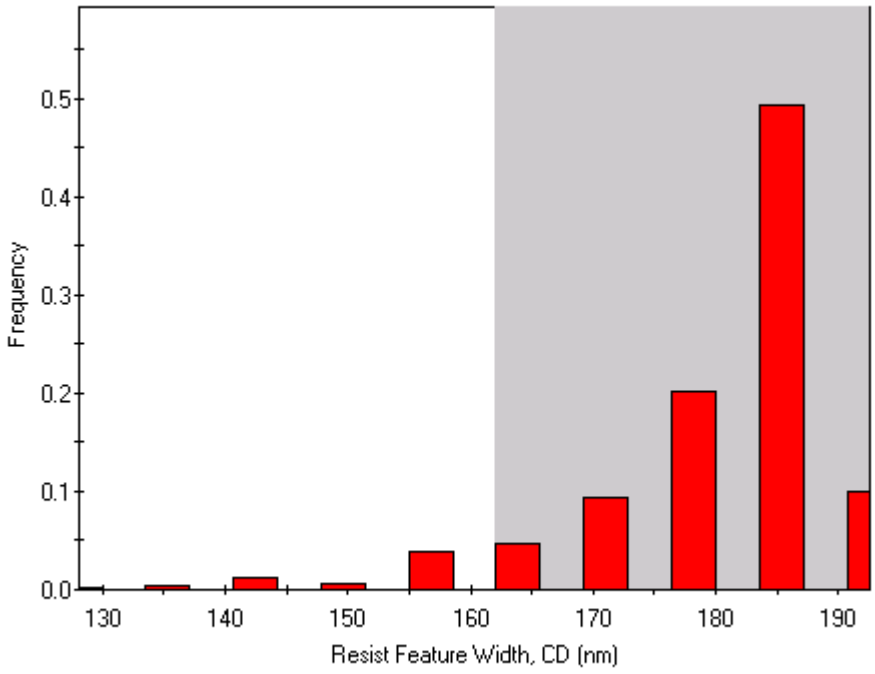

Figure 7: CD distribution for BARC thickness errors with a standard deviation of 5 nm. The oxide thickness errors have a standard deviation of 10 nm. The CD limited yield is 93.3% and the C_{pk} is 0.47.

After you have set the input error distributions, you get an output histogram of any of the output variables in your simulation set. Change the Output variable to be Resist Feature Width. You will now get the histogram shown in Figure 6. The histogram shows the probability of getting a particular CD value. For example, the red bar around CD=160 shows that about 5 to 10% of the CDs will be about 160 nm, even though we are trying to make 180 nm lines.

The gray box on the histogram shows the range of CD values that are within the CD specification on the Metrology input view. Notice that the histogram shows that many of the CDs fall outside of the CD specification – this indicates you have a low yield. Directly above the histogram is a group of Output Statistics. Among the calculated statistics are the mean of CD distribution, the standard deviation of the CDs, the CD Limited Yield, and the C_{pk}. The mean value is 180 nm, which indicates that the process is well-centered, but the standard deviation is 13 nm, which leads to low values for the CD limited yield and C_{pk} – the CD limited yield is 86%, and the C_{pk} is 0.44.

You can also change the granularity of the histogram by adjusting the "Number of Bins" on the left side of the screen. With "Automatic Sizing" of the bin size, you can select a different number of bins. If you choose "Manual Bin Settings", you can change both the number of bins and the size of the bins to customize the CD histogram. These graph customizations do not impact the values of the statistics displayed above the histogram

plot, because the statistical values are calculated directly from the input error distributions and the simulation set response surface.

Now that we have calculated a CD distribution, it is interesting to see which input variables have the biggest impact on yield and C_{pk}. For this example, we can look at whether reducing errors in the BARC thickness or errors in the oxide thickness will increase yield more. First, change the standard deviation for the thickness of layer #2 (the BARC thickness) from 10 to 5. The resulting CD distribution is shown in Figure 7. Notice that the yield goes up to 93%, but C_{pk} only goes up to 0.47. Next, examine the impact of oxide thickness errors. Change the standard deviation for the BARC back to 10, and change the standard deviation for layer #3 (the oxide) from 10 to 5 nm. We obtain about the same results – the yield goes up to 94%, but the C_{pk} remains low at 0.49.

From this analysis, it looks like C_{pk} does not improve much, even if we reduce the errors in the film stack. Can we choose a BARC thickness that improves yield and C_{pk}? We can investigate this with a "Distribution Analysis". A Distribution Analysis allows you to make plots of the statistics related to the CD histogram as a function of the set points (mean values) of the input variables. We will use these plots to maximize the CD limited yield and the C_{pk}. However, if we want to look at a large range of BARC thicknesses, it is possible that there will be a different optimal dose value for each BARC thickness. For this reason, we will optimize the breadth of the distribution separate from the mean of the distribution, and after we find a BARC thickness that reduces the standard deviation of the CD distribution, we can "re-center" the process by choosing a different exposure dose.

The first step is to set the standard deviation for the oxide thickness back to 10 nm. Next, click on the radio button labeled "Distribution Analysis", and then create a graph of standard deviation of the CD distribution versus the set point (mean value) for the BARC thickness. To do this, select Standard Deviation as the y-axis variable, and select Thickness Layer #2 as the x-axis variable. The resulting plot is shown in Figure 8. From the plot, we see that the standard deviation of the CD distribution goes to zero for very large BARC thicknesses. This physically makes sense, because we are only analyzing errors in the oxide thickness and in the BARC thickness, and eventually the BARC becomes so thick that errors in these parameters become unimportant. We do not want a BARC that is too thick, because this will lead to problems with our etch process. From the plot, it looks like 140 nm is thick enough, since the standard deviation is less than 2 nm for this thickness.

The next step is to make sure that the process is still well-centered with a BARC thickness of 140 nm. To do this, change the Standard Deviation plot to a plot of the mean of the CD distribution by choosing "Mean" as the y-axis variable. As shown in Figure 9, the mean of the CD distribution is around 180 nm for a BARC thickness of 140 nm, so the process should remain centered if we change the BARC thickness. Finally, we can evaluate both the breadth of the distribution and centeredness by plotting C_{pk}. Again, do this by changing the y-axis variable in the Distribution Analysis plot, and you should get the result shown in Figure 10. The local maximum in C_{pk} for a BARC thickness of 140 nm confirms that our new process is tighter and well-centered.

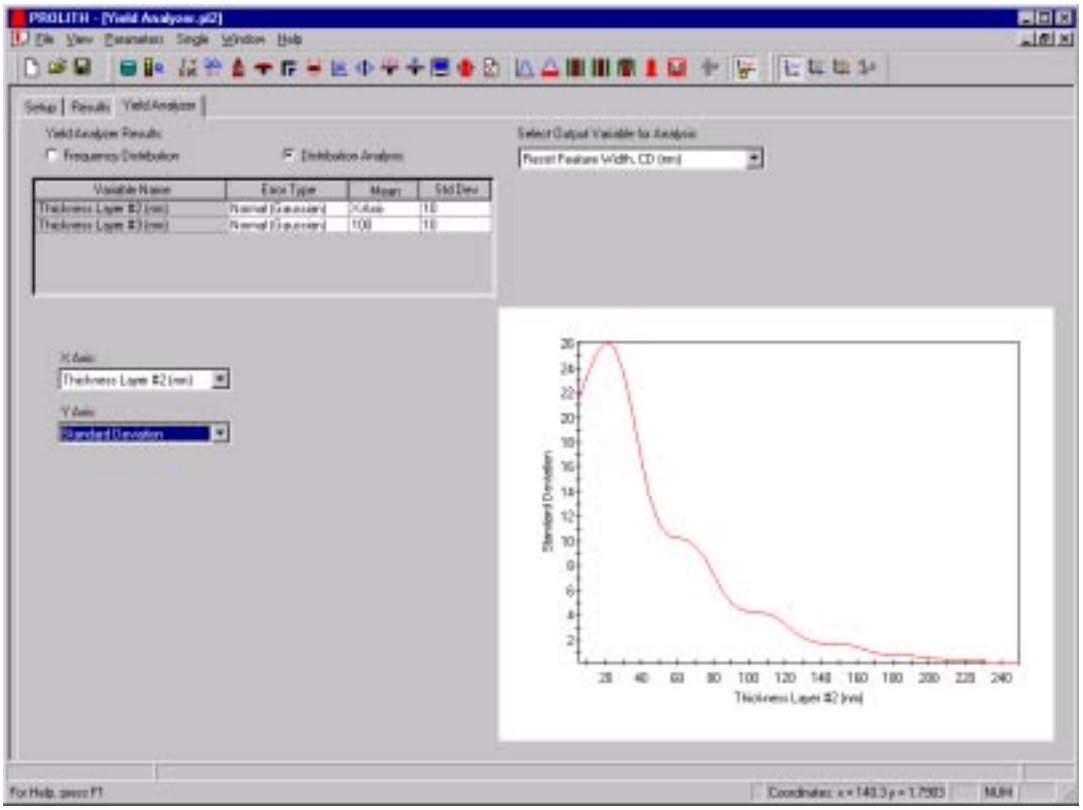

Figure 8: Distribution analysis of standard deviation of the CD distribution as a function of the nominal BARC thickness.

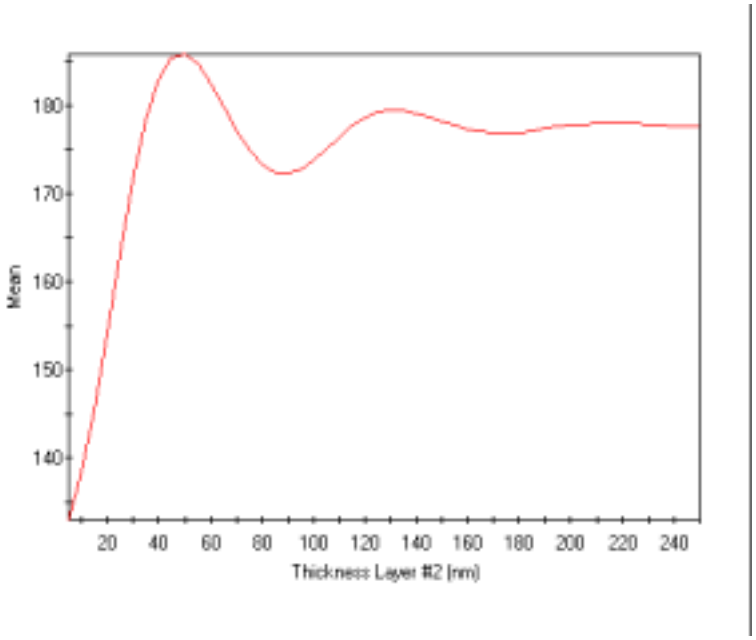

Figure 9: Distribution analysis of the mean of the CD distribution as a function of nominal BARC thickness.

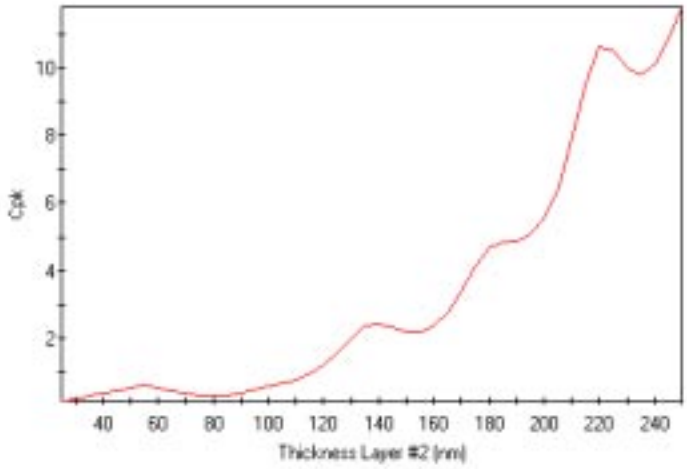

Figure 10: Distribution analysis of Cpk as a function of the nominal BARC thickness.

Click on the "Frequency Distribution" radio button, and return to the CD histogram. Change the mean value for the thickness of layer #2 (BARC) to 140 nm. Notice that the Yield is now 100% and C_{pk} is now 2.32. Next, examine the impact of reducing your film stack errors. We already performed this investigation for our original process – except now we will see better results for the improved process. First, change the standard deviation for the thickness of layer #2 (BARC) from 10 to 5. Notice that the C_{pk} goes up to 3.00. Next, change the standard deviation for the BARC back to 10, and then change the standard deviation for layer #3 (oxide) from 10 to 5 nm. Now the C_{pk} goes up to 3.16. From this analysis, we find that we have a process that is much less sensitive to errors, and a process that can be more dramatically improved when we reduce the errors in the film stack thicknesses.

You can perform this type of analysis for any set of PROLITH input variables, and view results for any output variable. For example, we can look at a histogram of substrate reflectivity. To do this, change the output variable from Resist Feature Width, to Substrate Reflectivity. For the new process, the standard deviation for the reflectivity distribution is 0.0064. If you return to the BARC thickness of 45 nm, then the standard deviation of the reflectivity distribution is 0.0428. This just re-emphasizes that increasing the BARC thickness makes the substrate reflectivity less sensitive to errors in your film stack.

Summary

The Yield Analyzer allows you to examine the impact of errors on your process. We have used the CD limited yield and the C_{pk} metrics to optimize a BARC thickness so that our process is less sensitive to variations in the BARC thickness and the thickness of the underlying oxide. This powerful technique can be used to optimize any process and improve CD limited yield and C_{pk}.

Questions

See Appendix A for answers.

1. When optimizing a BARC, it is very common to calculate the substrate reflectivity as a function of BARC thickness, and then choose one of BARC thickness values that minimizes the substrate reflectivity. Perform this analysis for the film stack in this chapter. Where are the initial and optimized BARC thicknesses on this curve?
2. Use the Yield Analyzer to find the optimal BARC thickness when there are no errors in the oxide thickness, but there are errors in the resist thickness. For the error distribution in the resist thickness, use a mean thickness of 500 nm and a standard deviation of 10 nm. Perform a distribution analysis and look at the standard deviation of the CD distribution as a function of BARC thickness. Where are the minimums in the standard deviation compared with the reflectivity minimums you calculated in question 1?
3. Find the optimal BARC thickness when errors are present in the oxide, BARC, and resist thicknesses. How do these results compare with the results in this chapter, and the results found in the questions above?

Further Information

For further information on the application of statistical process control to lithography, see

Lithography Process Control, by Harry J. Levinson, SPIE Press (1999).

Further examples of the Yield Analyzer can be found in the paper

"Yield Modeling and Enhancement for Optical Lithography," by C.A. Mack, and E.W. Charrier, *Proc. SPIE,* **2440** (1995) pp 435-447.

Chapter 10
Speed and Accuracy of PROLITH Simulations

Objective

In this example, we will consider the effects of the Speed Factor on simulation accuracy, and the tradeoffs that a user must make between speed and accuracy when running PROLITH simulations.

Introduction

The Speed Factor (specified on the Numerics View) has a direct influence on the lithography simulations performed by PROLITH in many ways. The first and most obvious influence of Speed Factor is on the number of grid points in the simulation volumes (the simulated 3D spaces that cover the wafer and resist). But the Speed Factor also determines the number of wavelengths used in broadband illumination calculations, the grid used to calculate the point spread function, the number of points used to define an illumination source, the maximum number of diffraction orders used for incoherent illumination calculations, etc. Through these mechanisms, the Speed Factor controls both the simulation speed and accuracy.

In this workbook chapter, you'll learn how to:

- Set the Speed Factor for a PROLITH simulation;
- Insure that your Speed Factor selection allows a valid simulation to be performed.
- See the influence of Speed Factor on both the speed and accuracy of the simulations performed;
- Choose a Speed Factor to maximize the efficiency of your PROLITH simulations.

Theory

Number of grid points along each axis of the simulation region - From the number of grid steps along each axis of the simulation volume and the size of the simulation region specified on the mask, the actual grid step size is calculated as:

grid step size = (simulation region size) / (number of grid points – 1)

It is this grid step size that has the most direct influence on accuracy. In particular, we can not examine features smaller than the grid step size. In fact, the desired feature size should be at least a few grid steps in width. Conversely, having a grid spacing that is much smaller than the relevant feature size makes the simulation slower than is required.

The number of grid points on each axis of the simulation volume is determined by the Speed Factor, and is set on the numerics view. The number of steps for a given Speed Factor is shown in Table 1:

Speed Factor	1	2	3	4	5	6	7	8
Number of Steps	301	201	141	101	71	51	37	27

Table 1: Number of steps for a given speed factor.

Number of wavelengths for broadband illumination - Whenever the wavelength range set in the *Imaging Tool* view is greater than 0, broadband calculations are performed that calculate images in resist for different wavelengths. Using the illumination spectrum (or a flat spectrum if NONE is specified), calculations are performed at specific wavelengths in the range. The number of wavelengths is determined by the Speed Factor according to Table 2.

Speed Factor	1	2	3	4	5	6	7	8
Number of Wavelengths	21	17	13	11	9	7	5	3

Table 2: Number of wavelengths for a given speed factor.

Point spread function - When calculating the point spread function (PSF) from the Imaging Tool view, the 2D image simulation volume is set separately from the normal single run volumes. The number of steps in both X and Y are set according to Table 3.

Speed Factor	1	2	3	4	5	6	7	8
Number of X and Y Steps	101	81	61	51	41	31	27	23

Table 3: Number of X and Y steps for a given speed factor.

Number of source points - The number of source points used in the source integration for High NA Scalar, Full Scalar, and Vector imaging models is determined by the Speed Factor and the source shape. First, a square grid is set up over the full potential size of the source (from –1 to 1 in relative pupil coordinates). The number of grid points on each side is given by Table 4.

Speed Factor	1	2	3	4	5	6	7	8
Number of Source Grid Points	101	63	51	41	35	31	25	17

Table 4: Number of source grid points for a given speed factor.

Second, the source shape is overlaid on this grid and the number of grid squares that overlap the source shape determines the actual number of source points used in the image calculations.

For the Standard (Low NA) image calculation mode, the integration over the source is analytic in the Y dimension. Therefore, only the number of source steps in the x direction is determined by the Speed Factor, as shown in Table 5.

Speed Factor	1	2	3	4	5	6	7	8
Number of Source X Grid Steps	300	200	150	120	80	60	40	30

Table 5: Number of source steps in the x direction for a given speed factor.

Number of diffraction orders used for incoherent illumination - For isolated or near isolated mask patterns, there are a very large number of possible diffraction orders in the diffraction pattern. However, only those orders that can make it though the objective lens need to be calculated. This number is a function of the wavelength and the numerical aperture, but is also a function of the size of the source (the larger the source, the more diffraction orders get through for certain source points). For incoherent illumination, the size of the source is infinite and, therefore, all possible diffraction orders affect the image. However, any practical calculation must limit the number of diffraction orders used. For this reason, PROLITH limits the size of the source for the purposes of calculating and using the diffraction pattern according to Table 6 (in "sigma" units):

Speed Factor	1	2	3	4	5	6	7	8
Incoherent Source "Effective Radius"	100	71	50	45	32	20	14	10

Table 6: Incoherent source "Effective Radius" for a given speed factor.

Number of focus steps for image in resist - When calculating the image in resist for Standard and High NA Scalar image calculation models, the aerial image is calculated at several focal planes within the resist. The number of focal planes used (and thus the number of aerial images that are calculated) is a complicated function of the Speed Factor and the estimated DOF of the image. It is determined at runtime.

Procedure

Changing the Speed Factor is a simple matter in PROLITH. Go to the Numerics View by pressing the Numerics toolbar button or selecting "Numerics" from the Parameters menu. In the Speed Factor box, move the slider control to select the desired Speed Factor. The main Speed Factor sets all of the items discussed above as well as the size of the X and Y grids. The Alternate Z Speed Factor can be set to independently vary the grid size in the Z direction. Here we have selected Speed Factor 4.

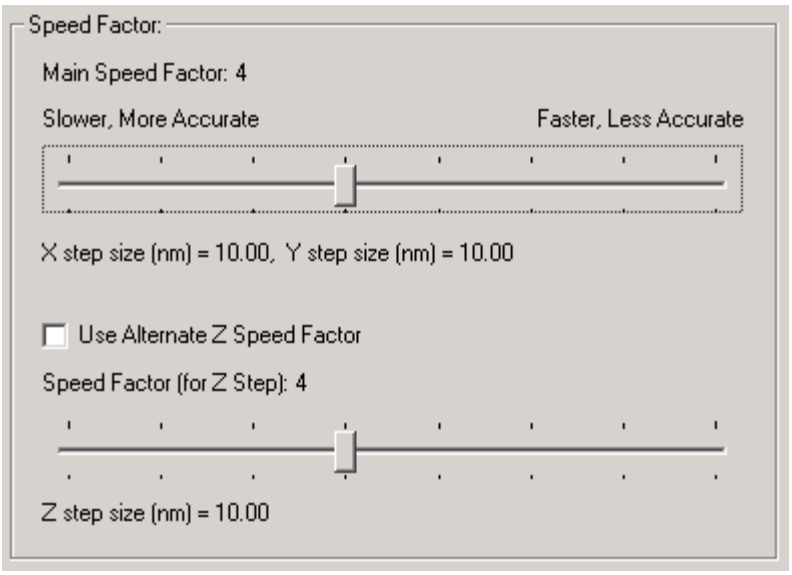

Figure 1: Adjusting the speed factor.

Notice that PROLITH says Speed Factor 4 corresponds to a 10 nm grid. If we looked at the Mask View, we would find that the Simulation Region was a 1 micron box (1000 nm):

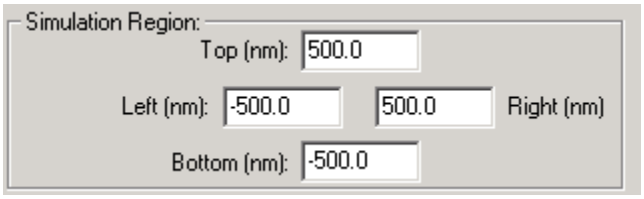

Figure 2: The simulation region.

From Table 1, we know there are 101 grids in a Speed Factor 4 Simulation Volume, and thus the Grid Step Size is: 1000 nm / (101-1) = 10 nm, as PROLITH has indicated. One of the most important facts to keep in mind as we run simulations is this: ***the simulator can never resolve features smaller than the grid size***. This will be true even if the "feature" of interest is a standing wave corrugation on a resist profile. Thus, the size of the features you are interested in dictate the maximum Speed Factor and simulation region size that should be used. Ideally, any spatial feature of interest should be many grid spacings in size.

From a practical standpoint, insuring that the grid is appropriately scaled is vital to the simulations. Once that restriction is met, it is likely that the other parameters controlled by the Speed Factor will be set to an acceptable value. You can always use the data in Tables 1-7 to insure your requirements are met.

Maximizing Simulation Efficiency - We have learned in the preceeding sections that the Speed Factor affects many different simulation parameters. We have placed some limits on the maximum acceptable Speed Factor setting. But let's suppose that we are considering a simulation for which all Speed Factors meet the minimal acceptable

requirements (several grid points per feature). How are we to choose which Speed Factor to use?

Let's take a concrete example. Open a new PROLITH document, and make the following changes:

Film Stack:

Layer 1: 800 nm of SPR 500
Layer 2: Silicon substrate

Mask:

Mask type: 2D Parametric
Feature type: Line End Shortening - Tee
Feature Width: 250 nm
Gap Width: 300 nm

Imaging Tool:

Wavelength: 365 nm
Numerical Aperture: 0.6

At Speed Factor 8, the grid spacing is 38.46 nm. This gives at least 6 grids (=250 nm/38.46 nm) in the smallest feature dimension that we are concerned with. This is on the minimal side, but may still be acceptable. At Speed Factor 1, we'd get 75 grids in the 250 nm feature width, more than enough for an accurate simulation.

In the figure below, we see the results of this simulation run using Speed Factor 8 and Speed Factor 2. The basic information obtained in each run is approximately the same. There is more faceting of the resist in the Speed Factor 8 simulation, characteristic of the larger grid. The gap between the lines measured at Speed Factor 8 is 442.3 nm, where in the Speed Factor 2 simulation, the result is a more accurate 455 nm, a difference of 12.7 nm, or 2.8%. It may be that the Speed Factor 8 result is good enough for our purposes, and it does run much faster—seconds instead of minutes. Or it may be that the higher accuracy is required.

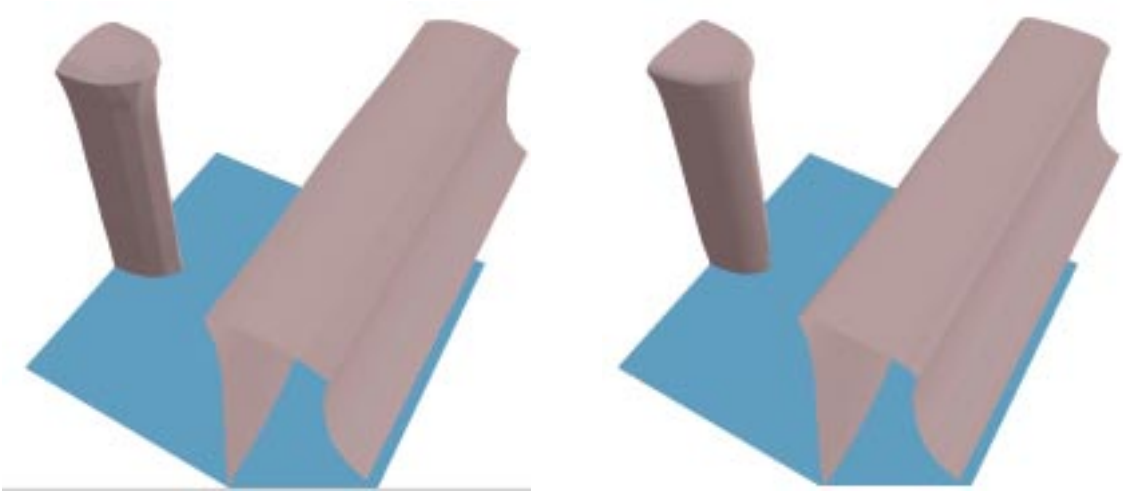

Figure 3: Resist simulation with speed factor variation. Speed Factor 8 (left) and Speed Factor 2 (right).

In the end, you must judge for yourself how much error is tolerable. Because of the complexity of the simulations, no hard rules apply, but some estimates can be made. In the following table, we present a very approximate comparison of speed and accuracy. To generate the table, we ran about 250 simulations covering a wide variety of lithographic parameters using all 8 Speed Factors. An average speed increase and relative error in the final stage (Resist CD) was then calculated for each simulation (errors in earlier stages will be smaller). Everything in the table is relative to the Speed Factor 1 simulation, which, by definition, is our slowest and most accurate result. The speed increases are given as a multiplicative factor and the error is a relative error assuming that the Speed Factor 1 result was exact. Thus a Speed Factor 6 simulation runs about 210 times faster than a Speed Factor 1 simulation, and gives approximately 3.9% more error. Because of the nature of the averaging, and the wide variety of PROLITH simulation parameters, any given simulation is not likely to follow these numbers exactly, but the table still offers some guidance.

Speed Factor	1	2	3	4	5	6	7	8
Relative Speed Increase	1.0	2.9	10	19	63	210	460	1000
Average Relative Error (Resist Feature Width)	0.0	0.20%	0.71%	0.99%	1.9%	3.9%	5.9%	11%

Table 8: Approximate trade-offs between speed and numerical accuracy for the various speed factors.

Summary

We have given an explanation of the Speed Factor for PROLITH simulations. We have seen how to change the Speed Factor, and have learned what effects changes have on various aspects of the simulation. We have included in Tables 8 a quick guide for comparisons between speed and accuracy.

Questions

See Appendix A for answers.

1. How much slower would you expect a Speed Factor 3 simulation to be than a Speed Factor 6?
2. Why would we expect the errors in Resist Feature Width to be larger than the errors in Image CD?
3. Does the same Speed-and-Accuracy relation which occurs for Single Simulations also hold for Simulation Sets?
4. My machine is drastically slower at low speed factors than the results in Table 8 indicate. What could be causing this?

Further Information

You can find more information about the internal workings of PROLITH in the book *Inside PROLITH* by Chris Mack. The following technical publications may also be helpful for understanding simulation and its limits:

Chapter 11
Etch Simulation for Lithographers

Objective

In this example, we will describe the inputs to the etch simulator and consider its abilities and limitations. Describe the process for matching an etch simulation to experimental cross-sectional SEM data. Briefly describe the process for tuning and using 3D etch simulations.

Introduction

Traditional lithographic simulations begin with a design layout and model the optical and chemical processes involved in reproducing the design as a 3-dimensional photoresist pattern. What we are really after, however, is information about the pattern, as it would appear in silicon. To achieve this goal, we devise an etch algorithm whose inputs include a full lithography simulation and minimal information about an intended etch process. Namely, we take as inputs the horizontal and vertical etch rates for each material in the film stack, the angular distribution of the incoming ion flux, and possibly a fitting coefficient for physical sputtering processes. We then produce a set of output metrics-before and after etch-including the CD, sidewall angle, resist loss, etch depth, etc.

Theory

The PROLITH etch simulator treats the surface of the filmstack in an etch process as an advancing wavefront. This interface moves perpendicular to itself with a speed that depends on the materials that make up the filmstack, on the shape of the profile, on the etch process, etc. That is to say, the position of the interface advances in time according to the specified material etch rates and the shape of the evolving profile.

To minimize the complexity of the etch simulations, we have lumped all of the physics into a few simple parameters - the kinds of parameters that can be obtained from a series of cross-sectional SEM images. We do not attempt to calculate etch rates from plasma chemistry, ion energies, and film stack materials. Instead, we take measured etch rates for each material in the film stack. For plasma etching, we take the flux of incoming ions to be a simple distribution - either uniform and purely vertical, or with a Gaussian profile in the flux angle about the vertical. Using the ion flux information, we compute visibility and shadowing effects. Materials exposed to the ion source directly etch faster than those hidden from the source. We also treat the nonlinear angular dependence of the physical sputtering yield with a single, materially dependent, fitting parameter.

In detail, the full inputs to the PROLITH etch simulator are:

Resist Profile:

A full resist profile from a PROLITH simulation(either 2D or 3D).

Etch Rates:

The etch rates for each material in the film stack in both the horizontal and vertical directions measured in nanometers per second. For plasma etching, the full vertical rate is applied to regions of the surface which are fully exposed to the ion source. The horizontal rate is applied to the entire surface. Because the surface always moves perpendicular to itself with a rate equal to the combined horizontal and vertical rates, the vertical rate can be thought of as the anisotropic etch rate, and the horizontal rate as the isotropic rate. This also means that to simulate chemical or wet etching, we just set the horizontal and vertical etch rates equal.

Ion Spread:

The angular spread of the incoming ion flux, measured in degrees. If this angle is zero, the ions are assumed to be purely vertical. If non-zero, a Gaussian profile in flux density is assumed, and the angle is the 3-sigma value of the distribution.

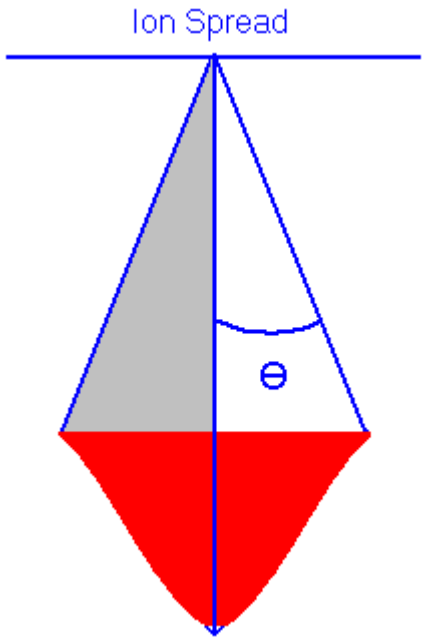

Figure 1. Ion Spread Angle

Faceting Parameter:

A fitting parameter called the faceting parameter, which gives additional material faceting if desired. It describes the nonlinear angular dependence of the physical sputtering yield, and crresponds to the variable A in the equation:

$$yield \sim (1 + A\sin^2\theta)\cos\theta \qquad (1)$$

Where θ is the angle of incidence measured from the normal. If this value is zero, the process has no sputtering component, and the maximum etch rate occurs for normally incident ions. If non-zero, the process is driven, at least in part, by physical sputtering, and the maximum etch rate occurs for ions incident at some shallower angle.

We see this function plotted in Figures 2 and 3 for the cases A=0 and A=2.

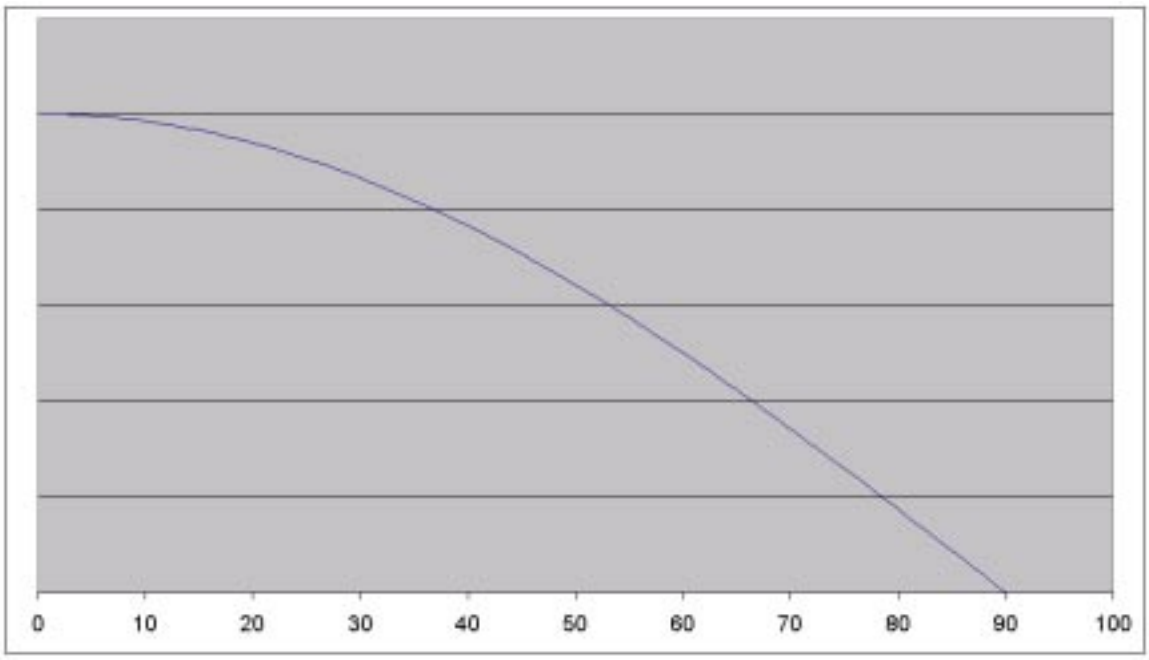

Figure 2. Sputtering Yield for A=0

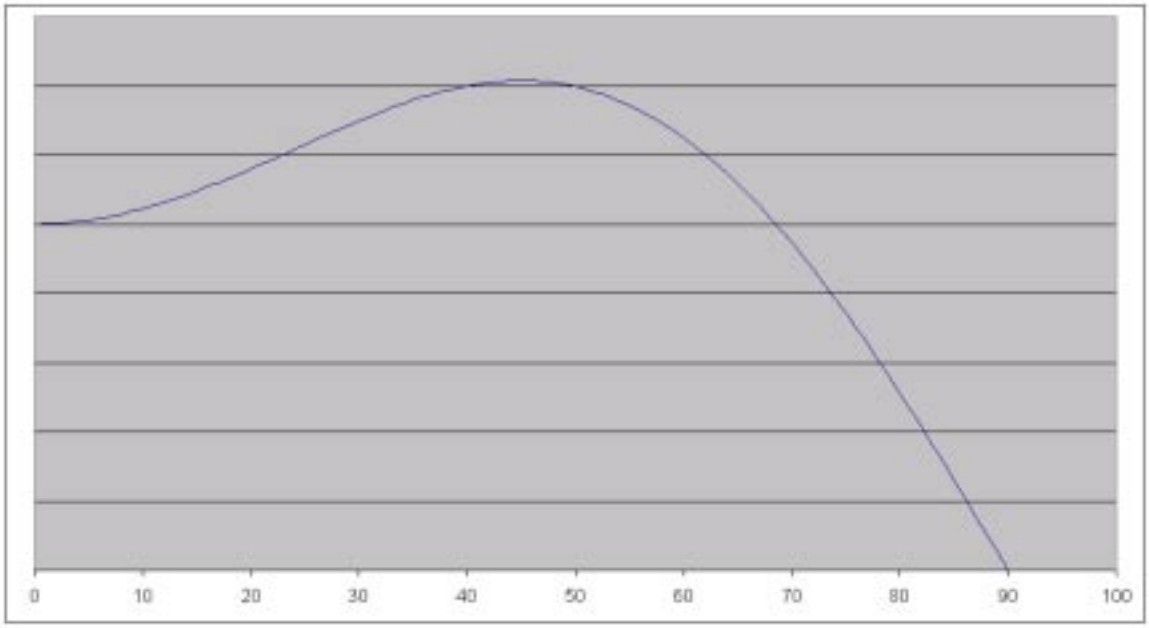

Figure 3. Sputtering Yield for A=2

By taking several sets of etch rate data, ion spread, and faceting parameters, we can model real world plasma chemistries which vary over the course of a full etch process. Using a set of cross-sectional SEM images from a series of wafers at various stages of the etch process, we extract our model input parameters as we fit our simulated profiles to the experimental data. Once we have a tuned etch model, corresponding to a full etch process, we are free to vary any lithographic input or even the etch model parameters. With this technique, we can consider both the effect of varying lithographic inputs on final etch profiles and etch process windows, and different etch processes and chemistries as correlated to etch model inputs.

NOTE: For even more technical information about the etch simulator, refer to the SPIE publication ML4691-133.pdf (which is available in the same folder as this tutorial).

Procedure (Matching 2D Etch Simulations to Experimental Data)

For purposes of this tutorial, we will assume that we can match a lithography result. That is, we assume we can get a good resist profile match with experimental data. Also for the sake of example, let's say we were trying to print 275 nm isolated lines.

Open the etchdemo.pl2 file. This file contains an already tuned resist profile. Generate a resist profile. You should see something like this:

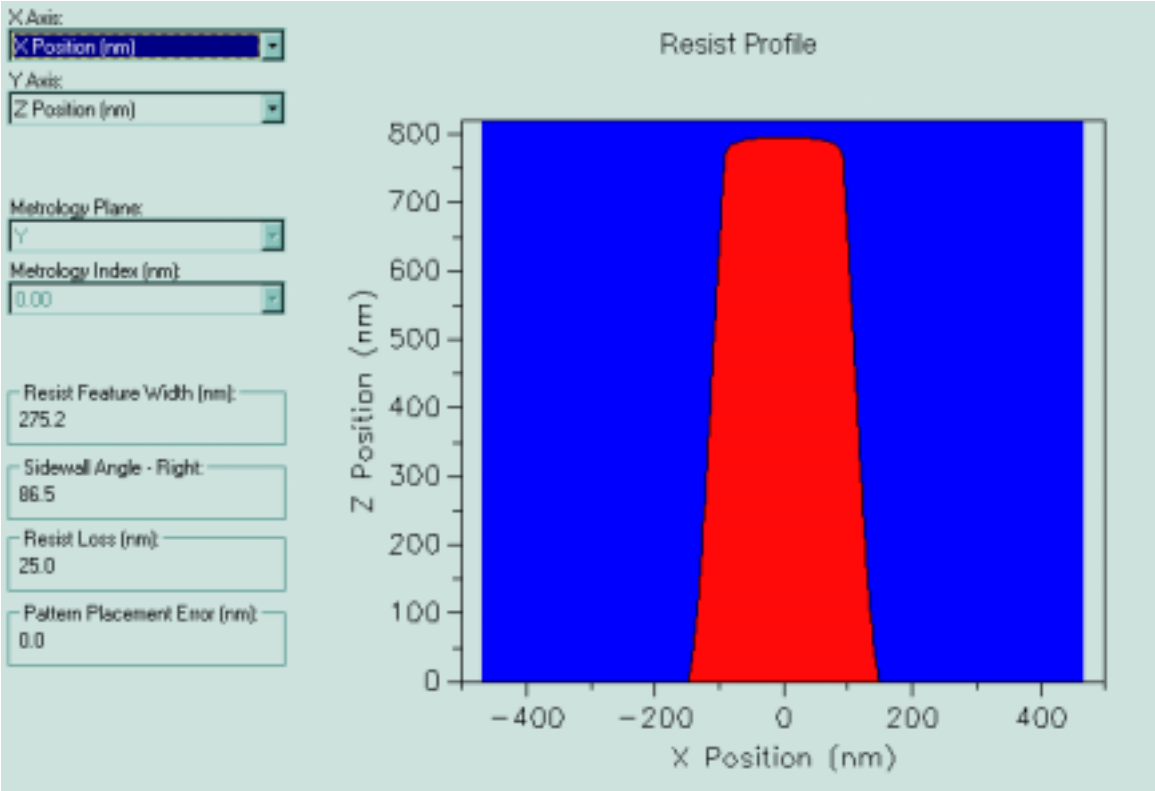

Figure 4. A resist profile for a 275 nm line.

Note that the CD as measured is 275.2 nm, which is what we'd expect from a simulation tuned to make 275 nm lines.

Load the "Before Etch.bmp" bitmap file (shown below in figure 5). Compare it to the cross section. It matches pretty well in terms of height, width, and shape. The profile in the image is a bit more vertical (and thus measures a bit narrower at the base) but we have a good enough fit to proceed. This is the first input to the etch simulation - a correct resist profile. Now we can start our etch simulation.

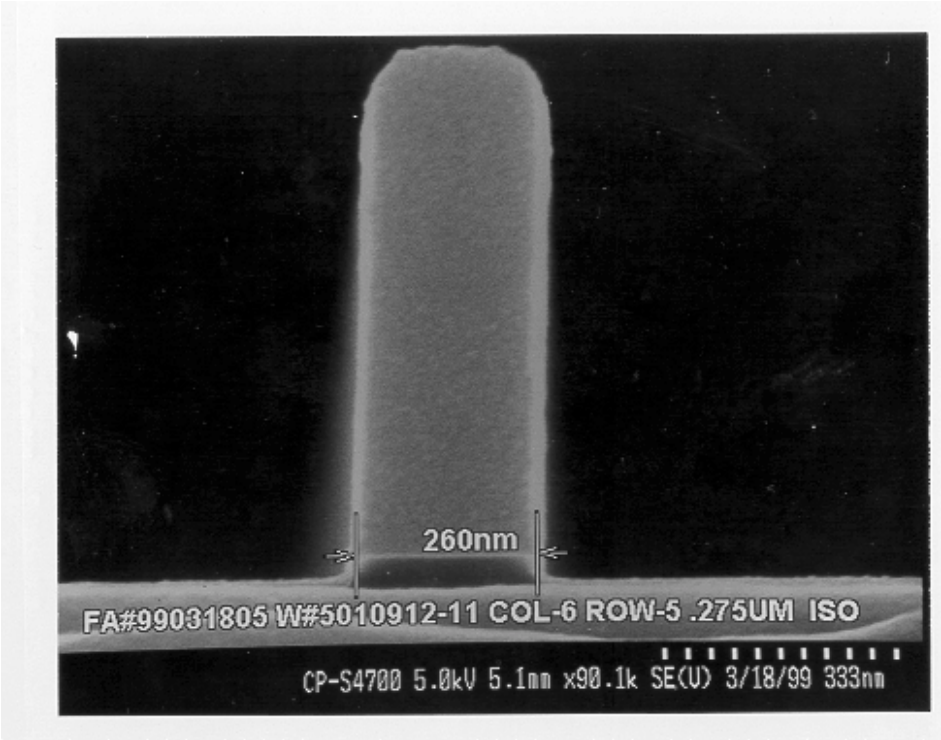

Figure 5. An isolated 260 nm line before etch.

Let's assume that we are going to try to match a two-stage etch process. The first stage is a 15 second breakthrough etch designed to get through the ARC, followed by a 60 second main etch to cut through the poly layer below. Say we have a couple of cross sectional SEM images we are going to use for this purpose. Say the first cross section (of the break through etch stage) looks like this ("Break Thru Etch.bmp"):

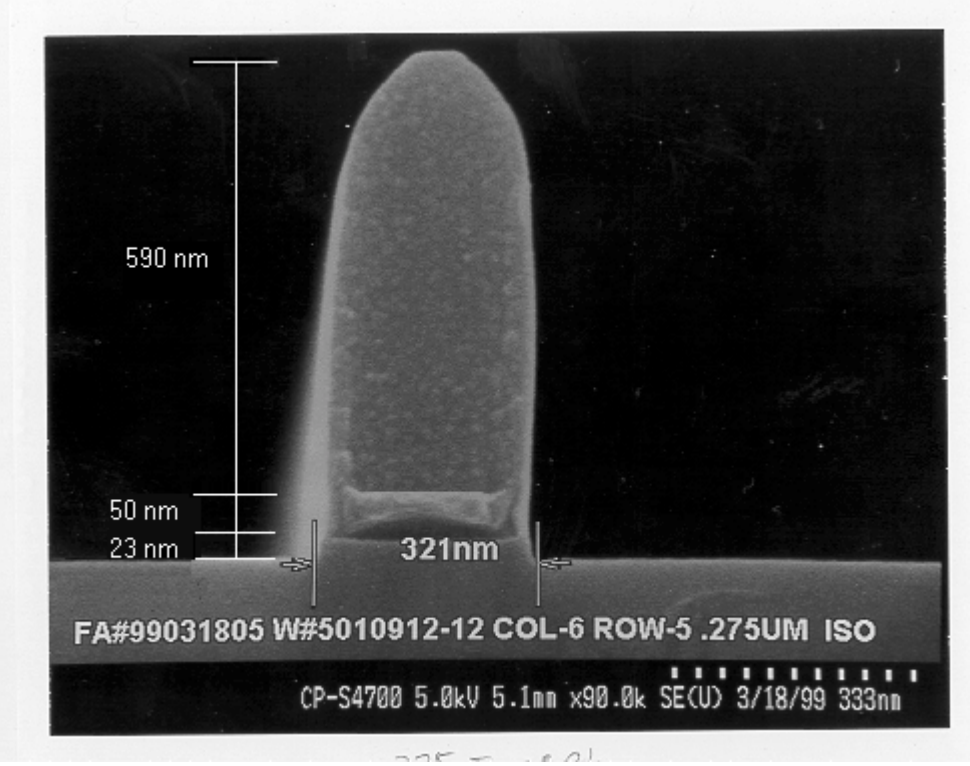

Figure 6. An isolated line after break-thru etch.

We see in the image that the Resist profile is 590 nm tall. It sits atop the 50 nm layer of ARC. The ARC is completely cut through and the polysilicon below is etched 23 nm. From the picture, we can approximate the etch rates by subtracting the final resist heights and CDs from the initial resist heights and CDs and dividing by 15 seconds of etch time.

(820 nm - 590 nm)/15 s = 15.3 nm/s for the resist in the vertical direction.

(260 nm - 321 nm)/2/15 s = -2 nm/s for the resist in the horizontal direction (where we have divided by two since a horizontal etch occurs on both sides of the line).

For the ARC etch rate, we need a bit more information (or some more cross sections). But just as an example, let's say we know that our ARC/Poly selectivity is 5.45:1. In the 15 seconds of etch we cut through all 50 nm of the ARC and 20 nm of the silicon. This is a total of 73 nm in 15 s, but the first 50 nm is cut through 5.45 times faster. After a bit of algebra, we find that the etch rates must be about 12 for the ARC and about 2.2 for the poly in the vertical direction. In the horizontal, we find that they are about -1 and -0.8 respectively.

So let's enter these numbers into the etch inputs screen. Go to the Etch Inputs Screen by pressing the Etch button. Type in the values from above. When you are done the table should look like Figure 7 below:

Stage	Etch Time (s)	Ion Spread (deg)	Material	Vertical Etch Rate (nm/s)	Horizontal Etch Rate (nm/s)	Faceting Coefficient
1	15.00	0.00	APEX E	15.30	-2.00	0.00
			Brewer ARC CD1	12.00	-1.00	0.00
			Silicon	2.20	-0.80	0.00

Figure 7. Etch inputs for the break-thrue etch stage.

Run the etch simulation by pressing the Etch button. (For your convenience, a completed simulation is saved in "Break Thru Trial 1.pl2"). Your output should look something like this:

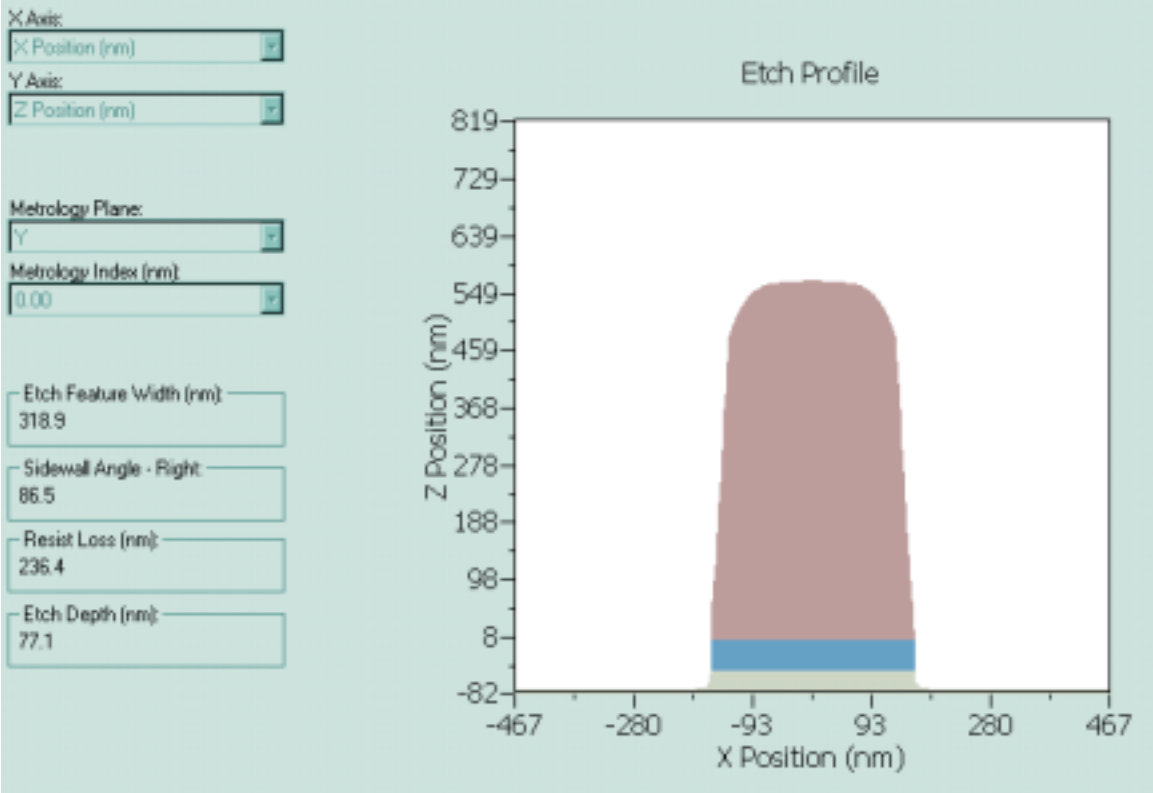

Figure 8. Etch profile after break-thru etch.

Comparing this to the SEM image, we see that we are lacking the faceting of the resist. We are also a bit narrow. Playing around with the parameters, and especially adding some faceting is in order.

Let's try the following set of input parameters shown in Figure 9:

Stage	Etch Time (s)	Ion Spread (deg)	Material	Vertical Etch Rate (nm/s)	Horizontal Etch Rate (nm/s)	Faceting Coefficient
1	15.00	0.00	APEX E	15.20	-2.50	0.40
			Brewer ARC CD1	12.00	-1.12	0.00
			Silicon	2.20	-0.80	0.00

Figure 9. Etch inputs for break-thru etch (trial 2).

Running this simulation gives us a very nice match to the SEM. (For your convenience, a completed simulation is saved in “Break Thru Trial 2.pl2”). Your output should look like the following:

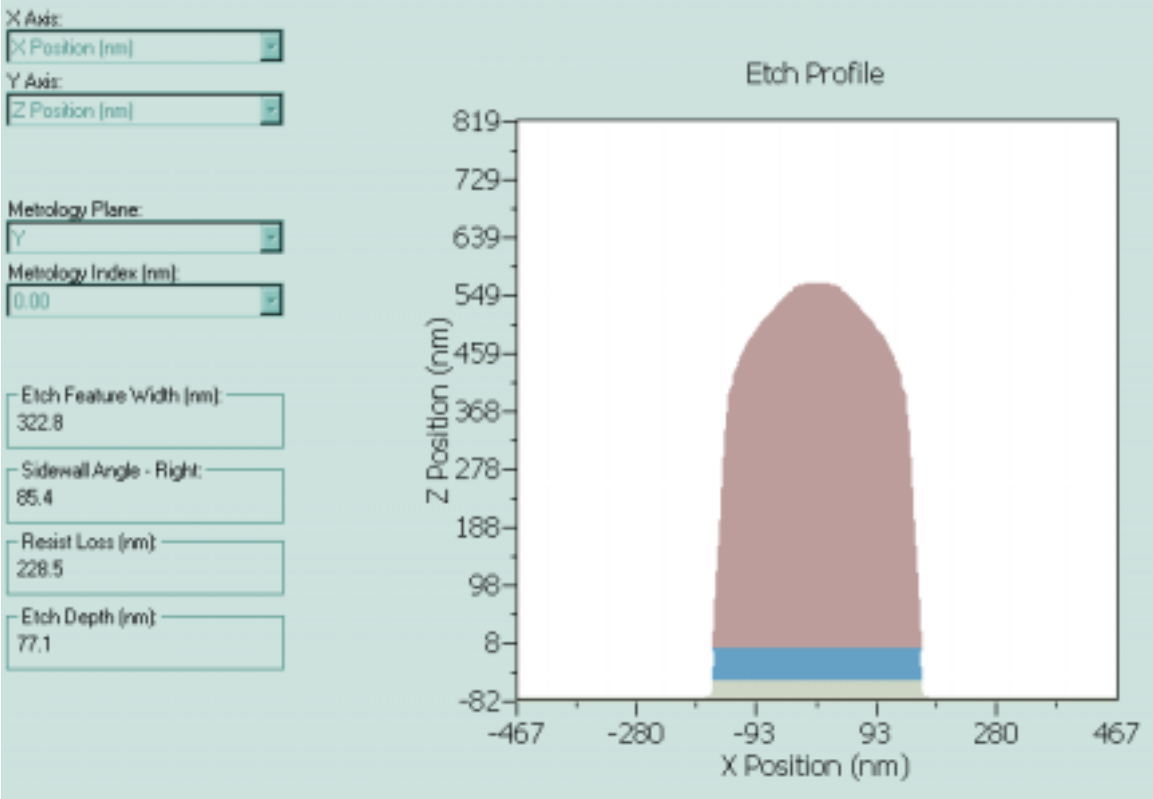

Figure 10. Etch profile after break thru etch (trial 2)

Use the right mouse button to measure the profile at several heights. Right-Click to the left of the profile, hold down the button and drag to the right side of the profile, then release. The measured CD appears below the image.

We now need to try and match on the main etch stage. We repeat the process using the next SEM image, (“Main Etch.bmp”), shown in Figure 11:

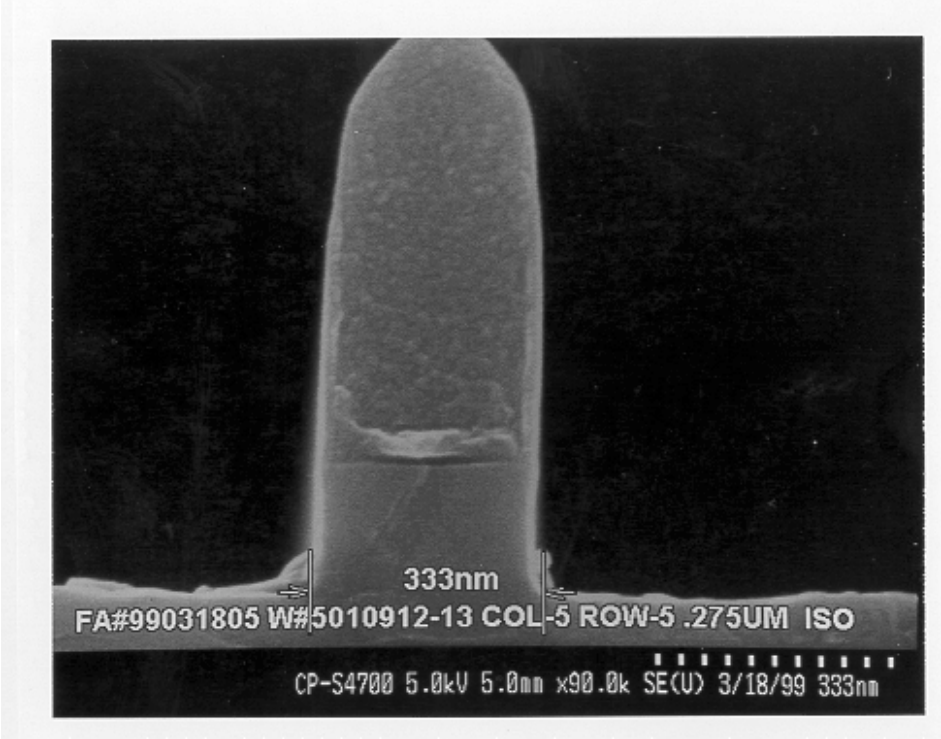

Figure 11. Cross sectional profile after main etch.

We add another stage to the etch on the etch inputs screen, and add the following parameters, as shown in Figure 12:

Etch Model: Standard Number of Etch Stages: 2

Stage	Etch Time (s)	Ion Spread (deg)	Material	Vertical Etch Rate (nm/s)	Horizontal Etch Rate (nm/s)	Faceting Coefficient
1	15.00	0.00	APEX E	15.20	-2.50	0.40
			Brewer ARC CD1	12.00	-1.12	0.00
			Silicon	2.20	-0.80	0.00
2	60.00	0.00	APEX E	0.50	0.00	0.00
			Brewer ARC CD1	2.80	0.10	0.00
			Silicon	2.80	0.10	0.00

Figure 12. Etch inputs for the break-thru and main etch stages.

Running this simulation gives us a very nice match to the SEM as seen in Figure 13. (For your convenience, a completed simulation is saved in "Main Etch.pl2"). Your output should look like the following:

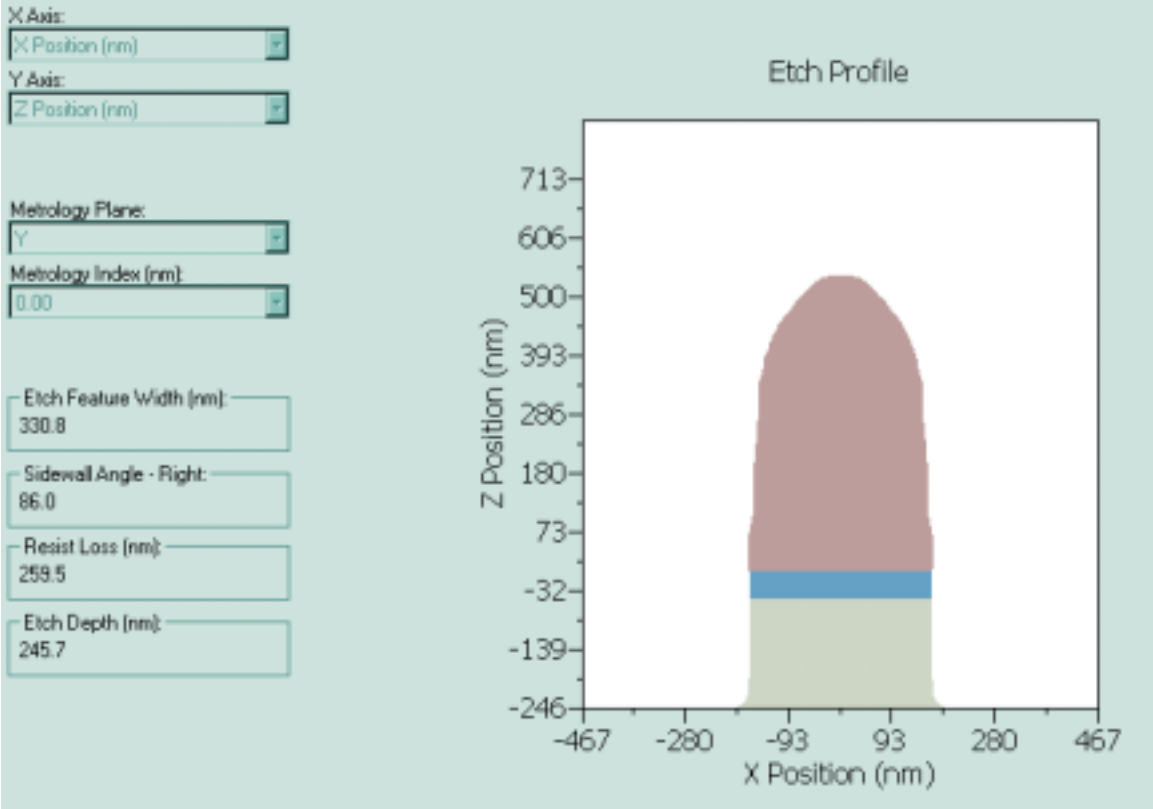

Figure 13. Etch profile after main etch.

This gives a basic overview of the etch process. We have taken experimental data and matched the profiles with a simulation. If we consider this a tuned etch model, we can now begin running experiments. We could, for example, run a simulation set where we vary the pitch of our 1D mask. Or we could vary thicknesses in the filmstack and look at etch variations. Or we could run any number of other interesting simulations.

Procedure (Extending 2D Etch Simulations to 3D)

Now, let's consider a 3D etch problem. *Because we will always begin with cross-sectional SEMs*, *we always tune our model using a simple 1D mask.* Thus the procedure for setting up a 3D simulation should always include setting up a 2D simulation first. Then, using the same set of tuned etch parameters, we convert to a comparable 2D mask. We have already tuned a model for 275 nm lines in the previous example, so lets switch a mask to a 2D mask made of 275 nm lines. Suppose, for example, that we wanted to look at a line-end shortening problem. We could use a T-shaped mask made of 275 nm lines as shown at the right in Figure 14.

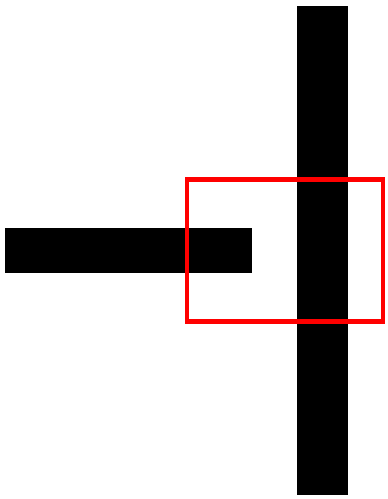

Figure 14: T-mask.

Open the file “MainEtch.pl2” in the tutorial folder.

Go to the numerics view. Change the speed factor to 7 for a faster calculation.

Go to the mask view. Then select the 2D parametric mask “Line End Shortening - Tee.” Set the feature width to 275 nm and the gap width to 300 nm.

Because etch simulations can take a while, we’ll bring up the Queue window so that we can watch the progress bar.

Run a resist profile and have a look at the resulting 3D resist image. It should look something like Figure 15:

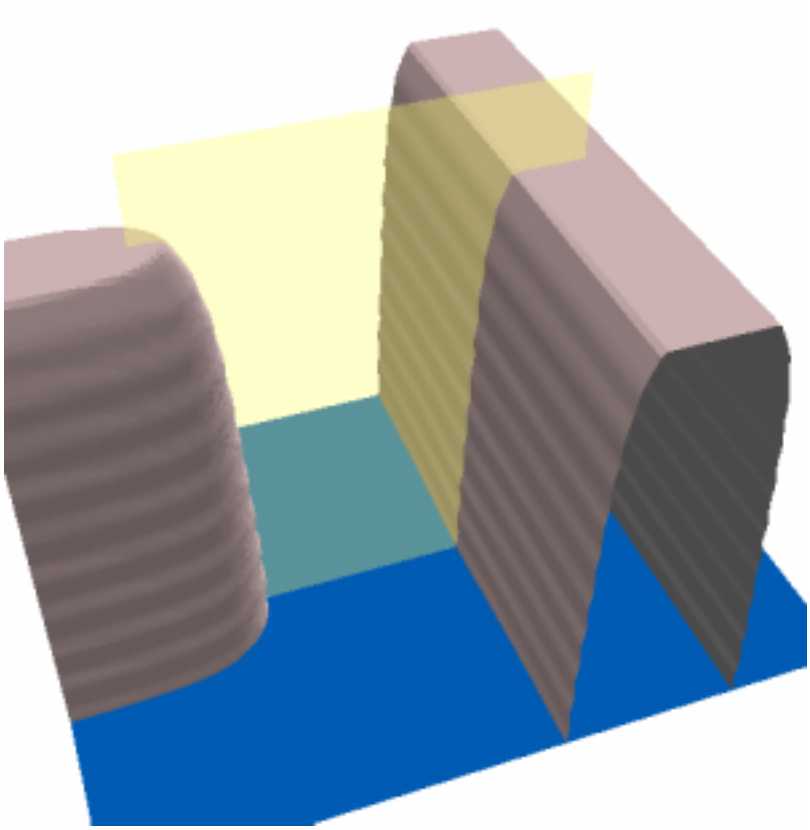

Figure 15. 3D resist profile for the T-mask

Go to the etch profile view. Note: Etch processing can take a long time, especially on slower machines. For your convenience, we have precalculated the results of this etch simulation and stored the result in the tutorial folder. You can load the file "3D Etch Demo.pl2" and go to the etch profile view by pressing the button. The output should look like Figure 16 (for a Y-metrology plane):

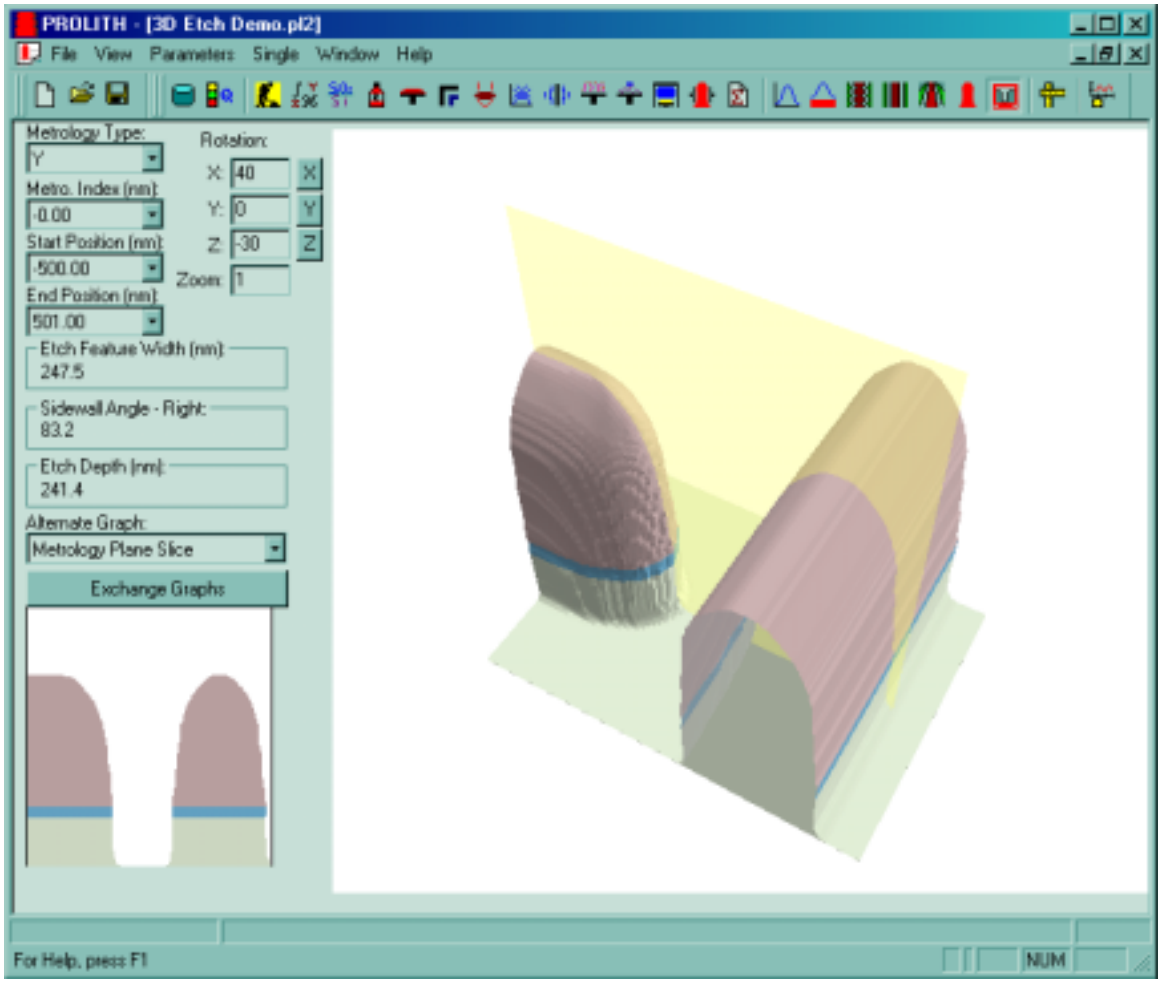

Figure 16. Etch profile after main-etch for the T-mask

Note that the resist has been faceted and that the cross section is consistent with our 2D results. The interesting thing here, then, is that we could consider many different interesting lithography effects (e.g., OPC variations, focus and dose variations, etc.) and look at their after etch effects.

Note: this file is saved at a low speed factor - the total computation time is measured in hours (so don't start any 3D etch simulations from this document without changing the speed factor, or you're in for quite a wait.)

Press the "Exchange Graphs" button. Use the right mouse button to measure the width of the gap just like we did with the 2D profile. The output should be similar to Figure 17 below:

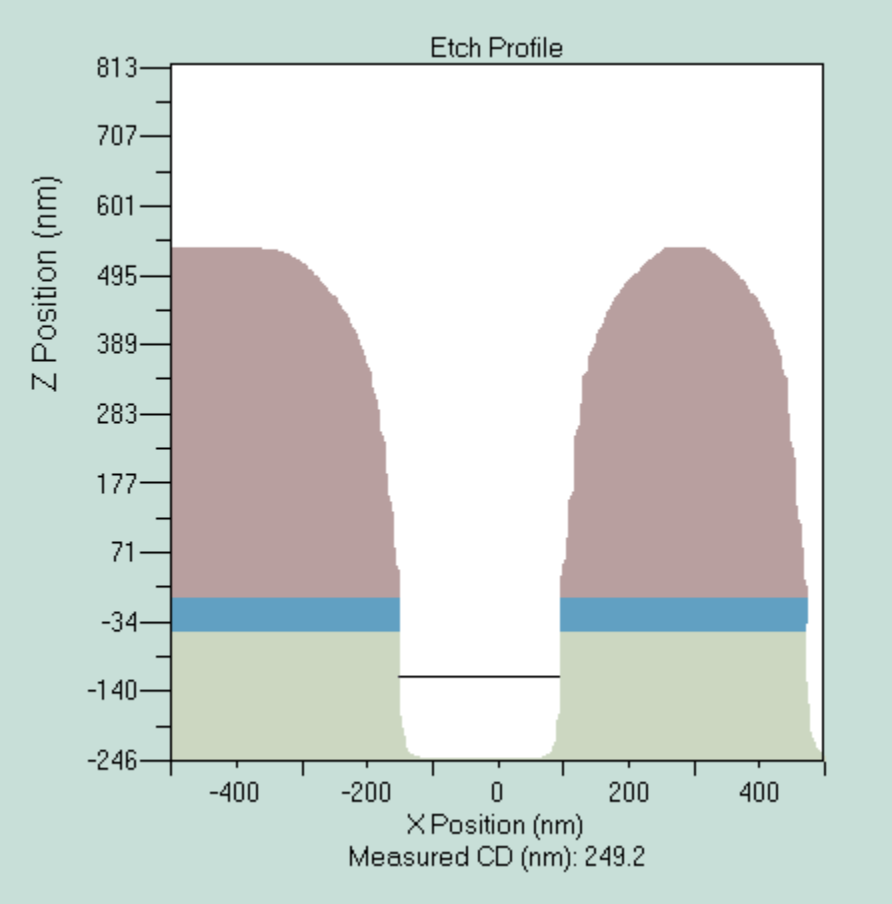

Figure 17. Measuring the CD on the 2D cross sectional profile.

Summary

The PROLITH etch model takes only a few simple inputs, yet yields many powerful and interesting results. Combined with an optical lithography simulator, we can now simulate the entire pattern transfer process. We can tune the model to match experimental data for a wide range of etch processes, and use the predictive value of the model to simulate many lithographic and etch processing conditions. The usefulness of the model to the lithographer will come foremost with the ability to optimize a lithographic process to obtain desired after etch results, but also with the instructive value the model has for lithographers trying to understand etch processing and its limitations.

Questions

See Appendix A for answers.

1. Why would I want to run an etch simulation?
2. How do I simulate chemical or wet etching?
3. To what physical process does a negative horizontal etch rate correspond?
4. What kind of experimental data is needed to get the inputs for the PROLITH etch simulator?

5. Can PROLITH etch simulations show undercutting?
6. Does the PROLITH etch simulator include any aspect ratio dependent etching effects?
7. How do the input parameters change when we switch from a 2D to a 3D etch simulation?

Appendix A
Answers to questions

Chapter 1 - Using NILS to Judge Aerial Image Quality

1. As shown in Figure 5, decreasing the wavelength gives a larger NILS value for small amounts of defocus. For large amounts of defocus, the NILS values are not very different when the wavelength is changed. So, the choice of an optimal wavelength will depend on what value of NILS your resist need to print. For the example in Figure 5, we see that if the new resist requires a NILS of 2, then changing the wavelength will not as important as if the new resist requires a NILS of 3.5.
2. The results are qualitatively the same for isolated features.
3. The source shape can also be adjusted on most steppers. For conventional illumination, optimization of the partial coherence of the source shape can be performed by making plots similar to Figures 5 and 6. For more complex source shapes, such as quadrupole or annular, the optimization is a little more complicated because there are more parameters. However, the image quality can vary dramatically with numerical aperture and source shape, so maximizing NILS is a very powerful approach to optimizing your stepper settings.

Chapter 2 – Defining Depth of Focus

1. The CD Process window (shown in dashed yellow) is much smaller than either the Sidewall Angle or Resist Loss process windows. So, our desire for tight CD control is the limiting factor; or conversely, we have plenty of latitude in our process for producing acceptable Sidewall Angles and Resist Loss.
2. The process window drastically shrinks; we lose half of our depth of focus and nearly half of our exposure latitude. Also, the best focus and best exposure points are moved—we need more defocus and a higher exposure to achieve even a marginal process latitude.
3. The plot doesn't change, as we aren't constrained by the resist loss process window.

Chapter 3 – Optimizing Resist Thickness using a CD Swing Curve

1. CD Uniformity = Max CD – Min CD across range of resist thickness inputs. CD Uniformity @732 nm = CD Max (735 nm)-CD Min(729 nm) = 241.3-235.3= 6 nm variation across wafer. CD Uniformity @754 nm = CD Max (754 nm) - CD Min (751 nm) = 252.4-252.1= 0.3 nm variation across wafer.
2. For contact holes and spaces CD max occurs at roughly the same thickness as the E0 min and the CD min occurs at roughly the same location as the E0 max.

3. Resist absorbance or B parameter causes the resist feature (lines) width to increase from one CD min to the next higher CD min location. Increasing B parameter increases the amount of change. Between consecutive CDmin values, and decreasing B parameters decreases the amount of change between consecutive CDmin values.

Chapter 4 – Optimizing a Bottom Antireflective Coating

1. No, the results are not the same. The optimal thickness with this erroneous analysis would be 60 nm.
2. Set the BARC thickness to 60 nm in the film stack view. In the simulation sets, set *Min, Max* and *Step* values to 0.0, 60.0 and 30.0 nm respectively. The resultant multi-line graph will show that none of these thicknesses provides an optimized BARC.

Chapter 5 – Optimizing a Film Stack for Reflectivity Control

1. From Figure 4 k~0.65 has the lowest reflectivity in this thickness range. Looking in Table 1 this absorbance corresponds to an N_2O flow rate of ~105 sccm. At this flow rate the resulting refractive index is found from Table 1 as ~1.96. Re-simulating the substrate reflectance as a function of SiON thickness yields an optimal thickness for this processing condition of 45 nm. Using this BARC (d=45 nm, n=1.96, k =0.65) yields a less than 0.25% substrate reflectivity and a low CD swing. The choice between the thick and the thin BARC materials requires consideration of many things, e.g., coating uniformity for each process condition, etch selectivity, substrate variability, etc. If etch selectivity is a concern then the thinner ARC may be preferable. If the thickness of the oxide under the BARC varies due to coating non-uniformity or topography then the thicker BARC is preferable. The reader should verify this last statement by repeating the experiment shown in Figure 9 using the thin BARC material a verify a larger CD variation with oxide thickness.
2. The addition of the oxide would increase the substrate reflectivity to ~1.5%. Re-simulating Figure 7 using a 5 nm oxide cap shows than the BARC has the best performance (lowest substrate reflectivity) with a k value ~0.31. This lower k value is obtainable using ~200 sccm flow rate. The refractive index for the SiON material changes slightly to 1.82 so the ideal thickness must be increased to 118 nm.

Chapter 6 – Influence of PEB on Standing Waves

1. Isolated features give similar results to those shown in Figures 7 and 8, except that the isolated features have greater depth of focus. As the results are the same, analysis of either feature type should lead to a suitable bake time.
2. The isolated features print larger for short bake times (50 nm larger), but the iso-dense print bias decreases with increasing PEB time. At a bake time of about 190 seconds, the isolated and the dense lines are about the same size. However, as shown in Figure 8, correcting iso-dense print bias with PEB time would be detrimental to the process depth of focus.

Chapter 7. – Exposure vs. Thermal Dose for Chemically Amplified Resists

1. The general shape and trends are the same. The location of the CD Error = 0 line is for the dense line is shifted to the left relative to the isolated graph. For example, for an exposure dose of 15 mJ/cm^2, the isolated line case will have a 0-error point at a temperature of 89 degrees and the dense line case will have a 0-error point at a temperature of 88.5 degrees.

Chapter 8 – Effects of the Aberration Coma

1. For the original 5 bar pattern with the "Coma_20" aberration and a dose of 180 mJ/cm2, the image placement error on the center line is 53.5 nm. If you increase the partial coherence from 0.5 to 0.6, the image placement error becomes 75.3 nm. For this case, it appears that increasing the partial coherence causes the diffraction pattern to sample parts of the lens with greater wavefront deviation, so the effects of coma are exaggerated.
2. As shown in the Procedure above, features oriented along the x-axis will not be as influenced by x-coma as features oriented along the y-axis. For the features oriented along the y-axis, coma will cause an error in the CD and in the pattern placement. One way to account for these differences is to overlap the process windows for both orientation in order to find a common process window where both orientations will print with acceptable CDs and pattern placement errors.

Chapter 9 – Using the Yield Analyzer Option to Predict CD Distributions

1. The BARC thickness in the original process was the first minimum in the reflectivity curve, and the BARC thickness in the new process is a little thicker than the second minimum (located around 125 nm).
2. There are two minima in the standard deviation curve at the same BARC thicknesses as the minima in the substrate reflectivity. The standard deviation minimum at the 45 nm BARC thickness is about 8 nm, while the standard deviation is about 5 nm at the second reflectivity minimum (125 nm BARC).
3. For errors in the BARC, oxide, and resist thicknesses each with a standard deviation of 10 nm, a plot of the standard deviation of the CD distribution versus the mean BARC thickness has an even more dramatic minimum at the second reflectivity minimum at the BARC thickness of 125 nm. Shown below are the CD limit yield, standard deviation, and Cpk values for the three BARC thicknesses that we have discussed in this chapter. As shown in the table, the second reflectivity minimum (125 nm) gives slightly better results. The most dramatic improvement is seen by moving away from the 45 nm BARC thickness.

BARC Thickness	Yield	Standard Deviation	Cpk
45 nm	83%	13.3	0.32
140 nm	100%	6.1	0.94
125 nm	100%	5.6	1.02

Chapter 10 – Speed and Accuracy of PROLITH Simulations

1. By consulting the data in Table 8, you can see that a typical Speed Factor 3 simulation is 21 times slower than a typical Speed Factor 6 simulation.
2. Because we build the results at each stage from the results at previous stages, errors cascade through all the calculations. Thus, because the Resist CD measurement is one of the last calculations performed, it includes all errors which have occurred in previous stages, and is therefore more prone to error.
3. Yes. The Simulation Set is just a collection of Single Simulations, so the same relation holds.
4. By increasing the Speed Factor, you also increase the memory requirements for the simulations (roughly in proportion to the Number of Steps shown in Table 1 squared for 2D simulations or cubed for 3D simulations). If your machine doesn't have enough RAM to hold a simulation completely in memory, it may be paging to disk, which will introduce giant delays (it will be at least 1000 times slower if it must go to disk). This usually only happens at low Speed Factors. To solve this problem, install more memory on your computers.

Chapter 11 – Etch Simulation for Lithographers

1. To simulate the entire pattern transfer process, to determine the impact of the final resist profile shape on the quality of the etched pattern in the substrate, to understand the effect of changing lithography input variables on the final etch profile, or to simulate bilayer resist processes.
2. Set the horizontal and vertical etch rates for each material equal to each other.
3. A negative etch rate corresponds to deposition of material. For a PROLITH etch simulation, only the horizontal etch rate is allowed to be negative.
4. All the inputs for a PROLITH etch simulation can be obtained through matching simulated etch profiles to cross-sectional SEM images taken at various times throughout the etch process.
5. Yes, if the horizontal etch rate of a layer is greater than the etch rate of the layer above it.

6. Only though the ion spread parameter and the shaddowing effect that slows the etching of deep trench features relative to shallow ones.
7. The etch model extends naturally to three dimensions with no additional parameters. In this case, the horizontal etch rate means the uniform etch rate in the x- and y-planes. The ion spread parameter becomes the half angle of the 3D cone of visibility rather than a 2D triangle. The other parameters have no alternate interpretation.